UNIVERSITÄT ZU LÜBECK

Research Center Borstel
Leibniz Lung Center
Director: Prof. Dr. Ulrich Schaible

Macrophage-specific Arginase-1 – a susceptibility factor in *Mycobacterium tuberculosis* infection

Dissertation
for Fulfillment of
Requirements
for the Doctoral Degree
of the University of Lübeck

from the Department of Natural Sciences

Submitted by

Anna Baumann
From Hamburg

Lübeck 2022

First Referee: Prof. Dr. Ulrich Schaible

Second Referee: Prof. Dr. Jürgen Westermann

Date of oral examination: 31.01.2023

Approved for printing. Lübeck, 08.02.2023

Table of contents

List of Figures

List of Tables

List of Abbreviations

A. dest.	*Aqua destillata*, Lat. „destilliertes Wasser“
ANOVA	analysis of variance
Arg-1	Arginase-1
B. malayi	*Brugia malayi*
BCG	*Mycobacterium bovis* bacille Calmette-Guerin
BMC	bone marrow chimeric
BMDM	bone marrow derived macrophages
bp	basepairs
BSA	bovine serum albumin
BSL	biosafety level
CAM	classically activated macrophage
CCL	chemokine C-C motif ligand
CD	cluster of differentiation
cDNA	complementary DNA
CFH	cubic foot per hour
CFU	colony forming units
CTLA	cytotoxic T lymphocyte antigen
d	day
DC	dendritic cell
DKO	double knockout
DMEM	Dulbecco’s Modified Eagle Medium
DMSO	dimethylsulfoxid
DNA	deoxyribonucleic acid
dNTP	deoxyribonucleosid triphosphate
DO	diverse outbread
DTH	delayed-type hypersensitivity
EDTA	ethylenediaminetetraaceticacid
et al.	*et alii*, Lat. „and others“
EtOH	Ethanol
G-CSF	granulocyte colony–stimulating factor
GM-CSF	granulocyte-macrophage colony-stimulating factor
GSEA	genome set enrichment analysis
GV	Gentiana violet
H&E	hematoxylin and eosin
HIV	human immunodeficiency virus
i. e.	*id est*, Lat. „that is” / “that means“
IFN-γ	interferon-gamma
IL	interleukin
iL3	infectious third-stage larvae
IL-4δ2	interleukin-4-delta-2
IL-4Rα	interleukin-4-receptor alpha-chain
IRG	immunity-related 47-kilodalton (p47) guanosine triphosphatases
IVC	individually ventilated cage
L.	*Litomosoides*

L-Arg	L-arginine
LC	light cycler
L-NIL	L-*N*6-(1-iminoethyl)-lysine
log_{10}	decadic logarithm
LRG-47	47-kilodalton (p47) guanosine triphosphatase (murine orthologue of Irgm1)
LTBI	latent tuberculosis infection
mφ	macrophage
M.	*Mycobacterium*; *cave*: → *Mycobacterium tuberculosis*
M.O.M.	mouse on mouse
MDR-TB	multidrug-resistant TB
MHC	major histocompatibility complex
mRNA	messenger ribonucleic acid
Mtb	*Mycobacterium tuberculosis*
N.	*Nippostrongylus*
NADP	Nicotinamide adenine dinucleotide phosphate
NADPH	Nicotinamide adenine dinucleotide phosphate (reduced form)
NO	nitric oxide
NOHA	N^{ω}-hydroxy-L-Arginine
NOS2	nitric oxide synthase 2
O.	*Ornithonyssus*
OADC	oleic albumin dextrose catalase
OAT	ornithine aminotransferase
ODC	ornithine decarboxylase
PAMP	pathogen-associated molecular pattern
PBS	phosphate buffered saline
PCR	polymerase chain reaction
PD	programmed death
PMN	polymorphonuclear cells
PPD	purified protein derivative
PRR	pattern recognition receptor
RNI	reactive nitrogen intermediate
ROS	reactive oxygen species
RT	room temperature
S.	*Strongyloides; cave*: →*S. mansoni*
s. c.	subcutaneous, subcutaneously
S. mansoni	*Schistosoma mansoni*
SDS	sodium dodecyl sulfate
SEA	*S. mansoni* egg antigen
SOCS3	suppressor of cytokine signaling 3
SPF	specific pathogen-free
TB	tuberculosis
TBS	tris-buffered saline
Th	T helper cell
TLR	Toll-like receptor
TNF	tumor necrosis factor
UPL	universal probe library
VL	visceral leishmaniasis

WHO	World Health Organization
wk	week
WT	wild type

1 Introduction – Of Mycobacteria, Mice, and Man

Mycobacterium tuberculosis (Mtb), the most common causative agent of tuberculosis (TB), is a rod-shaped, obligate aerobic bacterium first identified by Robert Koch in 1882 (1). Caseating granulomas in the lung constitute the hallmark of TB. In the human host, granulomas are stratified and may display hypoxia/anaerobiosis, low pH, and presence of long-chain fatty acids which account for the difficulties of identifying Mtb in the center of granulomas (2). Despite considerable research efforts, the underlying mechanisms of pathology and disease susceptibility are not entirely clear to this day.

1.1 The Epidemiology of Human TB

TB remains a major global health threat with approximately 10 million new cases worldwide in the year 2020. The World Health Organization (WHO) estimates that the TB incidence may rise in the coming years due to the impact of the coronavirus disease 2019 (COVID-19) pandemic on the time to diagnosis, reporting, treatment and mortality. In the human immunodeficiency virus (HIV)-negative population, 1.3 million TB deaths were reported and 214,000 deaths in the HIV-positive population in 2020 alone (3). The estimated TB incidence in 2020, for countries with at least 100,000 incident cases, is illustrated in Figure 1. Approximately 3% to 4% of new cases were reported to be at least rifampicin-resistant or multi-drug-resistant (MDR). Emerging drug-resistance is one problem that complicates the eradication of TB, despite drug-susceptibility testing being more widely available (3). In countries with a high incidence of TB disease, the exposure to Mtb is higher (4), patients may carry highly virulent strains (5) and helminth infections are prevalent (3,6–8). The risk to develop TB is higher in immunocompromised individuals or people who had recent contact with Mtb. Co-infection with HIV is possibly the most significant comorbidity that has been identified as a risk factor for TB (9). No large studies are currently available to characterize concomitant COVID-19 as a potential risk factor for TB (10). Also, host and Mtb genotypes – and certain combinations thereof - may predispose for increased disease susceptibility (9). Other hurdles in the way of eradication of TB are the lack of correlates of protection and an effective vaccine. Vaccination of children with *Mycobacterium* (*M.*) *bovis* bacille Calmette-Guerin (BCG) remains the gold standard vaccination against Mtb until today. Additionally, difficult identification and treatment of latently infected individuals adds to the difficulties in eradicating the Mtb reservoir (3). Therefore, TB represents a major threat to human health until this day and improving our understanding of the complex immune response to Mtb is key in facilitating the development of new medicines, diagnostic tools and treatment strategies.

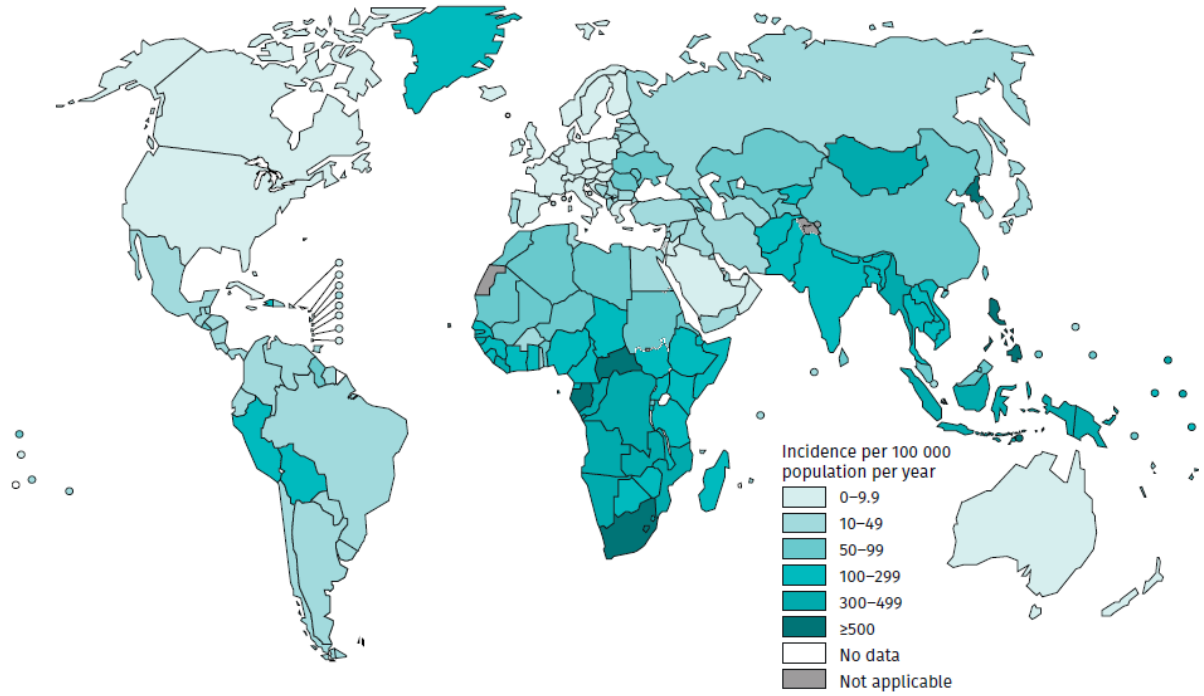

Figure 1 Estimated TB incidence rates in 2020 (3)
Among the endemic countries, the high-burden countries Nigeria, South Africa, Pakistan, India, Indonesia, the Philippines, Bangladesh, and China account for 67% of TB cases worldwide (3).

1.1.1 Clinical disease

Mtb is transmitted by droplet infection and establishes a focus of infection in the lung. Transmission may also occur by contact with a patient's contaminated secretions. Following infection, most individuals remain symptom-free. Rarely, unspecific symptoms such as fever and pleural effusion appear (2). The initial control of Mtb infection rarely fails, but few of infected individuals progress directly from infection to active disease (9), defined as primary-progressive TB. Primary-progressive TB is rare in immunocompetent patients but more frequently observed in immunocompromised patients. Signs and symptoms may resemble those of acute pneumonia. Cavitation may be absent if CD4+ T-cell responses are impaired and a delayed-type hypersensitivity (DTH) response is lacking, also known as nonreactive TB (2). Reactivation of latent TB gives rise to post-primary or secondary TB, which can show multiple, heterogeneous clinical presentations. Post-primary TB may be asymptomatic as long as the infection remains localized or bacilli remain dormant. When symptoms arise they are often non-specific, mild, and may be similar to those observed in other pulmonary disease such as pneumonia or lung cancer, thereby hindering timely diagnosis and treatment (9). Symptoms can be localized or systemic and may include fatigue, anorexia and weight loss, fever, night sweats, productive cough with purulent sputum and hemoptysis indicating tissue destructive cavitation. If the infection spreads to the surfaces of the pleura, inflammation and friction can give rise to chest pain (2,9,11). Establishment of bacteremia or dissemination along the lymphatic system can lead to extra-pulmonary TB, the symptoms of which may be nonspecific and manifestations will depend on the site(s) of infection (12). Caseous granuloma necrosis, liquefaction, and ultimately rupture of the granuloma lead to the characteristic cavitation. Granuloma erosion into a bronchus facilitates Mtb transmission via sputum expectoration (2).

1.1.2 The pathogenesis of human tuberculosis

Following aerosol transmission, Mtb predominantly infects macrophages, which then enter the subtending epithelium and initiate an inflammatory response. When the infected macrophage is unable to control the growth of Mtb, cell death leads to the release of viable bacilli, resulting in infection of more alveolar macrophages, release of pro-inflammatory signals, and recruitment of monocytes from the circulation to form an early inflammatory aggregate. Upon arrival of acquired immunity, early lesions develop into stratified granulomas, the hallmark of TB (13). Monocytic progenitor cells differentiate into multinucleated giant cells whose high-cholesterol metabolism may facilitate Mtb survival (14). The generation of multinucleated giant cells appears to be induced by interleukin (IL)-4 (15,16) and IL-13 (17). Macrophages may also develop into foamy macrophages and epitheloid macrophages (18,19). Foamy macrophages likely contribute to caseous necrosis within the granuloma. These cells comprise the core of the granuloma below a layer of fibroblasts that deposit collagen to form a fibrous capsule, which is surrounded by CD4+ and CD8+ T cells and B cells in the marginal zone. Encapsulation and calcification of granulomatous lesions contribute to containment of bacilli (20). The metabolic state of dormant Mtb within the granuloma is incompletely understood, but a sustained immune response to Mtb is crucial to maintain latency (9). While granuloma formation prevents the spread of bacilli to neighboring tissues, it also prevents access of the immune system to the bacilli contained within the granuloma, thereby facilitating their persistence (21). Reactivation of Mtb can be triggered by various factors, including immunosuppression, re-infection, stress, and age but its precise mechanisms are still unclear. Adaptive immunity is essential for control of the infection, but comes with the limitation of significant tissue hypersensitivity. If the granuloma is unable to contain the multiplying bacilli, active TB ensues (22).

1.1.3 The mouse model of TB

The disease observed in the human host can differ considerably from that observed in animal models of experimental TB. The frequently used Balb/C or C57BL/6 mouse strains do not mimic the lung pathology observed in human TB entirely when infected with Mtb Erdmann or Mtb H37Rv strains. Nevertheless, these models allow to study different aspects of the immune response to Mtb. Various experimental animal models of tuberculosis employing different strains of the MTB complex have been developed over time. Of note, no model mirrors all aspects of human tuberculosis, but a variety of animal models is required to investigate different aspects of the immune response and the many heterogeneous presentations of latent and active TB seen in humans (23–25). Established models employ mice, rats, guinea pigs, rabbits, and non-human primates (9,26,27), but the choice of the model not only depends on scientific considerations but also on practicalities. In terms of the latter, the mouse model has the advantages of being relatively inexpensive and requiring less space and resources for maintenance compared to models using rats or bigger animals. Plenty of tools to manipulate the mouse model exist, ranging from genetic modification of mouse strains to the amounts of reagents and kits available for purchase. Due to extensive use in research over the past decades, the mouse model is also the best-characterized animal model to study TB (9,27). It should be noted though, that different mouse models may be associated with different manifestations of disease and immune response not only as a consequence of e.g. the genetic background of experimental mice, but also due to the strain and the

infectious dose of Mtb (28,29). With regards to disease manifestation, wild type mice develop a chronic infection without latency characterized by high bacterial loads. Human hosts most often develop a latent infection. Not unlike the human immune system though, the murine immune system controls the developing high bacterial load, inflammation, and lesion progression for prolonged amounts of time and up to several months without onset of symptoms (27,30). Chronic infection leads to ongoing immune activation and infection control over long periods of time. Ultimately, progressive immunopathology results in death due to lung failure (31).

Despite of the often limited overlap between the tissue pathology and disease progression observed in the mouse compared to the human host, the use of experimental mice has provided valuable information about the human immune response to Mtb infection. Experiments with mice have shown the essential role of CD4+ T cells (9). Important cytokines required for control of mycobacterial infection, including IL-12 (32), interferon (IFN)-γ (33), and tumor necrosis factor (TNF) (34) as well as the importance of nitric oxide synthase 2 (NOS2) (35) have been identified in the mouse model and confirmed in patients (9,36). Overall, these examples demonstrate the value of the mouse model as a tool for the field of infection immunology of TB.

1.2 Protective immune responses to Mtb infection

1.2.1 Mtb predominantly infects macrophages

Mtb exploits complement receptors, scavenger receptors, and mannose receptors on the macrophage to infect the cell and gain access to the endosome (37,38). The mycobacterial cell wall plays an essential role in protection of Mtb from antimicrobial defenses within the macrophage, but its components are also easily recognized by the immune system. Recognition of pathogen-associated molecular patterns (PAMPs) through pattern recognition receptors (PRRs) leads to release of chemokines and cytokines and consequently to attraction and activation of inflammatory cells (39). Toll-like receptors (TLR) such as TLR-2, TLR-4, and TLR-9 can recognize structures of Mtb (39), but their importance in the mouse model of TB is controversially discussed (40–43). In addition, cytoplasmic PRRs can be involved in sensing microbial deoxyribonucleic acid (DNA) and contribute to generation of cytokine responses (44). Following aerosol infection, mainly alveolar macrophages respond to the infection. Dendritic cells (DCs) can also become infected. Polymorphonuclear cells (PMNs) and monocyte/macrophages may be attracted and activated further down-stream (44). Although macrophages are able to phagocytose Mtb, they initially fail to control the infection and succumb to cell death, the precise form of which is a matter of discussion (45–47). Cell death promotes the spread of the infection through release of free bacteria and enhances inflammation and tissue destruction. DCs or macrophages deliver Mtb-antigens for antigen presentation to T cells and enhance protective immunity (9). Within the macrophage, Mtb ensures its survival by reprograming the endosomal microenvironment resulting in an increased pH, prevention of endosomal maturation and ultimately blocking phagolysosomal maturation (9,48).

1.2.2 Mtb infection triggers the release of pro-inflammatory cytokines and chemokines leading to protective Th1- and Th17A responses

In response to Mtb internalization, innate immune cells release pro-inflammatory cytokines including IFN-γ (33) and TNF (34). The principal sources of TNF are macrophages, although other producers include lymphocytes, endothelial cells, and other immune cells. TNF influences proliferation and differentiation of immune cells, as well as expression of chemokines and adhesion molecules on vascular endothelium in the lung, thereby facilitating recruitment of immune cells. Neutralization of TNF leads to decreased expression of chemokines that attract T cells, B cells, and innate immune cells including monocytes/macrophages and neutrophils. Also, TNF was shown to induce macrophages and neutrophils to release reactive oxygen species (ROS) and proteases (36).

Similar to TNF, IFN-γ is essential for survival of mice during infection with Mtb and can be produced by both lymphocytes and phagocytes (33,36,49,50). TNF and IFN-γ promote cellular infiltration and inflammation (34,51). An influx of inflammatory cells and large numbers of monocytes/macrophages initially benefits mycobacterial proliferation and development of granulomatous lesions by providing new host cells for bacterial replication while their antibacterial effector mechanisms have not yet been fully activated (52). Macrophage activation is dependent on IFN-γ (49) and this effect is potentiated in presence of TNF and IL-18 (53). Despite the presence of phagocyte-activating IFN-γ, growth control of Mtb also requires the presence of T cells to realize the full antibacterial potential of macrophages (54,55). In susceptible mice, IFN-γ also serves the purpose of limiting infiltration by PMNs, but this function appears to play a lesser role in the relatively resistant Balb/C and C57BL/6 mouse strains (56). Additionally, IFN-γ signaling can induce antimicrobial peptides in macrophages (57). Moreover, both IFN-γ and TNF appear to be required for maintenance of the granuloma during the chronic phase of infection (34,58).

TNF, IFN-γ and IL-1 can trigger production of IL-6 by different sources including myeloid and non-myeloid cells (36). IL-6 was shown to potentiate early IFN-γ expression, although its effects on susceptibility appear to be less pronounced during low-dose infection. Despite increased bacterial loads and a delay in IFN-γ responses following low-dose infection, IL-6 deficient mice were ultimately able to control the infection (59). In contrast, high-dose infection via the intravenous route in IL-6-deficient mice resulted in elevated levels of IL-4, decreased levels of IFN-γ, and impaired survival (60). Other than this, IL-6 was also linked to detrimental effects, such as decreasing surface expression of major histocompatibility complex II (MHC II) on macrophages and T cell inhibition in other mycobacterial infections (61,62).

Activated DCs produce IL-12, which consists of IL-12p35 and IL-12p40 subunits and is important for optimal IFN-γ production and generation of Th1 responses (32). Interestingly, the IL-12p40 unit may also form a homodimer, IL-12p$(40)_2$, which can agonize or antagonize the IL-12p70 heterodimer (p35+p40) although the factors determining agonizing or antagonizing roles of IL-12p$(40)_2$ remain to be elucidated (63). IL-12, chemokine C-C motif ligand (CCL)19, and CCL21 influence DCs to travel to the draining lymph node where they present Mtb-antigens to CD4+ T cells (9,36). In the lung, IL-12 plays an essential role in maintaining the expanded IFN-γ/Th1 response (64). Interestingly, it was revealed by Schreiber *et al.* that neolymphoid follicles in the lungs are formed when interactions in the lymph node are compromised. This allowed priming, activation and expansion of effector cells nonetheless and mice

were able to control mycobacterial growth, therefore demonstrating that lymph node involvement was not crucial in TB (65).

Next to the Th1 population, the Th17 subset that produces IL-17A, IL-17F and IL-22 has been identified as a minor cell population in immunity to TB and is largely dependent on IL-23, which is produced by activated DCs after uptake of Mtb (66,67). Overall, the IL-23/IL-17 axis appears of lesser importance in initial control of Mtb infection in the low-dose model, but has been implicated in vaccine-induced immunity (68).

1.2.3 IFN-γ-dependent NOS2 induction: classical activation of macrophages

IFN-γ release from Th1 cells induces classical activation of macrophages resulting in the maturation of phagolysosomes and auto-phagolysosomes as well as enhanced antigen-presenting capacities (44). IFN-γ induces NOS2 in macrophages which leads to production of nitric oxide (NO) and reactive nitrogen intermediates (RNI) as well as formation of nitrite and nitrate (69) which is key in the antimycobacterial defense. Due to the oxidative damage to many different parts of the bacilli it is effective at killing Mtb (35,70,71). If NOS2 is absent or inhibited, Mtb grows uncontrollably resulting in lethality (35,72). Classically activated macrophages (CAMs) will also generate hydroxyl radicals such as superoxide anions and hydrogen peroxide via NADP(H) oxidase and the interaction between NO and superoxide can lead to the production of toxic peroxynitrite (71). In addition to NOS2, IFN-γ also induces an immunity-related 47-kilodalton (p47) guanosine triphosphatase (IRG). The murine orthologue (Lrg-47) promotes phagosome maturation in macrophages and was shown to contribute to controlling the multiplication of Mtb in mice (73). Interestingly, the human orthologue of LRG-47 appears to be involved in autophagy and growth control of Mtb as well (74). These IFN-γ-dependent effector mechanisms are key functions of CAMs (Figure 2, upper part) and accordingly *Nos2* and *Lrg47* serve as prototype markers for this state of activation.

Immune cell infiltration into the lung results in amorphous, predominantly cellular lesions of infected macrophages interspersed with lymphocytes. Mtb-infected mice develop unstructured granulomatous lesions, sometimes displaying interstitial fibrosis. Fibrosis may develop over time, leading to the characteristic “honeycomb” morphology which resembles human fibrosis (31). However, no discernible strata are formed. Granulomatous lesions in mice lack a fibrous capsule, central necrosis, liquefaction, and cavitation (27,30,75). Also giant cells are absent in mice and the developing lesions are vascularized and seem to lack hypoxia (24,76). While much effort has focused on discerning the factors underneath those striking differences in granulomatous lesion morphology between the human host and the mouse model, the mechanisms have not been elucidated entirely.

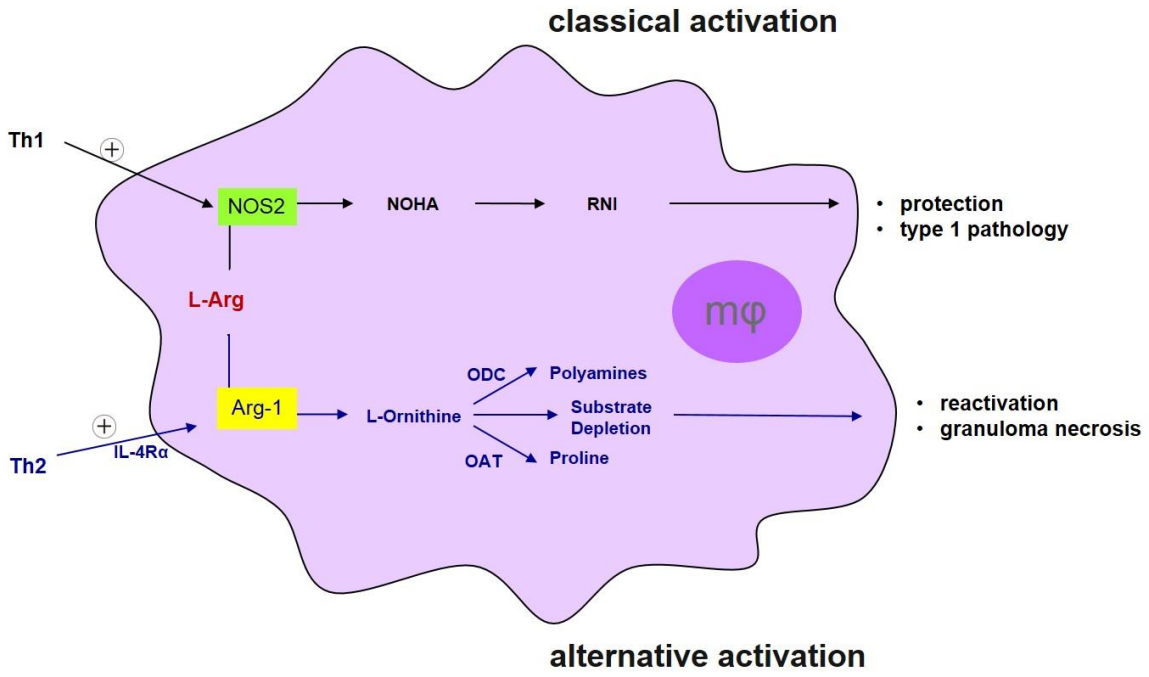

Figure 2 Classical vs. alternative activation of macrophages (references in text)
IFN-γ induces classical activation of macrophages characterized by the expression of their hallmark enzyme NOS2. NOS2 uses L-Arg as a substrate to generate RNI, mainly NO, which is critical in the antimycobacterial defense to destroy Mtb. In between, NOHA is formed, an endogenous inhibitor of Arg-1. Alternative activation of macrophages may occur via type 2 cytokines such as IL-4 and IL-13 that share the common IL-4Rα-chain. IL-4Rα-signaling induces the hallmark enzyme of alternative macrophage activation, Arg-1. Arg-1 competes with NOS2 for the substrate L-Arg and catalyzes the reaction of L-Arg to L-Ornithine and urea. L-Ornithine is metabolized via ODC to polyamines or via OAT to proline. Proline may provide building blocks for collagen and facilitate development of fibrosis. Polyamines may potentially be used by Mtb for growth.

Arg-1, Arginase-1; IFN-γ, interferon-gamma; IL, interleukin; IL-4-receptor alpha, IL-4Rα; L-Arg, L-Arginine; mφ, macrophage; Mtb, *Mycobacterium tuberculosis*; NO, nitric oxide; NOHA, N^{ω}-hydroxy-L-Arginine; NOS2, nitric oxide synthase 2; OAT, ornithine aminotransferase; ODC, ornithine decarboxylase; RNI, reactive nitrogen intermediates; Th, T helper cell;

1.3 Subversive immune responses in TB

While Th1 responses that lead to induction of CAMs are considered protective and essential in immunity to TB (9), a potentially subversive role has been ascribed to Th2 cytokines including IL-10, IL-4, and IL-13. This is illustrated by reports of increased levels of IL-10 and IL-4 in patients with active TB (77–79) although IL-4 involvement is inconsistently reported in literature (79). Nevertheless, mixed Th1 and Th2 immune responses are also described in patients with progressive TB and they were characterized by elevated IL-4 and IL-13 levels which in turn were associated with the extent of disease and cavitary status (78,80). Genetic mutations may further facilitate the susceptibility to TB. A variant of the IL-4-receptor alpha (IL-4Rα)-chain was implicated in increased susceptibility to TB. This supports the notion that Th2 responses can drive detrimental outcomes in human TB (81). This genetic association study in TB patients showed that a mutation in *IL4RA*, the human gene encoding the IL-4Rα chain, predisposed for severe asthma and enhanced IL-4 and IL-13 signal transduction which was associated with the degree of pathology observed in TB (81). Interestingly, increased Th2 responses were are also observed in TB patients in developing countries with a high exposure to Mtb (28,82,83). PBMCs (84) and T cells (80) have been described as sources of IL-4 in TB patients. When comparing TB patients to household contacts, patients with active TB had elevated plasma levels of IL-4 (77–79). In contrast, expression of the IL-4-antagonist IL-4-delta-2 (IL-4δ2) was increased in patients with high Th1 responses and control

of latent Mtb infection (85,86). However, it is unclear how and why Th2 responses arise in TB. Moreover, the mechanisms through which Th2 responses may mediate increased susceptibility to TB are unclear and difficult to examine in murine models of TB. This is due to the fact that a Th2 component is not usually observed in mice in response to low-dose Mtb infection. It has been shown that the infectious dose is a determinant for Th1- or Th2-polarization in mice infected with *M. bovis* BCG. Indeed, Balb/C mice showed Th2 responses after high but not low-dose infection (87). High-dose infection of Balb/C mice has been developed as a model for TB in developing countries where patients face high exposure to mycobacteria and show elevated Th2 responses during infection with Mtb (83). IL-4 deficiency and IL-4 depletion in a high-dose infection model in Balb/C mice resulted in significantly improved control of Mtb infection which could be reconstituted by IL-4 administration (88–90). Following high-dose infection, bacterial reactivation correlated with the arrival of IL-4 producing lymphocytes (28). A Th2 response after high-dose infection may also be involved in the breaking of the growth plateau during the chronic phase of infection as bacterial reactivation was shown to correlate with the arrival of IL-4 producing lymphocytes (28) Moreover, increased Th2 responses in Balb/C mice appear to correlate with tissue injury in TB (91,92). In contrast, no such role for IL-4 or IL-10 could be observed during low-dose infection of Balb/C and C57BL/6 mice. Indeed, susceptibility to TB early after infection was unaffected in mice lacking IL-10, IL-4, IL-4/IL-13, IL-4Rα or STAT-6 (93,94). However, bacterial growth was increased to some extent in IL-4Rα- and STAT-6-deficient mice late during infection and IL-4/IL-13-deficient mice showed higher gene expression levels of *Ifng* and *Nos2* than wild type (WT) mice (94). *In vitro* data have also shown that IL-4 may inhibit transcription factors downstream of IFN-γ-signaling and suppress gene expression of *Nos2* (95). Given the absent Th2 induction during low-dose infection in mice, mice deficient for Th2 cytokines may not necessarily be a suitable model to investigate the effects of Th2 cytokines in murine TB. In order to study the effect of increased Th2 responses in low-dose infection, murine models have employed transgenic mice that overexpress the cytokines IL-10 or IL-13. IL-10^{tg} and IL-13^{tg} mice demonstrated an increased susceptibility to Mtb infection compared to WT mice (96,97). Overexpression of IL-10 led to reduced RNI production and diminished control of Mtb infection. In IL-10^{tg} mice, macrophages were the predominant source of IL-10, which promoted alternative activation of macrophages (Figure 2) instead of classical activation and correlated with impaired infection control, outweighing IFN-γ–induced effector functions of CAMs (96). Over-expression of IL-13 after Mtb infection led to development of necrotic lesions and reactivation, further underpinning a role for Th2-mediated mechanisms in the development of pathology and disease susceptibility. These IL-13-dependent effects were mediated through IL-4Rα-signaling, which was associated with elevated expression of Arginase-1 (Arg-1), the hallmark enzyme of AAMs (97). However, little is known about the role of Arg-1 in TB and its importance for disease susceptibility.

1.4 Does Arg-1 mediate susceptibility to TB?

1.4.1 Arg-1 – undermining protective anti-mycobacterial immune responses?

Arg-1 expressing AAMs have been found in the granulomas of patients with progressive TB and in Mtb-infected non-human primates (77,78,83,98,99). Human PBMCs from TB patients showed elevated

levels of arginase activity, which was associated with increased levels of IL-10 and reduced proliferation and cytokine responses of T cells (100). Moreover, alternate activation of macrophages appeared to be increased in patients with MDR-/XDR-TB compared to patients with drug-susceptible TB but was also associated with use of pyrazinamide-containing treatment regimens (101).

In fact, AAMs appear less well able to produce RNI compared to CAMs when infected with Mtb *in vitro* (96). Specifically, Arg-1 metabolizes L-Arginine (L-Arg) to urea and L-ornithine. Therefore, substrate competition for L-Arg may provide a mechanism by which Arg-1 regulates RNI production via NOS2 (102). Also, depletion of extracellular L-Arg by arginase activity has been shown to mediate T cell dysfunction due to impaired CD3ζ-chain expression (103). In addition to substrate competition, another mechanism through which Arg-1 induction may undermine macrophage effector functions in intracellular infections was shown for *Leishmania major* (104). L-ornithine is metabolized via the enzyme ornithine decarboxylase (ODC) as part of the biosynthetic pathway of polyamines (105), which provide a proliferative advantage to *L. major* for growth (104). IL-13 and IL-10 release during infection with *L. major* led to increased induction of AAMs, increased proliferation of *L. major*, and higher disease susceptibility (104,106). Additionally, L-ornithine can be metabolized via ornithine aminotransferase (OAT) to the amino acid proline which is required for collagen synthesis and may affect tissue repair and fibrosis (105). When grown on L-Arg in liquid cultures, Mtb was also able to utilize L-Arg for proline synthesis and growth (107).

Conditions that promote AAM induction include Th2 responses that have been described in human TB patients and are also observed in helminth infections. *In vivo*, Arg-1 induction in macrophages has been described for intracellular pathogens such as *L. major* (104) but also for *M. bovis* BCG (108). It should be noted, that mycobacteria have also been shown to induce Arg-1 independently of Th2 signaling and Stat-6 but via an IL-6/Arg-1 axis and/or TLR/MyD88-mediated mechanisms *in vitro* (108,109).

Overall, the available evidence suggests a detrimental role of Arg-1 induction in the context of intracellular infections. In TB in particular, induction of Arg-1 appears to correlate with disease susceptibility (96,97).

1.4.2 Does helminth-induced Arg-1 promote susceptibility to TB?

In the context of Th2 responses, Arg-1 expressing AAMs are better known from helminth infections during which AAMs serve the purposes of wound healing and tissue repair, dampening inflammatory responses, but also contribute to direct inhibition of helminth motility and expulsion of helminths from mucosal sites (110). Since Th2 responses are known to inhibit Th1 responses and given the co-endemicity of TB and helminth infections (3,6–8), studies reporting compromised Th1 immune responses in TB patients with concomitant helminth-infections (111,112) appear to be expected. Yet others have published beneficial effects of helminth co-infection (113) or no effect on susceptibility to infection with mycobacteria at all (114). Another recent publication showed that co-infection with *Schistosoma mansoni* and Mtb led to increased Arg-1 induction, exacerbated inflammation and increased disease severity, but did not affect macrophage-mediated control of mycobacterial growth, instead implying T cell responses. These effects were ameliorated in bone marrow chimeric (BMC) mice lacking Arg-1 in macrophages (115). While these results seem initially compelling, pre-existing infection

with the intestinal nematode *Nippostrongylus* (*N.*) *brasiliensis* showed conflicting results in another Mtb co-infection model (116). Here, *N. brasiliensis* infection led to increased lung bacterial loads during co-infection with Mtb which was dependent on IL-4Rα-signaling and implied a role for AAMs, but found no evidence for impaired T cell responses (116). Thus, the importance of helminth-induced AAMs and the mechanisms affecting susceptibility to TB remain controversial. It seems obvious that different helminth species with different tissue tropisms may have different requirements for AAM induction and employ different immunomodulatory effects. To add insult to injury, the variability of data in literature is considerable and differs in their granularity and experimental approaches. This complexity calls for models which investigate several different helminth species in the context of co-infection with Mtb in one well-defined Mtb infection model with a high level of consistency in potential confounding factors such as housing effects, specific-pathogen-free (SPF)-conditions in animal facilities and microbiota, and taking into account not only acute but also chronic helminth infections.

1.4.3 Mtb induces Arg-1 in CAMs

Mycobacteria have been shown to induce Arg-1 independently of Th2 signaling and Stat-6 but via an IL-6/Arg-1 axis and TLR/MyD88-mediated mechanisms *in vitro* (108,109). In the context of Mtb infection, it has been shown that IL-6 can induce Arg-1 and NOS2 in macrophages, with Arg-1 preceding NOS2 expression. Mtb showed preferential growth in Arg-1-expressing macrophages which was counter-regulated by SOCS3 (117). Infection with *M. bovis* BCG induced MyD88-signaling and production of IL-6, IL-10, and granulocyte colony–stimulating factor (G-CSF) which in turn induced Arg-1 in macrophages via autocrine/paracrine signaling (109). Mtb was also able to induce Arg-1 in macrophages through TLR/MyD88-mediated mechanisms via CCAAT/enhancer-binding-proteins (C/EBP) and independently of Stat-6 during low-dose infection with Mtb H37Rv *in vitro* (108). The same authors report that mice lacking Arg-1 in macrophages were better able to control Mtb growth following low-dose aerosol infection with 200 CFU Mtb *in vivo* (108). Controversially, Arg-1 induction in response to low-dose Mtb infection is not consistently observed. When examining WT mice, no Arg-1 induction by Mtb H37Rv was observed in previous publications that used an infectious dose of 100 CFU (96,97). This differential induction of Arg-1 by the same Mtb strain could imply that Arg-1 induction may be a function of the infectious dose of Mtb H37Rv, but experimental *in vivo* evidence to this effect is lacking. Some evidence suggests an association between the virulence of the Mtb strain used and the level of *Arg1* mRNA induction. When macrophages were infected with the clinical Mtb isolates CDC1551 and HN878 *in vitro*, *Arg1* gene expression could be observed in response to infection with both strains, but *Arg1* mRNA levels were higher in macrophages infected with the HN878 strain (109). Whether Arg-1 induction depends on the virulence of the infecting Mtb strain *in vivo* is currently unknown. Additional experimental evidence for Arg-1 as a susceptibility factor in TB derives from animal experiments in WT mice in which arginase activity was artificially increased (97). L-*N*6-(1-iminoethyl)-lysine (L-NIL) stimulates Arg-1 activity by inhibiting NOS2. In the NOS2-mediated reaction that metabolizes L-Arg and O_2 to NO and L-citrulline, the intermediate N^{ω}-hydroxy-L-Arg (NOHA) is formed (118). NOHA is an endogenous Arg-1 inhibitor (119). L-NIL inhibits NOS2 activity leading to relief of Arg-1 from NOHA-mediated enzyme inhibition. When WT mice were infected with Mtb and were then administered L-NIL, WT mice developed recrudescent Mtb growth and necrotic granulomatous lesions in the lung (97). Also,

NOS2$^{-/-}$ mice showed potentially Arg-1-mediated pathology in hypoxic granulomatous lesions in a dermal infection model of Mtb (120).

Overall, these data suggest a role for Arg-1 in mediating adverse effects in TB, but direct experimental evidence *in vivo* is scarce. No experimental proof exists whether the degree of Arg-1 induction promotes susceptibility and pathology during Mtb infection *in vivo*. Also, it is unclear if the infectious dose of Mtb and strain virulence can be linked to the level of Arg-1 induction *in vivo*.

1.4.4 Aim

TB susceptibility and pathology appear to be correlated with Arg-1/AAM induction (96,97,108), but no direct proof of this exists so far. Th2-mediated Arg-1 induction in macrophages has been extensively described during helminth infections, which are co-endemic with TB (3,6–8). Mtb alone may induce Arg-1 in macrophages to subvert NOS2 activity and create a niche that favors bacterial growth although this is not consistently observed and mostly based on indirect observations (96,97,108). The present thesis aims to answer whether acquisition of TB susceptibility and pathology are mediated by macrophage Arg-1 induction resulting from helminth co-infection or Mtb infection alone. In case of the latter, this may depend on the degree of Arg-1 induction as a function of strain virulence and the infectious dose. To this end, the following questions are addressed:

- Does helminth-induced Arg-1 lead to increased susceptibility to TB and pulmonary pathology during acute and chronic co-infection with different helminth species *in vivo*?
- Does highly virulent Mtb HN878 infection lead to Arg-1-mediated disease susceptibility and pathology?
- Does the degree of Arg-1 induction depend on the infectious dose of Mtb and does this translate into increased susceptibility and pathology *in vivo*?
- Is L-NIL-mediated Mtb reactivation and granuloma necrosis dependent on macrophage-specific Arg-1 *in vivo*?

These questions will be addressed using WT mice and Tie2cre^{neg} Arg1$^{f/f}$ and Tie2cre^{pos} Arg1$^{f/f}$ mice that carry a conditional deletion for the *Arg1* gene in macrophages (108). Tie2cre (cre^{pos} designating transgene, cre^{neg} designating Arg-1-competent littermates) is a hematopoietic deleter, but since lymphoid lineage cells rarely express Arg-1, this provides a system for investigating the role of Arg-1 in macrophages during Mtb infection *in vivo* (108). The following approaches are used to induce Arg-1 during Mtb infection:

- Co-infection with helminths: *N. brasiliensis*, *S. ratti*, and *L. sigmodontis* in WT mice
- Virulent Mtb HN878 infection in Tie2cre^{neg} Arg1$^{f/f}$ and Tie2cre^{pos} Arg1$^{f/f}$ mice
- High-dose vs. low-dose Mtb H37Rv infection in Tie2cre^{neg} Arg1$^{f/f}$ and Tie2cre^{pos} Arg1$^{f/f}$ mice
- L-NIL stimulation of Arg-1 activity during Mtb H37Rv infection in Tie2cre^{neg} Arg1$^{f/f}$ and Tie2cre^{pos} Arg1$^{f/f}$ mice

2 Materials and Methods

2.1 Consumable supplies

If not indicated otherwise, all disposable plastic supplies were obtained from Sarstedt (Nümbrecht, Germany). Syringes were obtained from BD (Heidelberg, Germany) and needles from Braun (Melsungen, Germany). If not indicated otherwise, all solutions were obtained from Merck (Darmstadt, Germany), and all chemicals were obtained from Sigma-Aldrich (St. Louis, USA).

2.2 Culture media for primary cells

- Dulbecco's Modified Eagle Medium (DMEM)-complete-medium (PAA Laboratories, Pasching, Austria) supplemented with 10% heat-inactivated fetal calf serum (Merck Biochrom, Darmstadt, Germany), 100 U/ml penicillin, 100 µg/mL streptomycin, 2 mM L-Glutamin (PAA Laboratories, Pasching, Austria)
- freezing medium: DMEM-complete-medium supplemented with 20% FCS and 10% dimethylsulfoxid (DMSO)
- Plutznik medium: DMEM-complete-medium supplemented with 10% FCS, 5% horse serum (PAA Laboratories, Pasching, Austria), 30% L929-supernatant (lab internal production), 2 mM L-glutamine, 100 U/ml penicillin, 100 µg/mL streptomycin, 1 mM sodium pyruvate (PAA Laboratories, Pasching, Austria), and 100 µM 2-mercaptoethanol

2.3 Culture media for bacteria

- Difco Middelbrook 7H10 agar (BD, Heidelberg, Germany) supplemented with 10% heat-inactivated bovine serum (Biowest, Darmstadt, Germany) and 0.5% glycerol (AppliChem, Darmstadt, Germany)
- Difco Middelbrook 7H9 broth (BD, Heidelberg, Germany) supplemented with 0.05% Tween80, 0.2% glycerin (autoclaved or sterile filtered), 10% oleic albumin dextrose catalase (OADC) (BD, Heidelberg, Germany)

2.4 Solutions

- alpha-isonitrosophenon (6% alpha-isonitrosophenon in 100% Ethanol (EtOH))
- azocarmine G solution (0.1% azocarmine in *A. dest.*, 1% glacial acetic acid)
- bovine serum albumin (BSA)/tris-buffered saline (TBS) (3% BSA in TBS)
- citrate buffer (10 mM citric acid monohydrate ($C_6H_8O_7$) in *Aqua* B. Braun (Braun, Melsungen, Germany))

- eosin (1% eosin Y di-sodium-salt in tap water, filtered pre-use, acidified with 2-3 drops glacial acetic acid)
- formalin (4% formalin in phosphate buffered saline (PBS))
- Gentiana Violet (0.01% Gentiana Violet (GV) in *Aqua* B. Braun, acidified with 100% acetic acid)
- Gill's hematoxylin (0.6% hematoxylin, 0.06 % sodium iodate ($NaIO_3$), 5.28 % aluminum sulfate hydrate ($Al_2(SO_4)_3 \cdot H_2O$), 25% ml ethylene glycol, 6% glacial acetic acid, in tap water)
- Ketanest/Rompun anesthetic for *L. sigmodontis* infection of mice (10% Ketanest/Ketavet (WDT, Garbsen, Germany) and 2.5% Rompun (Bayervital, Leverkusen, Germany) in 0.9% NaCl)
- L-arginine (L-Arg) solution (0.5 M L-Arg in *A. dest.*, pH 9.7)
- L-*N*6-(1-iminoethyl)-lysine (L-NIL; Alexis, Lörrach, Germany) (0.01 M L-NIL in drinking water)
- lysis buffer for arginase assay (0.04% triton X-100, 23.8 mM Tris-hydrochloride (HCl), 4.76 mM manganese chloride ($MnCl_2$) in *Aqua* B. Braun, pH 7.5)
- lysis buffer for genotyping (5 mM ethylenediaminetetraaceticacid (EDTA) (pH 8), 200 mM NaCl, 0.2% sodium dodecyl sulfate (SDS), 100 mM Tris/HCl (pH 8), 10 g/ml Proteinase K (Roche) in *Aqua* B. Braun)
- manganese chloride ($MnCl_2$) (100 mM $MnCl_2$ in ddH_2O, stored at 4°C)
- PBS (2.7 mM KCl, 1.5 mM potassium dihydrogen phosphate (KH_2PO_4), 137 mM NaCl, 9 mM sodium dihydrogen phosphate (NaH_2PO_4), pH 7.4 in *Aqua* B. Braun)
- PCR Mastermix (1x Reaction buffer (NEB, Frankfurt am Main, Germany), 0.2 mM deoxyribonucleosid triphosphates (dNTPs; PEQLAB, Erlangen, Germany), 10 U/ml Taq DNA polymerase (NEB, Frankfurt am Main, Germany) in *Aqua* B. Braun), 0.25 µM primer sense, 0.25 µM primer antisense)
- protease inhibitor solution for organ homogenization (1 tablet cOmplete™, Mini, EDTA-free (Roche, Basel, Switzerland) in 10 ml PBS)
- reverse transcription (RT) mix LC®480 System (1x reaction buffer (Thermo Fisher Scientific, Waltham, USA), 1 mM deoxyribonucleosid triphosphates (dNTPs) (Thermo Fisher Scientific, Waltham, USA), 20U RiboLock (Thermo Fisher Scientific, Waltham, USA), 200U RevertAid (Thermo Fisher Scientific, Waltham, USA))
- RT-qPCR LightCycler (LC) master mix for Universal Probe Library (UPL) system (50% 2x LC® 480 Probes Master (Roche, Basel, Switzerland), 0.625 mM primer sense, 0.625 mM primer antisense, 1% UPL probe (Roche) in *Aqua* B. Braun)
- SDS solution (1% SDS in TBS)
- 0.5 M stop solution for arginase assay (sulfuric acid (H_2SO_4) (96%), phosphoric acid (H_3PO_4) (85%), in *Aqua* B. Braun (1/3/7, v/v/v)
- Tris-buffered saline (TBS; 150 mM NaCl, 10 mM Tris in *Aqua* B. Braun, pH 7.4)
- Tris-hydrochloride (50 mM Tris in ddH_2O, adjusted to pH 7.5 with hydrochloric acid (HCl))
- Triton x-100 (0.1% Triton x-100 in ddH_2O)
- urea (CH_4N_2O) (1% CH_4N_2O in *A. dest.*)

2.5 Bacteria

Mtb H37Rv was cultivated in OADC-supplemented Middelbrook 7H9 broth at the Research Center Borstel. Bacteria were harvested at medium logarithmic phase and frozen in 1 ml aliquots at -80°C until use.

2.6 Helminths

2.6.1 Nippostrongylus brasiliensis

N. brasiliensis larvae were obtained from Prof. Dr. David Voehringer from the University of Erlangen. The life cycle of *N. brasiliensis* was established and maintained in CD(IGS) rats at the Research Center Borstel according to the protocol established by Dr. Adriana Turqueti-Neves. For life cycle maintenance, serial passage of *N. brasiliensis* was performed in CD(IGS) rats every 6-8 weeks. CD(IGS) rats were infected subcutaneously with a dose of 2500 iL3 *N. brasiliensis* into the scruff of the neck. From day 7 to 10 post infection, rat feces were collected daily for generation of fecal cultures. To this end, infected rats were placed on metal grids overnight that allowed for the feces to fall through. Cage bottoms were fitted with moist layers of pulp to prevent the fecal pellets from drying out. Rats were placed on regular bedding during the day. The pellets were collected into falcon tubes, covered by a layer of tap water and left to soak for 30 min. Subsequently, pellets and water were poured into a beaker and homogenized with a fork. Activated charcoal was added gradually to achieve a brittle texture that retained sufficient consistency to form loose “bricks”. Petri dishes with vents were fitted with one layer of Whatman cellulose paper (Sigma-Aldrich, St. Luis, USA). The paper had a diameter approximately 1-2 cm short of the rim of the petri dish and was moistened with tap water by use of a plastic Pasteur’s pipette. A loose brick of this feces-charcoal mass was formed in the middle of the paper by use of two rectangular spatulas. The cultures were then placed in the dark in a humidity chamber. Hatched larvae migrate from the brick to the rim of the paper where they can be seen with the naked eye after approximately 1 week, therefore the hatching of larvae was inspected visually after 7 days. Depending on the amount of visible larvae, bricks were removed between day 7 and day 14 after start of culture at the latest. The charcoal feces cultures were stored in a humidity chamber for up to 8 weeks. Moist pulp was exchanged and chambers were disinfected once a week. Larvae were harvested from the cultures by means of a Baermann apparatus. To remove the iL3 from the rim of the Whatman paper, PBS was warmed to 37°C in a water bath and poured into the funnel of the Baermann apparatus, the lower end of which was fitted with approximately 5 cm of rubber sleeve and closed with a serrefine. A layer of gauze was placed ca. 2 cm deep into the PBS in the funnel to serve as a filter to retain paper and pieces of charcoal. The rim of the Whatman paper was cut off and placed on the gauze layer. Larvae were allowed to sink down to the serrefine for 1 h after which they were collected in a glass tube, followed by washing 3x by suspension in 37°C warm PBS, sinking down for 20 min, careful removal of the PBS standing over the pellet, and subsequent suspension in warm PBS again. The larvae were placed in droplets under a stereomicroscope and only the motile larvae were counted.

2.6.2 Strongyloides ratti

Strongyloides (*S.*) *ratti* larvae for infection experiments were provided by PD Dr. Minka Breloer from the Bernhard-Nocht-Institute for Tropical Medicine (BNITM) Hamburg. The life cycle of *S. ratti* was maintained by weekly passage in Wistar rats and charcoal feces cultures at the BNITM by Marie-Luise Brunn and Dr. Martina Reitz. Rat feces were collected daily from day 7 – 14 post-infection and larvae were cultivated in charcoal feces cultures for 7 days before iL3 *S. ratti* were harvested for infection experiments.

2.6.3 Litomosoides sigmodontis

Litomosoides (L.) sigmodontis-infected arthropod vectors, (*Ornithonyssus (O.) bacoti* mites, for infection experiments were provided by PD Dr. Minka Breloer from the BNITM, Hamburg. The life cycle of *L. sigmodontis* was maintained in cotton rats (*Sigmodon hispidus*) at the BNITM by Dr. Wiebke Hartmann and Dr. Irma Haben. Naïve *Ornithonyssus bacoti* mites were allowed to feed on infected cotton rats. *L. sigmodontis* larvae reach the infectious 3rd stage in the mite approximately two weeks following uptake by mites, which were then used as vectors to transmit the infection via the next blood meal.

2.7 Rat and mouse strains

All experimental WT animals (Balb/C mice, C57BL/6 mice, and CD(IGS) rats) were obtained from Charles River Laboratories (Wilmington, Massachusetts, USA). Tie2cre Arg1$^{f/f}$ mice were obtained from Prof. Peter Murray from the St. Jude Children's Research Hospital (Memphis, Tennessee, USA) and were subsequently bred at the animal facility of the Research Center Borstel (RCB). Infected animals were housed in individually ventilated cages (IVCs) at the biosafety level (BSL)-3 laboratory of the Research Center Borstel under SPF conditions. All animals were free from viral, bacterial, and parasitic infections other than specified in the experimental procedures outlined in the present thesis. All animal experiments were performed in accordance with the German Animal Protection Act and were approved prior to start by the animal research ethics board of the Ministry for Agriculture, Environment, and Rural Areas of Schleswig Holstein under the following numbers: V311-72241.123-3 (44-3/12), V311-72241.123-3 (59-4/13), and V311-72241.123-3 (46-3/12).

Table 1 Overview of experimental animals used

Animals	Genetic background	Literature reference
Wild-type mice	C57BL/6	-
Wild-type mice	Balb/C	-
CD(IGS) rats	outbred	-
Tie2cre^{neg} Arg1$^{f/f}$ mice Tie2cre^{pos} Arg1$^{f/f}$ mice	C57BL/6	(108)

2.8 Animal experiments

All experimental mice were matched for age, sex, and genetic background.

2.8.1 Aerosol infection with Mtb

Experimental animals were separated into the individual compartments of aerosol cages (Marine & Industrie Technik, Hamburg, Germany). Aerosol cages were set into the inhalation exposure system (Glas-Col, Terre Haute, USA). Standardized bacterial suspensions were prepared as follows: midlog culture aliquots of Mtb H37Rv were thawed and passed 10x through a 26G needle to break bacterial aggregates. The resulting homogenous bacterial suspension was diluted in sterile *A. dest*. to an approximate concentration of 2.5 x 10^6/ml bacteria in a final volume of 6 ml. A serial 1:10 dilution was generated from 0.5 ml of this infection suspension and plated on Difco Middelbrook 7H10 agar plates supplemented with bovine serum for retrospective determination of the bacterial concentration achieved. The remaining 5.5 ml of the infection suspension were loaded into the nebulizer of the inhalation exposure system. The main air stream was set to 60 CFH (cubic foot per hour; 1,68 m^3/h) and the compression air stream for nebulizing the infection suspension was set to 11 CFH (0.28 m^3/h) to generate an aerosol cloud of 3-5 mm particles. The inhalation exposure phases with duration in seconds are summarized in Table 2.

Table 2 Inhalation exposure cycle for Mtb aerosol infection

Phase	duration [s]
system warm up	900
nebulizing of the infection suspension	2400
aerosol removal	2400
decontamination	900

For each experiment, 4 additional mice were infected as controls to be sacrificed on day 1 p.i. with Mtb for retrospective control of the infectious dose. To this end, complete lungs of four mice were plated on Difco Middelbrook 7H10 agar plates supplemented with bovine serum for determination of CFU counts.

2.8.2 Helminth infections

2.8.2.1 N. brasiliensis infection

Larvae were prepared for injection as described in section 2.6.1. Experimental mice were injected s.c. with 500 iL3 *N. brasiliensis* into the scruff of the neck 5-10 days before infection with Mtb.

2.8.2.2 S. ratti infection

Larvae were prepared for injection as described in section 2.6.2. Experimental mice were infected with 2000 iL3 *S. ratti* s.c. into the scruff of the neck 3 days before aerosol infection with Mtb.

2.8.2.3 L. sigmodontis infection

Experimental mice were infected with *L. sigmodontis* via the natural route by exposure to infected vectors: *O. bacoti* mites carrying the infective third-stage *L. sigmodontis* larvae. Before exposure to vectors, experimental mice were anaesthetized by injection of 200-300 µl Ketanest/Rompun to prevent reduction of the exposure time due to grooming behavior.

2.8.3 Mouse Scoring

All infected experimental mice were monitored for the development of signs and symptoms of disease following helminth- and/or Mtb infections. Before onset of visible symptoms, mice were weighed once a week. A score that quantified the severity of disease was assigned based on physical activity, body weight, general condition, and spontaneous behavior as classified according to Table 3. When mice reached a disease score of >4 or a body weight loss of ≥25%, animals were euthanized.

Table 3 Mouse scoring criteria

Disease score	Activity	Body weight	General condition	Spontaneous behavior
1	very active	unchanged or increasing	smooth and shiny coat, clean body orifices, eyes shiny and bright,	Normal
2	Active	reduction by less than 10%	coat defects (abnormally low or high grooming behavior)	minor changes
3	less active	reduction by 10-20%	dull and unkempt coat, unclean body orifices, increased muscle tone	unusual changes, impaired motor activity or hyperkinetic
4	hardly active	reduction by 20-30%	dirty coat, sticky or wet body orifices, abnormal posture, eyes dull, high muscle tone	self-isolation, lethargic, hyperkinetic, stereotypy, loss of coordination
5	lethargic	reduction by more than 30%	cramped posture or paralysis of trunk musculature / extremities, respiratory sounds, mouse feels cold to the touch	noises indicative of pain when touched, self-amputation (auto-aggression)

2.8.4 Inhibition of NOS2

The NOS2 inhibitor L-NIL (Alexis, Lörrach, Germany) was administered to experimental mice at a concentration of 0.01 M in drinking water *ad libitum* from d50 to d120 post-infection.

2.9 Harvesting blood, organs, and bone marrow from experimental mice

2.9.1 Puncturing of the inferior vena cava

Experimental mice were sacrificed by CO_2 asphyxiation and incisions were made to open the abdominal cavity. The intestines were pushed to the side and blood was drawn from the inferior vena cava by means of a 25 G needle and 1 ml plastic syringe. Blood was collected in a serum separator tube (BD,

Heidelberg, Germany) for centrifugation at 4020 x *g* for 10 min. Serum separators were stored at -80°C until analysis.

2.9.2 Organ harvesting from infected animals

Livers, lungs, and spleens of experimental mice were removed aseptically and weighed to determine partial and total organ weights. For determination of colony forming units (CFU), two lobes of the right lung were transferred into 3 ml protease inhibitor (Roche, Mannheim, Germany) solution with 6-8 ¼"-sized ceramic spheres for homogenization (MP Biomedical, Eschwege, Germany); partial lobes of the liver and one half of the spleen were transferred into 8 ml 0.5% Tween-80-*Aqua* B. Braun each. For determination of gene expression, the middle lobe and post-caval lobes of the right lung were transferred into 2 ml peqGold Trifast (PEQLAB, Erlangen, Germany). For analysis of histology, the left lung, half a spleen, and two partial lobes of the liver were placed in an embedding cassette (SIMPORT, Bernard-Pilon, Canada). The left lung lobe was injected with 4% formalin solution to avoid tissue compression. The embedding cassettes were closed and the tissue was fixated in 4% formalin solution for 24 h. The tips of the tails were collected in 1.5 ml tubes and frozen at -80°C until genotyping. For determination of intestinal worm counts, the intestines were removed by severing the superior duodenum from the stomach. The superior duodenum was gripped with a forceps and pulled upwards, while stripping off the mesenteries by gently moving a pair of spread scissors in a downward motion along the intestine. The inferior end of the large intestine was severed short of the rectum and whole intestines were transferred to petri dishes for determination of worm counts.

2.9.3 Bone marrow harvesting from Tie2cre^{pos} Arg1$^{f/f}$ mice

The femora of Tie2cre^{pos} Arg1$^{f/f}$ mice were collected for generation of bone marrow derived macrophages (BMDMs), that were subsequently used for confirmation of arginase deficiency in macrophages. Whole femora were removed at the hip and knee joint without opening the bone marrow channel, cleaned, and placed in 2 ml DMEM medium on ice. Bone marrow was harvested from femora by cutting off the upper and lower ends of the bone, flushing it with DMEM-complete-medium by means of a 25 G needle and a 20 ml syringe. Cells were collected in 50 ml Falcon tubes and centrifuged (10,000 rpm, 10 min, 4°C). Pellets were resolved in approximately 10 ml DMEM-complete-medium for counting. Cell counts were determined by use of a Neubauer hemocytometer (0.1 mm depth, 0.0025 mm^2; Laboroptik Ltd, Lancing, UK) and the following formula:

$$cells\ per\ \mu l = \frac{counted\ cells}{counted\ surface\ are\ (mm^2) \times chamber\ depth\ (mm) \times dilution} \quad [1]$$

2.10 Parasitological methods

2.10.1 Determination of worm counts

2.10.1.1 Adult worm counts of N. brasiliensis and S. ratti

In order to determine adult worm counts in the small intestine, infected animals were sacrificed and the intestines were removed. The intestines were sliced open longitudinally, and placed into petri dishes with 37°C warm tap water. Intestines were washed once by slewing in water and placed at 37°C for 2 h to allow for detachment of nematodes from the intestinal mucosa. The intestines were inspected for remaining nematodes by microscopy (BX41, Olympus, Tokio, Japan). Petri dishes were placed on a microscopy grid and adult helminths were counted to determine total adult worm counts per mouse.

2.10.1.2 L. sigmodontis worm counts

Fourth-stage *L. sigmodontis* larvae (L4), adult stages, and worm granulomata were collected from sacrificed mice by making a small incision into the peritoneum through which the thoracic cavity was rinsed with 8-10 ml PBS by use of a plastic Pasteur's pipette. Worms were collected in 24-well plates and counted by use of microscopy.

2.10.1.3 Determination of L. sigmodontis microfilaremia

For quantification of microfilaremia, blood of infected animals was added to EDTA tubes (Kabe Labortechnik, Nümbrecht, Germany). Out of this, 20 µl blood were diluted in 100 µl *aqua* B. Braun and centrifuged at 10.000 × *g* for 5 min. The supernatant was removed and the pellet resolved in 20 µl of Gentiana violet (GV) for counting of microfilariae.

2.11 Cell Biological methods

2.11.1 Cultivation of primary macrophages from bone marrow

Bone marrow cells were seeded into petri dishes at a density of 3×10^6 cells in 10 ml Plutznik medium and cultivated at 5% CO2 and 37°C for 3 days. On day 3, 10 ml Plutznik medium was administered and cells were cultivated for 4 more days to generate BMDMs. On day 7, medium was removed and the cells were washed with warm PBS. Cells were incubated with 3 ml warm Accutase (37°C, 5 min) and collected in 50 ml Falcon tubes for centrifugation at 1000 rpm, 10 min, 4°C. Supernatants were discarded and the pellets were resuspended in 10 ml DMEM complete medium for counting. Cells were seeded into 48 well plates at a density of 5×10^5 per well and left to adhere for at least 4 hours or overnight before stimulation.

1.1.1 Stimulation of arginase activity in BMDM

BMDM were stimulated with IL-4 at a concentration of 500U/ml for 24 – 48 hours in DMEM complete medium at 5% CO_2 and 37°C. Control wells received DMEM complete medium without IL-4. Following stimulation, cells were washed 3x with warm PBS and lysed by use of 100 µl cold lysis buffer (5 min, 4°C) per well. Lysates were collected in 1.5 ml tubes. Wells were washed with 400 µl cold ddH_2O to

increase lysis which was added to the collected lysate. Cell lysates were vortexed and either stored at -20°C until further use or directly used for determination of arginase activity (see section 2.15.1).

2.12 Microbiological analyses

2.12.1 Determination of colony forming units

In order to determine CFU counts for lung, liver, and spleen, organs were distributed into different tubes during organ harvesting as described in section 2.9. Partial lungs, livers and spleens were homogenized by means of the reciprocating homogenizer system FastPrep-24™ (MP Biomedicals, Illkirch, France). Six 6.35 mm ceramic spheres (MP Biomedicals, Illkirch, France) per tube were used to homogenize lung tissue, and 8 ceramic spheres for liver and spleen samples each. Lung, liver, and spleen were homogenized twice for 30 seconds. Subsequently, homogenates were serially diluted 1:10 in 0.05% Tween80 *Aqua* B. Braun for plating on Difco Middelbrook 7H10 agar plates supplemented with 10% heat-inactivated bovine serum (Biowest, Darmstadt, Germany) and 0.5% glycerol (AppliChem, Darmstadt, Germany). Plates were incubated at 37°C for 3 to 4 weeks until determination of CFU counts. The total CFU counts per whole organ were calculated by means of the partial and total organ weights and dilution factors of the serial dilution at which colonies could be counted.

2.13 Molecular biological analysis and techniques

2.13.1 Genotyping of mice

DNA was isolated from tail or ear biopsies of experimental mice and breeding stock and used for genotyping by means of polymerase chain reaction (PCR). Biopsies were incubated overnight in 300 µl genotyping-lysis buffer with 0.2mg/ml Proteinase K (peqLab, Darmstadt, Germany) at 56°C and 800 rpm on a thermomixer (Eppendorf, Hamburg, Germany). After incubation, tubes were centrifuged at 4020 × *g* for 10 min at room temperature. The supernatants were transferred to new 1.5 ml tubes and the DNA was precipitated by addition of 500 µl isopropyl alcohol (Sigma-Aldrich, St. Luis, USA). The DNA was centrifuged at 11180 × *g* for 10 min at room temperature. Supernatants were discarded, the DNA left to dry for approximately 5 min and then dissolved in 100 µl *A. dest*. for 20 min at 56°C. For PCR, 1 µl DNA solution was amplified using specific primer pairs (Table 4) and cycling conditions (Table 5). Agarose gels (1.2%) were prepared by dissolving 1.2 g agarose (peqLab, Darmstadt, Germany) in 100 ml electrophoresis-buffer Tris-Borat-EDTA by boiling. The agarose solution into a gel tray with combs and left to solidify for 60 min. DNA samples were loaded on 1.2% agarose gels followed by gel electrophoresis (Sub-Cell GT system, BioRad, Feldkirchen, Germany) and detected with ethidium bromide (Sigma-Aldrich, St. Luis, USA).

Table 4 Primer sequences and product sizes for genotyping

Genotype	Primer sequence (s, sense; as, antisense)	Product [bp]
Arg1$^{f/f}$ (floxed allele)	s: TGC GAG TTC ATG ACT AAG GTT as: AAA GCT CAG GTG AAT CGG	Flox: ca. 300 WT: ca. 210
Tie2cre (transgene)	s: GCG GTC TGG CAG TAA AAA CTA TC as: GTG AAA CAG CAT TGC TGT CAC TT	ca. 100
Tie2cre (internal positive)	s: CTA GGC CAC AGA ATT GAA AGA TCT as: GTA GGT GGA AAT TCT AGC ATC ATC C	ca. 324

Table 5 PCR cycling conditions for genotyping

Genotype	Step	Temperature [°C]	Duration time [sec]	Number of Cycles
Arg1$^{f/f}$	Denaturation	94	10	1
	Amplification	94	40	35
		53	40	
		72	1	
	Cooling	72	5	1
		10	forever	
Tie2cre	Denaturation	94	3	1
	Amplification	94	30	35
		51,7	1	
		72	1	
	Cooling	72	2	
		10	forever	

2.13.2 RNA isolation from lung homogenates

For analysis of gene expression, lung tissue was homogenized in glass homogenization tubes with 1 ml Trifast reagent (PeqLab, Darmstadt, Germany) per 0.1 mg tissue by use of the PotterS tissue homogenizer (Glas-Col, Terre Haute, USA) and sterile PTFE plungers (RETTENBERG, Göttingen, Germany) (10 repeats, 4°C). Cells from pleural effusion were collected by placing a small incision and rinsing. Cells were pelleted by centrifugation and resuspended in 1 ml of Tri-fast reagent (PeqLab) and vortexed for approx. 10 seconds. The nucleoprotein complex was allowed to dissociate for 5 min at room temperature before storage of samples at -80°C until further use. For RNA isolation, samples were thawed on ice and centrifuged (12,000 × *g*, 10 min, 4°C) to remove insoluble material. Clear supernatants were collected in new 2 ml RNAse-free tubes, followed by addition of 200 µl Chloroform per 1 ml of Trifast reagent. Samples were mixed for 15 sec, incubated at room temperature for 5 min, and centrifuged again (12,000 × *g*, 5 min, 4°C) for phase separation. The upper aqueous phase was transferred to new 1.5 ml RNAse-free tubes followed by addition of 500 µl cold 100% isopropyl alcohol per 1 ml Trifast reagent. The samples were mixed followed by RNA precipitation on ice for 15 min and subsequent centrifugation (12,000 × *g*, 10 min, 4°C). The isopropyl alcohol was discarded and pellets were washed twice with 1 ml 75% ethanol (12,000 × *g*, 10 min, 4°C). After the final washing step, the RNA was allowed to air dry for approximately 5 min before they were dissolved in 50 – 100 µl *Aqua* B.

Braun (10 min, 55 – 60°C). RNA concentration and purity were measured by use of the Nanodrop1000 (Thermo Scientific) and determination of the 260/230 and 260/280 ratio for phenol and protein contamination, respectively. RNA samples were stored at -80°C until further use.

2.13.3 Reverse transcription

For reverse transcription of RNA into complementary DNA (cDNA), 1.5 µg RNA in 11.5 µl *Aqua* B. Braun were mixed with 1 µl hexamer primer solution (Fermentas, Burlington, Kanada) and incubated at 65°C for 5 min, followed by addition of 7.5 µl reverse transcription (RT) mix (LC®480 System; Fermentas, Burlington, Kanada). Samples were incubated according to the scheme outlined in Table 6.

Table 6 Reverse transcription

Step	Temperature [°C]	Duration time [min]
1	25°C	10 min
2	42°C	60 min
3	70°C	10 min

The cDNA tubes were transferred from 70°C to an ice bucket. Per tube, 5 µl samples were pooled in one 1.5 ml tube in order to generate a concentrated cDNA solution. The pooled cDNA mixture was used for generation of a dilution series for the gene expression standard curve. The remaining cDNA were diluted 1:10 in *Aqua* B. Braun. cDNA samples were stored at 4°C for use in gene expression analysis or at -20°C or at -80°C for long-term storage.

2.13.4 Gene expression analysis

Gene expression was measured and quantified using real-time quantitative PCR (RT-qPCR) and the LC480® II system, the system's own software LC480® software 1.5.0 SP3 (Roche), and the Universal Probe Library (UPL) system (all Roche, Basel, Switzerland). The standard curve for quantification of gene expression relative to housekeeping gene expression (Hypoxanthine-guanine phosphoribosyltransferase; HPRT) was generated based on concentrated, pooled cDNA from all samples as described in section 2.13.3. The standard curve consisted of a 1:2 dilution series ranging from undiluted to a dilution of 1:1024. RT-qPCR master mix without cDNA served as the negative control for contamination. For analysis of gene expression, 9 µl RT-qPCR master mix was combined with 1 µl cDNA. Reaction cycles of the RT-qPCR protocol applied for all genes universally are listed in Table 7. RT-qPCR-primer and -probe sequences are listed in Table 8. RT-qPCR results were quantified using the LightCycler-Software LCS480 1.5.0.39.

Table 7 RT-qPCR reaction cycles

Step	Temperature [°C]	Duration time [sec]	Number of Cycles
Denaturation	95	300	1
Amplification	95	10	50
	60	20	
	72	1	
Cooling	40	30	1

Table 8 RT-qPCR primer pairs and corresponding probe numbers

protein	encoding gene	primer pairs (s, sense; as, antisense)	probe number
Arg-1	*Arg1*	s: 5‘-CCT GGA ACT GAA AGG AAA G-3‘ as: 5‘-TTG GCA GAT ATG CAG GGA GT-3‘	2
Fizz-1	*Retnla*	s: 5‘-TAT GAA CAG ATG GGC CTC CT-3‘ as: 5‘-GGC AGT TGC AAG TAT CTC CAC-3‘	3
HPRT	*Hprt*	s: 5‘-TCC TCC TCA GAC CGC TTT T-3‘ as: 5’-CCT GGT TCA TCA TCG CTA ATC-3‘	95
IFN-γ	*Ifng*	s: 5‘-ATC TGG AGG AAC TGG CAA AA-3‘ as: 5‘-TTC AAG ACT TCA AAG AGT CTG AGG TA-3‘	21
IL-4	*Il4*	s: 5‘-CAT CGG CAT TTT GAA CGA G-3‘ as: 5‘-CGA GCT CAC TCT CTG TGG TG-3‘	2
IL-6	*Il6*	s: 5‘-GCT ACC AAA CTG GAT ATA ATC AGG A-3‘ as: 5‘-CCA GGT AGC TAT GGT ACT CCA-3‘	6
IL-12p40	*Il12b*	s: 5‘-ATC GTT TTG CTG GTG TCT CC-3‘ as: 5‘-GGA GTC CAG TCC ACC TCT ACA-3‘	78
IL-13	*Il13*	s: 5‘-CCT CTG ACC CTT AAG GAG CTT AT-3‘ as: 5‘-CGT TGC ACA GGG GAG TCT-3‘	17
LRG-47	*Lrg47*	s: 5‘-AAG GCC ACT AAC ATC GAA TCA-3‘ as: 5‘-TGC CTT ATC TCA CTT AAT ACT CCT-3‘	82
NOS2	*Nos2*	s: 5‘-CTT TGC CAC GGA CGA GAC-3‘ as: 5’-TCA TTG TAC TCT GAG GGC TGA C-3‘	13
TNF	*Tnf*	s: 5‘-TGC CTA TGT CTC AGC CTC TTC-3‘ as: 5’-GAG GCC ATT TGG GAA CTT CT-3‘	49
Ym-1	*Chil3*	s: 5’-GAA CAC TGA GCT AAA AAC TCT CCT G-3’ as: 5’-GAG ACC ATG GCA CTG AAC G-3’	88

2.14 Histopathological and Immunohistochemical Analysis

2.14.1 Formalin fixation and processing of organs

Organs were fixed in 4% formalin for 24 h followed by dehydration by means of an autotechnicon (Hypercenter XP, SHANDON, Pittsburgh, USA) and an ascending alcohol series (Table 9).

Table 9 Autotechnicon protocol: dehydration series

Dehydration step	Time [min]
4% formalin	60
70% alcohol	60
80% alcohol	60
90% alcohol	60
96% alcohol	60
abs. alcohol	60
abs. alcohol	60
abs. alcohol	60
Xylol	60
Xylol	60
Paraffin	90
Paraffin	90

Dehydrated tissue samples were then pre-incubated in paraffin at 65°C for 2 h and stored at 65°C before embedding in liquid paraffin by use of the Leica EG1140C paraffin embedding station (Leica, Nussloch, Germany). Hardened paraffin blocks were stored at 4°C until further use. For histological analyses, sections of 2 µm thickness were transferred into a cold water bath, and then placed into a 37°C water bath for removal of creases and straightening of sections before mounting onto SuperFrostPlus microscopy slides (Langenbrinck, Emmendingen, Germany). Slides were dried at 37°C overnight and stored at RT.

2.14.2 Histopathological stains

2.14.2.1 Hematoxylin and Eosin stain

Paraffin tissue sections were deparaffinized in three sequential Xylol (Carl Roth, Karlsruhe, Germany) cuvettes for 5 min each. Rehydration of sections was achieved in a descending alcohol series (Table 10) followed by incubation in *A. dest.* for 5 min.

Table 10 Hematoxylin and Eosin stain – rehydration in a descending alcohol series

Alcohol concentration [%]	Duration
Xylol/Ethanol (1:2, v/v)	1 min
100% Ethanol	2 x 5 min
100% Ethanol	Dipping
95% Ethanol	Dipping
80% Ethanol	Dipping
40% Ethanol	Dipping

Organ sections were stained with Gill's hematoxylin for 20 min. The slides were rinsed for 3 min in *A. dest.* and blueing-up was achieved under running tap water for 5 min. Organs were stained with 1% eosin (acidified) for 3 min. Slides were rinsed twice in *A. dest.* followed by dehydration in an ascending alcohol series (Table 11), clearing, and mounting with Entellan (Merck, Darmstadt, Germany).

Table 11 Hematoxylin and Eosin stain – final ascending alcohol series

Alcohol concentration [%]	Duration
Ethanol 70%	Dipping
Ethanol 96% I	Dipping
Ethanol 96% II	Dipping
Ethanol abs. I	Dipping
Ethanol abs. II	2 min
Xylol I	5 min
Xylol II	5 min
Xylol III	5 min

2.14.2.2 Azan trichrome stain for collagen

Organ sections were deparaffinized and rehydrated as described in section 2.14.2.1. Chromatin was stained for 1 h at 60°C in azocarmine solution, followed by 15 min of cooling down, and rinsing in *A. dest*. Sections were counter stained with aniline alcohol for 10 – 30 sec. Differentiation of nuclei was controlled by microscopy. The reaction was stopped by use of glacial acetic acid, followed by rinsing with *A. dest*. Sections were incubated for 3 h in 5% phosphortungstic acid. Collagen and connective tissue were stained in Anilineblau-Goldorange solution for 15 min and rinsed in *A. dest*. The sections were differentiated in 96% ethanol and dehydrated in an ascending alcohol series, treated with Xylol, and mounted with entellan.

2.14.3 Immunohistochemical stains

2.14.3.1 Arg-1 stain

Tissue sections were deparaffinized in Xylol for 10 min and rehydrated in a descending acetone series (Table 12), followed by rinsing in tap water and three sequential cuvettes of TBS.

Table 12 Arg-1 stain descending alcohol series

Ethanol concentration [%]	Duration
100%	10 min
70%	10 min
40%	10 min

Antigen retrieval was achieved by incubation in 1% SDS/TBS for 5 min at room temperature (RT). Slides were rinsed 3x in TBS followed by peroxidase blocking in 1% H_2O_2 for 20 min in the dark at RT. Then the slides were inserted into the Shandon humidity chamber (Sequenza™ Slide Rack and Coverplate™ system; Ted Pella Inc., California, USA) and rinsed 3x in TBS. The VECTOR avidin/biotin blocking kit (VECTOR, Burlingame, Canada) was used to block endogenous biotin. To this end, the tissue sections were incubated in Avidin D for 15 min in a wet chamber at RT to block avidin D binding sites, rinsed with TBS, and incubated in biotin for 15 min in a wet chamber at RT. Slides were rinsed 3x in TBS. The VECTOR mouse on mouse (M.O.M.) immunodetection kit (VECTOR, Burlingame, Canada) was used according to the manufacturer's instructions for blocking endogenous immunoglobulins. In brief, tissue sections were incubated in the immunoglobulin blocking solution for 1 h in the dark at RT, followed by rinsing in TBS. Slides were incubated in M.O.M. diluent in TBS for equilibration before incubation in mouse anti-mouse Arginase I (BD, Heidelberg, Germany) antibody (1:250 in M.O.M. diluent) over night at 4°C. The slides were rinsed 3x in TBS, followed by incubation in M.O.M. biotinylated anti-mouse IgG reagent for 10 min in a wet chamber at RT followed by rinsing 3x with TBS. Incubation in Vectastain ABC reagent (Vectastain Elite ABC-Peroxidase kit; VECTOR, Burlingame, Canada) for 10 min at RT was followed by rinsing 3x in TBS, before the slides were removed from the humidity chamber, and 3,3-diaminobenzidine (DAB) substrate (DAB peroxidase substrate kit; VECTOR, Burlingame, Canada) was applied. Development of stain intensity was controlled by microscopy and the reaction was stopped after 2 to 5 min with ddH2O. Gill's hematoxylin staining was performed for 5 min followed by blueing-up under running tap water, before mounting with Kaiser's glycerin (Merck, Darmstadt, Germany).

2.14.3.2 NOS2 stain

Tissue sections were deparaffinized and rehydrated as described in section 2.14.3.1. Antigen retrieval was achieved by boiling in citrate buffer for 45 min using the Retriever 2100 (Aptum Biologics Ltd., Southampton, UK). Tissue sections were washed 3x in TBS followed by peroxidase blocking (1% H2O2, 20 min, dark, RT). After this step, the slides were inserted into the Shandon humidity chamber. The slides were incubated in Avidin-Block for 30 min at RT before incubation with the primary antibody rabbit anti-NOS2 (Millipore, Massachusetts, USA) 1:800 in 3% BSA/TBS overnight in the dark at 4°C. Slides were then rinsed 3x in TBS to remove excess, unbound antibody followed by incubation in the secondary goat anti-rabbit antibody (Dianova, Hamburg, Germany) 1:200 in 3% BSA/TBS for 1 h min at RT in the dark. Slides were rinsed 3x in TBS, incubated in the Vectastain ABC reagent for 20 min at RT in the dark, and rinsed again 3x in TBS. After this step, the slides were removed from the humidity chamber, developed using DAB substrate, counter stained with hematoxylin, and mounted using Kaiser's glycerin as described in section 2.14.3.1.

2.14.4 Microscopic analysis

The Olympus BX41 light microscope (Olympus, Tokyo, Japan) with the software systems DS-Ri1 and NIS Elements D 3.1 (both Nikon, Melville, USA) were used for microscopy and photographic documentation.

2.15 Immunological Analyses

2.15.1 Determination of arginase activity in lung homogenates

Lung homogenates were thawed on ice and briefly vortexed. The debris was allowed to settle and 10 µl of lung homogenate were transferred into a new 1.5 ml tube. Lung homogenates were brought to a volume of 25 µl by addition of 15 µl *Aqua* B. Braun before addition of 25 µl lysis buffer. Arginase was activated for 7 min at 56°C. Then 50µl L-Arg solution (0.5 M) was added as substrate. The tubes were briefly vortexed followed by incubation at 37°C for 60 min to allow for L-Arg conversion into urea and L-ornithine. Then, 1:2 serial dilutions in *Aqua* B. Braun from 10 to 0.01 mg/ml urea were used as a standard for quantification of the urea concentration. The last tube contained no urea and served as a blank background control. The reaction was stopped by addition of 400 µl stopping solution directly followed by addition of 20 µl 6% α-isonitrosophenone per sample and standard. Samples and standard were incubated at 100°C for 30 min. For colorimetric determination of the urea concentration, 200 µl of samples and standard were transferred into a 96 F-well maxisorp plate (Nunc, Thermo Fisher Scientific) and analyzed at 550 nm by use of the Tecan microplate reader (Tecan, Männedorf, Switzerland).

2.15.2 Determination of arginase activity in BMDMs

Arginase activity was analyzed in lysates of IL-4 stimulated BMDMs from Tie2cre^{pos} Arg1$^{f/f}$ mice for retrospective exclusion of “leaky” mice that display arginase activity despite positive genotyping for the cre-transgene. To this end, 50 µl of lysates were transferred into a new 1.5 ml tube and incubated at 56°C for 7 min before addition of 50 µl L-Arg, mixing, and incubation at 37°C for 45 min to allow for conversion of L-Arg to urea and L-ornithine. A 1:2 serial dilution in *Aqua* B. Braun from 10 to 0.01 mg/ml urea was used as a standard for quantification of the urea concentration. The last tube contained no urea and served as a blank background control. The reaction was stopped and the urea concentration quantified as described in section 2.15.1.

2.16 Statistics

The software GraphPad Prism 8 was used for statistical analysis. The results were determined as significant at a level of $\alpha \leq 0.05$. Multiplicity adjustment was carried out using Bonferroni’s post hoc text.

3 Results

So far, there is no direct experimental proof that the degree of Arg-1 induction promotes susceptibility and pathology in TB *in vivo*. Different means were employed to stimulate arginase activity in Mtb infection experiments described in the following sections: Mtb co-infection with helminths known to promote Th2-responses and arginase activity in the lung (section 3.1), high-dose Mtb infection (section 0), virulent Mtb HN878 infection (section 3.3) and stimulation of arginase activity by use of the NOS2 inhibitor L-NIL (section 3.4).

3.1 Helminth-induced Arginase-1 does not affect susceptibility to Mtb infection in Balb/C and C57BL/6 wild-type mice

Arg-1 induction in helminth infection models can be short-term as for *N. brasiliensis* (Supplementary Figure 1) and *S. ratti* infection (Supplementary Figure 2), but can also persist for longer periods of time as can be observed during chronic *L. sigmodontis* infection (Supplementary Figure 3). In order to investigate the impact of helminth-induced Arg-1 on subsequent Mtb infection, co-infection experiments were conducted with acute and self-limited *N. brasiliensis* and *S. ratti* infections and with chronic *L. sigmodontis* infection. The evaluation of the impact of helminth-induced arginase activity on susceptibility to Mtb infection was based on the analyses of different disease criteria indicative of tuberculosis progression at experimental endpoints 3, 6, and 14 weeks post-infection with Mtb H37Rv. Parameters that were recorded included mycobacterial growth, gene expression of cytokines and other markers associated with the anti-tuberculosis immune response, the enzyme activity of Arg-1, and analysis of lung histopathology in co-infected mice compared to mice infected with Mtb alone.

3.1.1 Different types of helminth-infections promote Arg-1 induction in the lung

The evaluation of the impact of helminth-induced Arg-1 on susceptibility to Mtb infection relied on a timing of helminth infections prior to Mtb infection that allowed for Arg-1 to be present at the time of Mtb infection. This was critical especially for transient helminth infections during which the window of Arg-1 expression was expected not to persist for longer periods of time (116). In order to define the time window during which migrating larvae and/or adult helminths promote a Th2-milieu with induction of Arg-1 in the lung, WT mice were infected subcutaneously (s.c.) with 500 iL3 *N. brasiliensis,* or 2000 iL3 *S. ratti* into the scruff of the neck, or with *L. sigmodontis* via the natural route through exposure to arthropod vectors, i.e. infectious third-stage larvae (iL3)-transmitting *O. bacoti* mites. Then, lung tissue samples for gene expression analysis were taken at minimum three different time points post-infection specific to the individual helminth life-cycles. In *L. sigmodontis*-infected mice, gene expression analysis was not only performed on lung homogenates but also on cells from pleural wash because AAM are potently induced in the thoracic cavity where immature adult and mature adult *L. sigmodontis* life stages reside in close proximity to the lungs (121). Moreover, due to recent reports on the induction of mixed AAM/CAM populations in response to helminth infection (113,122), and because CAM-hallmark enzyme NOS2 is known to play an essential role in the control of Mtb infection (44), CAM induction was assessed

by determination of *Nos2* gene expression. *Arg1* and *Nos2* gene expression were recorded as positive (+) or negative (-) based on gene expression analysis by real-time quantitative PCR (RT-qPCR) in lung homogenates and (for *L. sigmodontis* only) in cells from pleural wash (Table 13). The data show that *Arg1* started to increase at day 7 post-infection in *N. brasiliensis*-infected C57BL/6 mice. Peak *Arg1* gene expression levels were reached at day 10 after which *Arg1* gene expression declined rapidly (Supplementary Figure 1). Consequently, co-infection with Mtb H37Rv was set at day 5 post-infection with *N. brasiliensis*, i.e. just before onset of *Arg1* induction in order to allow for the longest possible time window of *Arg1* expression in the lung at the time of Mtb infection, also considering the initial lag phase of Mtb after deposition of bacilli in the lung. In *S. ratti*-infected C57BL/6 mice, *Arg1* induction in the lung was recorded on days 7 and 10 post-infection. Median *Arg1* gene expression was similar on day 7 and 10, but a statistically significant difference was only observed at day 7 (Supplementary Figure 2). Co-infection with Mtb was set at day 3 post-infection with *S. ratti. Nos2* induction in the lung was not observed in response to *N. brasiliensis* infection or *S. ratti* infection. For *L. sigmodontis*, *Arg1* expression became detectable in the lung and in cells from thoracic cavity wash at approximately 30 days post-infection in Balb/C mice and remained high on day 60. Balb/C mice were co-infected with Mtb 30 days post-infection with *L. sigmodontis.* It should be noted that some *Nos2* gene expression was detected in cells from pleural wash of *L. sigmodontis* infected Balb/C mice at day 60 (Supplementary Figure 3).

Table 13 Helminth infections promote *Arg1* gene expression in the lungs of infected WT mice
Experimental mice were infected with 500 iL3 *N. brasiliensis*, or 2000 iL3 *S. ratti* s.c. into the scruff of the neck, or with a natural dose of *L. sigmodontis* by exposure to larvae-carrying *O. bacoti* mites. At the indicated time points, gene expression of *Arg1* and *Nos2* in lung homogenates was recorded as positive (+) or negative (-) based on gene expression analysis by real-time quantitative PCR (Supplementary Figure 1, Supplementary Figure 2, Supplementary Figure 3). For *L. sigmodontis*, the thoracic cavity of mice was rinsed and cell homogenates in addition to lung homogenates were submitted to gene expression analysis by real-time quantitative PCR for *Arg1* and *Nos2* genes (Supplementary Figure 3).

	Time post-infection [d]					
relative gene expression [1/*HPRT*]	0	3	7	10	14	21
***N. brasiliensis* in C57BL/6 mice (lung homogenate)**						
Arg1	-	-	+	+	-	-
Nos2	-	-	-	-	-	-
***S. ratti* in C57BL/6 mice (lung homogenate)**						
Arg1	-	-	+	+	-	
Nos2	-	-	-	-	-	

	0	14	30	60
***L. sigmodontis* (lung homogenate) in Balb/C mice**				
Arg1	-	-	+	+
Nos2	-	-	-	-
***L. sigmodontis* (pleural wash) in Balb/C mice**				
Arg1	-	-	+	+
Nos2	-	-	-	+

3.1.2 Helminth-induced Arg-1 and Mtb CFU counts in the lung

In the context of helminth-Mtb co-infection, helminth infection was timed as such that mycobacteria would encounter rising Arg-1 levels in the lungs of helminth-infected mice. Arginase activity in lung homogenates was confirmed by arginase assay at week 3, 6, and 14 post-infection with Mtb H37Rv. Bacterial loads in lung homogenates were assessed by determination of CFU counts at week 3, 6, and 14 post-infection with Mtb. WT mice were infected with 500 iL3 *N. brasiliensis*, or 2000 iL3 *S. ratti* s.c. into the scruff of the neck, or with *L. sigmodontis* via the natural route. Then helminth-infected mice and control mice were infected with 100 CFU Mtb H37Rv via the aerosol route (5 days, 3 days, or 30 days after *N. brasiliensis*, *S. ratti*, and *L. sigmodontis* infections, respectively). Arginase activity and corresponding CFU counts in co-infected mice are shown in Figure 3.

3.1.2.1 Arginase activity and pulmonary CFU counts in the lungs of N. brasiliensis-Mtb co-infected Balb/C and C57BL/6 WT mice

Both C57BL/6 mice and Balb/C mice were used in co-infection experiments with *N. brasiliensis* to account for potential later use in genetically modified mice that were available only on different genetic backgrounds. In both Balb/C and C57BL/6 mice arginase activity in the lungs of *N. brasiliensis*-infected mice (Figure 3A) was significantly higher at the time of Mtb infection than in control mice at the time of Mtb infection (wk 0). Within 3 weeks, arginase activity decreased to background levels in co-infected mice and Mtb-infected control mice. No significant differences in arginase activity were detectable between Balb/C and C57BL/6 mice. CFU counts in Balb/C and C57BL/6 mice co-infected with *N. brasiliensis* at week 3 were similar to that of control mice (Figure 3B). Mycobacterial growth plateaued after week 3 and stayed at similar levels between co-infected mice and control mice. At week 14, co-infected Balb/C mice showed higher mycobacterial loads in the lung than control Balb/C mice ($p \leq 0.05$). In contrast, co-infected C57BL/6 mice continued to show similar bacterial loads compared to control mice for the remainder of the experiment.

Comparing Balb/C and C57BL/6 mice, co-infected Balb/C mice developed transiently higher bacterial loads in the lung than co-infected C57BL/6 mice at week 6 post-infection with Mtb.

In Balb/C mice, the biological significance of the difference observed at week 14 remains unclear as it could not yet be assessed in a second independent experiment. Looking at the mean CFU levels recorded at earlier time points, this difference at week 14 seems to reflect natural variation between individual mice, given that CFU counts at earlier time points were slightly higher already. In C57BL/6 mice, mycobacterial growth appeared to be unaffected by co-infection with *N. brasiliensis* during the entire experiment.

The difference observed between co-infected Balb/C and co-infected C57BL/6 mice appeared to be transient and resolved after week 6. Also, statistical significance was achieved in only one out of two independent experiments using C57BL/6 mice. Overall, these data suggest that mycobacterial growth appeared to be unaffected by *N. brasiliensis*-induced arginase activity independently of the genetic background of experimental mice.

3.1.2.2 Arginase activity and pulmonary CFU counts in S. ratti-Mtb co-infected C57BL/6 mice

Co-infection experiments with *S. ratti* were conducted in C57BL/6 mice due to significantly lower susceptibility of Balb/C mice to *S. ratti* infection. No difference in arginase activity was detected between co-infected mice and control mice at any given time point (Figure 3C). However, aerosol infection was timed in line with Arg-1 detection in pre-experiments and was scheduled just before the onset of *Arg1* gene expression in response to *S. ratti* infection (Supplementary Figure 2). Because *Arg1* expression declined within 14 days after *S. ratti* infection, this window is not visible here as the next time point after Mtb infection was week 3. This translates into 24 days post *S. ratti* infection. Lung bacterial loads reached approximately 10^7 CFU in the lungs of C57BL/6 mice at week 3 and remained constant (Figure 3D). Overall, mycobacterial growth was not affected by *S. ratti*-induced arginase activity in co-infected mice.

3.1.2.3 Arginase activity and pulmonary CFU counts in L. sigmodontis-Mtb co-infected Balb/C mice

Co-infection experiments with *L. sigmodontis* employed Balb/C mice due to reduced susceptibility of C57BL/6 mice to *L. sigmodontis* infection. C57BL/6 mice generally do not develop patent infection. *L. sigmodontis*-infected Balb/C mice showed significantly increased arginase activity compared to uninfected control mice at the time of co-infection ($p \leq 0.05$) (Figure 3E). Arginase activity then increased with time in co-infected animals, peaked at week 6 ($p \leq 0.001$), and was maintained at this level until week 14. Arginase activity in Mtb-infected control mice remained at baseline levels. Despite substantial Arg-1 induction by *L. sigmodontis*, co-infected Balb/C mice reached similar levels of mycobacterial loads in the lung compared to control mice infected with Mtb alone (Figure 3F).

Overall, induction of arginase activity in response to helminth infection could be confirmed for *N. brasiliensis* and *L. sigmodontis* infection, but was likely missed for *S. ratti* infection during the longer time intervals between measurements in co-infection experiments than in pre-experiments. Whereas *N. brasiliensis* induced transient arginase activity at the time of Mtb infection which then declined again, *L. sigmodontis* infection led to continuous arginase activity over the course of the experiment. Despite differences in the degree of Arg-1 induction and its longevity across experiments with all three helminth-species, mycobacterial growth was not affected at the observed time points. The biological significance of occasionally detected statistical differences in *N. brasiliensis*-Mtb co-infection remains unclear due to minor levels of magnitude and limited reproducibility. Therefore, under the experimental circumstances tested, helminth-induced arginase activity did not seem to affect susceptibility to Mtb infection in terms of bacterial growth in the lungs of Balb/C and C57BL/6 mice.

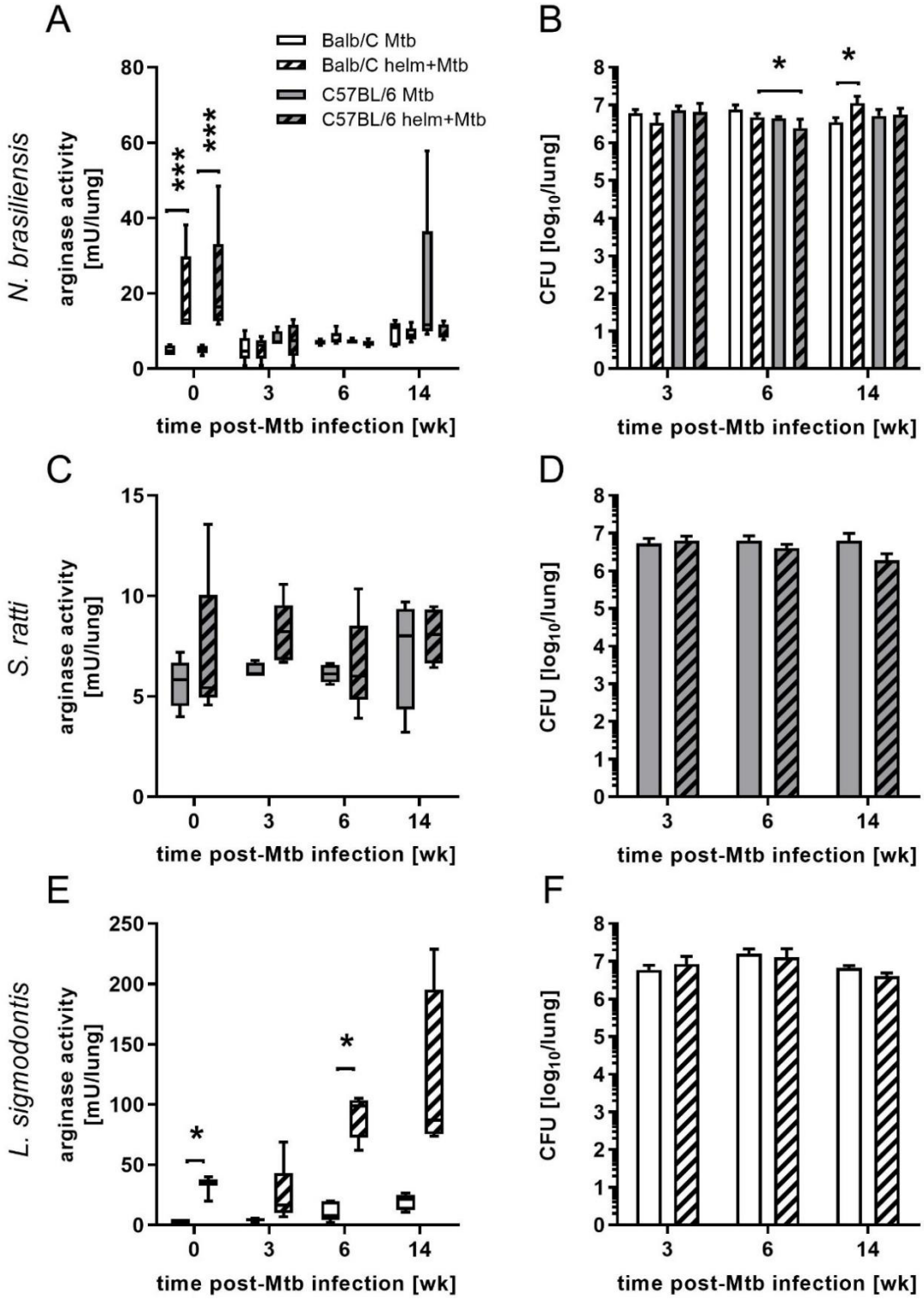

Figure 3 Arginase activity and mycobacterial loads in the lungs of helminth-Mtb co-infected Balb/C and C57BL/6 mice Balb/C and C57BL/6 mice were subcutaneously infected with (A-B) 500 iL3 *N. brasiliensis* or (C-D) 2000 iL3 *S. ratti* into the scruff of the neck, or (E-F) *L. sigmodontis* via the natural route 5 days, 3 days, and 30 days, resp., before infection with 100 CFU Mtb H37Rv via the aerosol route. Control mice were infected with Mtb alone. At the indicated time points, arginase activity (A, C, E) in lung homogenates was measured by L-Arg conversion into urea and quantified by spectrophotometric determination of the absorbance at 540 nm. Data represent the median, 25^{th}-75^{th} percentiles, and min. and max. values of 4-5 mice per group. Statistical analysis was performed using the Kruskal-Wallis test with Dunn's post-hoc test to define differences in arginase activity between Mtb-infected and co-infected mice, and between Balb/C and corresponding C57BL/6 groups as significant (*, p≤0.05; ***, p≤0.001). Bacterial burden (B, D, F) was assessed by determination of CFU in lung homogenates at the indicated time points. Data represent the mean+SD of five mice per group. Statistical analysis was performed using 2-way ANOVA with Bonferroni's *post-hoc* test to define differences in CFU counts between Mtb-infected and co-infected mice, and between Balb/C and corresponding C57BL/6 groups as significant (*, p≤0.05). For *N. brasiliensis* co-infection, the data shown is representative of two independent experiments; for Balb/C mice one experiment has been performed. For *S. ratti* co-infection, the data shown is representative of two independent experiments. For *L. sigmodontis* co-infection, one experiment has been performed.

In addition to arginase activity and CFU counts, parasite counts were determined to confirm successful helminth infection. Worm counts were determined for all three species. Additionally, microfilaraemia as a measure of patent *L. sigmodontis* infection is reported (Figure 4).

For *N. brasiliensis*, the time of Mtb infection corresponded to 5 days post-infection with *N. brasiliensis*, when L4 larvae reach the small intestine and mature into adults. Balb/C and C57BL/6 mice show similar intestinal parasite numbers at the day of Mtb infection (Figure 4A). Likewise, Balb/C and C57BL/6 mice cleared *N. brasiliensis* infection by week 3 post-infection with Mtb. Overall, *N. brasiliensis* elimination appeared to be similar between Balb/C and C57BL/6 mice at the time points observed.

Intestinal *S. ratti* parasite numbers at the time of Mtb aerosol infection correspond to 3 days post-infection with *S. ratti*. Peak adult *S. ratti* burden in the small intestine is usually reached by day 6 post-infection, but arriving larvae can be observed already. *S. ratti* infection was eliminated before week 3 post Mtb infection, similarly to *N. brasiliensis*, which is in line with the expected elimination time of 2-3 weeks for both helminths in respective mouth strains (Figure 4B).

L. sigmodontis adults were rinsed out of the pleural cavitiy and counted (Figure 4C). Additionally, *L. sigmodontis* microfilaremia (Figure 4D) was assessed to confirm patency. Though parasite numbers in the thoracic cavity decreased over time, patent infection was established as demonstrated by the occurrence of microfilaremia at week 6. Even at week 14 post-infection with Mtb, which corresponds to 18.5 weeks post-infection with *L. sigmodontis*, living adult parasites could still be found in one out of four Balb/C mice. Overall, *L. sigmodontis* infection progressed naturally according to its known life cycle. Of note, this conclusion is based on previous experience, accepting the limitation that no worm-only infected control group was available for comparison.

In conclusion, parasite burden of *N. brasiliensis*, *S. ratti*, and *L. sigmodontis* confirm successful helminth infection within a mostly normal range for the mouse strains tested. The lack of a worm-only infected control group remains a limitation of these co-infection experiments as it cannot be excluded that Mtb infection had some significance in the overall normal, but relatively low parasite burden.

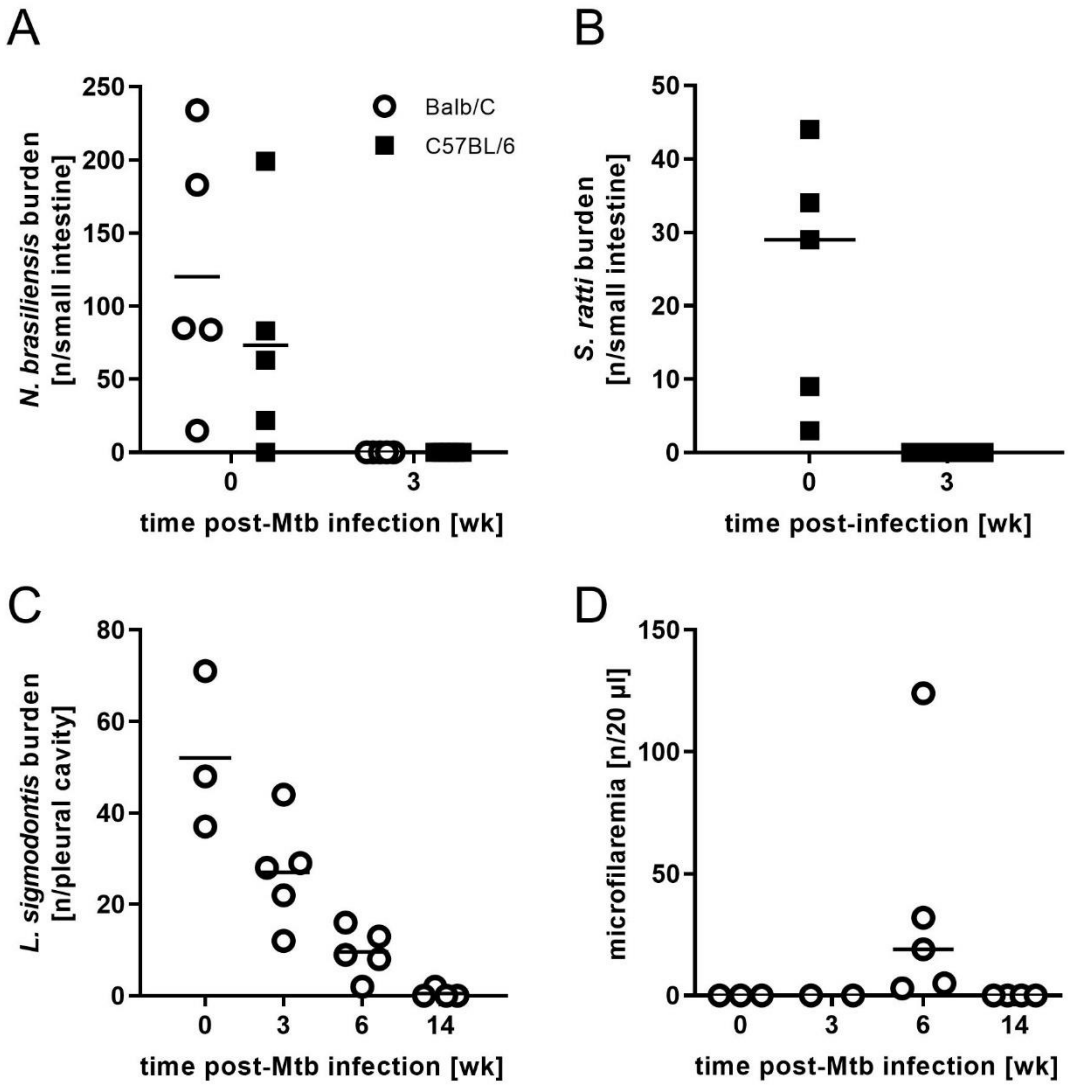

Figure 4 Parasite burden in co-infected Balb/C and C57BL/6 mice
Balb/C and C57BL/6 mice were subcutaneously infected with (A) 500 iL3 *N. brasiliensis* or (B) 2000 iL3 *S. ratti* into the scruff of the neck, or (C-D) *L. sigmodontis* via the natural route 5 days, 3 days, and 30 days, resp., before infection with 100 CFU Mtb H37Rv via the aerosol route. Control mice were infected with Mtb alone. At the indicated time points, *N. brasiliensis* and *S. ratti* were isolated from the small intestine, *L. sigmodontis* was isolated from the thoracic cavity, and *L. sigmodontis* microfilariae from the blood. Helminths were subjected to microscopic analysis and counted. Data represent the median of three to five mice per group. Microfilaremia of Balb/C mice was quantified by microscopic analysis of GV-stained blood samples and counting; group size n = 2-5. For *N. brasiliensis* co-infection, the data shown is representative of two independent experiments; for Balb/C mice one experiment has been performed. For *S. ratti* co-infection, the data shown is representative of two independent experiments. For *L. sigmodontis* co-infection, one experiment has been performed.

3.1.3 Gene expression of *Il13* and AAM-associated markers in the lungs of co-infected mice

In light of the surprising lack of impact of arginase activity on mycobacterial growth in the lung of co-infected mice, gene expression analysis in lung homogenates by real-time quantitative PCR was performed to obtain a picture of the Th2-milieu and alternative activation of macrophages. *Il13* was included as a marker for the Th2 response. Markers for alternative macrophage activation included *Arg1*, Found In Inflammatory Zone 1 (Fizz-1; encoding gene: *Retnla*), and the Chitinase-like 3 molecule Ym-1 (encoding gene: *Chil3*).

3.1.3.1 Il13 and AAM-associated markers during N. brasiliensis-Mtb co-infection

N. brasiliensis-infected Balb/C and C57BL/6 mice showed elevated gene expression of *Il13* at week 0 (Figure 5A). In line with IL-13-mediated induction of AAM, *Arg1*, *Retnla*, and *Chil3* levels (Figure 5B-D) followed this pattern in co-infected mice but not in control mice. Within 3 weeks post-Mtb infection, gene expression levels of *Il13*, *Arg1*, *Retnla*, and *Chil3* declined to background levels and remained comparable between co-infected and Mtb-infected animals for the remainder of the experiment. This was independent of the genetic background of experimental mice.

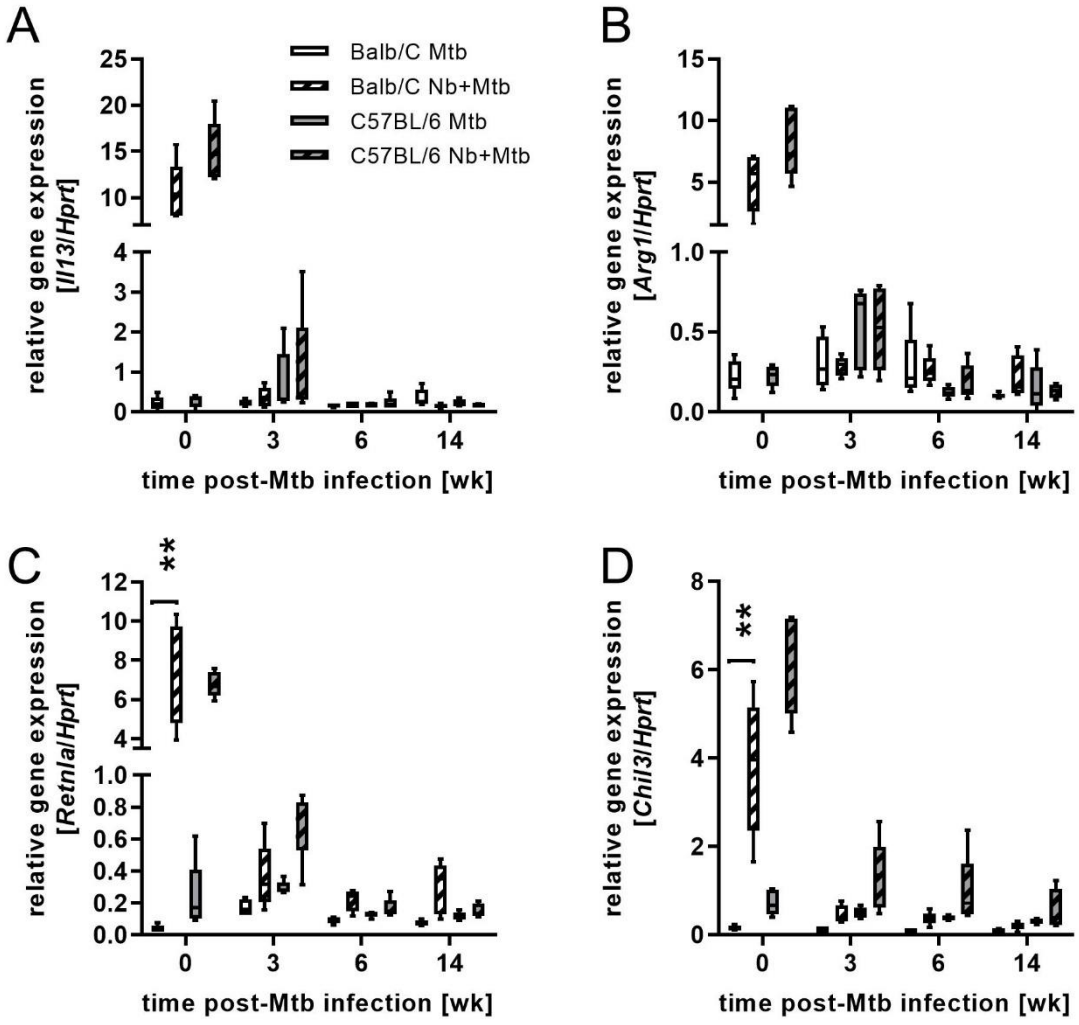

Figure 5 Relative gene expression of *Il13* and AAM-associated markers in the lungs of *N. brasiliensis*-Mtb co-infected Balb/C and C57BL/6 mice

Balb/C and C57BL/6 mice were subcutaneously infected with 500 iL3 *N. brasiliensis* (Nb) into the scruff of the neck 5 days before infection with 100 CFU Mtb H37Rv via the aerosol route. Control mice were infected with Mtb alone. At the indicated time points, RNA was isolated from lung homogenates and reversely transcribed into cDNA for gene expression analysis of (A) *Il13*, (B) *Arg1*, (C) *Retnla*, and (D) *Chil3* relative to *Hprt* housekeeping gene expression by real-time quantitative PCR. Data represent the median, 25th-75th percentiles, and min. and max. values of five mice per group. Statistical analysis was performed using the Kruskal-Wallis test with Dunn's post-hoc test to define differences between Mtb-infected and co-infected mice, and between Balb/C and corresponding C57BL/6 mice as significant (**, p≤0.01). For C57BL/6 mice, the data shown is representative of two independent experiments; for Balb/C mice one experiment has been performed.

3.1.3.2 Il13 and AAM-associated markers during S. ratti-Mtb co-infection

In C57BL/6 mice, gene expression of *Il13*, *Retnla*, and *Chil3*, but not *Arg1* was elevated in mice infected with *S. ratti* compared to control mice at the time of Mtb infection (*Il13*, *Retnla*, p≤0.01; *Chil3*, p≤0.01). A lack of statistically significant *Arg1* induction at the day of Mtb infection is not surprising, since co-infection was timed at just before the onset of *Arg1* gene expression (Supplementary Figure 2). At week 3, gene expression levels of *Il13*, *Arg1 Retnla*, and *Chil3* reached comparable levels between co-infected C57BL/6 mice and control mice. Although the spread of individual data points tended to be higher in co-infected C57BL/6 mice, the median relative gene expression of *Il13*, *Arg1*, *Retnla*, and *Chil3* remained similar to that of Mtb-infected controls until the end of the experiment.

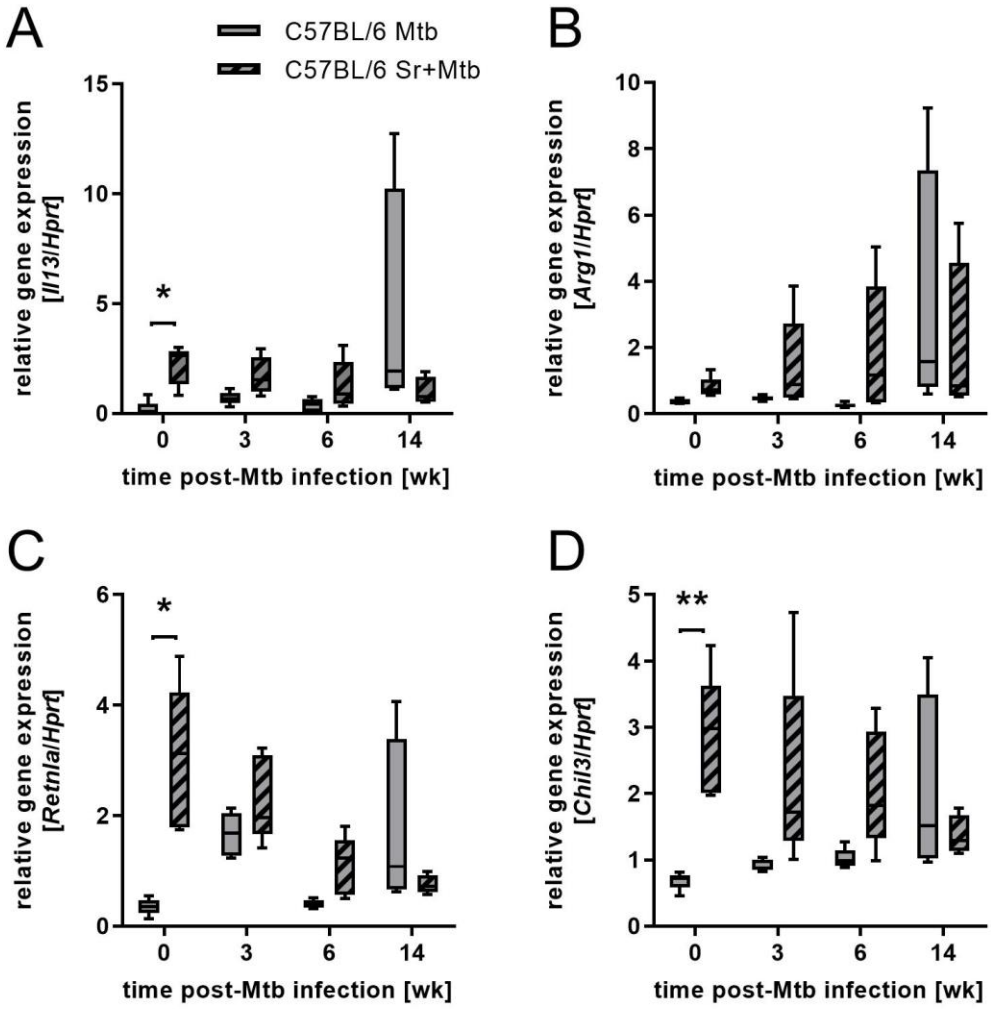

Figure 6 Relative gene expression of *Il13* and AAM-associated markers in the lungs of *S. ratti*-Mtb co-infected C57BL/6 mice

C57BL/6 mice were subcutaneously infected with 2000 iL3 *S. ratti* (Sr) into the scruff of the neck 3 days before infection with 100 CFU Mtb H37Rv via the aerosol route. Control mice were infected with Mtb alone. At the indicated time points, RNA was isolated from lung homogenates and reversely transcribed into cDNA for gene expression analysis of (A) *Il13*, (B) *Arg1*, (C) *Retnla*, and (D) *Chil3* relative to *Hprt* housekeeping gene expression by real-time quantitative PCR. Data represent the median, 25th-75th percentiles, and min. and max. values of four to five mice per group. Statistical analysis was performed using the Kruskal-Wallis test with Dunn's post-hoc test to define differences between Mtb-infected and co-infected mice as significant (*, p≤0.05; **, p≤0.01). The data shown is representative of two independent experiments.

3.1.3.3 Il13 and AAM-associated markers during L. sigmodontis-Mtb co-infection

L. sigmodontis-infected Balb/C mice showed elevated gene expression of *Il13*, *Retnla*, and *Chil3*, but not *Arg1* at the time of Mtb infection (Figure 7) compared to control mice ($p \leq 0.05$ and occasionally $p \leq 0.01$). *Il13* gene expression in co-infected mice but not Mtb-infected controls increased over time. Induction of *Arg1* gene expression was not yet detectable at the day of Mtb infection, not surprisingly since Mtb infection was timed before the onset of *Arg1* induction by *L. sigmodontis* (Supplementary Figure 3). *Arg1* gene expression increased over time, peaking at week 14 in co-infected Balb/C mice but not in control mice. *L. sigmodontis* appeared to induce AAM mainly in the thoracic cavity where adult parasites reside, whereas levels of gene expression induced in the lung are several orders of magnitude lower compared to expression levels in the thoracic cavity (Supplementary Figure 3). *Retnla* and *Chil3* (Figure 7C-D) gene expression levels were both significantly increased in co-infected mice compared to control mice at the time of Mtb infection (week 0). Gene expression levels in co-infected mice decreased again after week 0, but still showed higher gene expression levels by trend than control mice.

Considering *Il13* and AAM-associated markers across helminth co-infection experiments overall, *N. brasiliensis* and *S. ratti* infection caused a transient *Il13* induction resulting in alternative activation of macrophages in co-infected mice. *L. sigmodontis* infection induced *Il13* and AAM-associated markers during co-infection with Mtb in Balb/C mice. One mature, adult *L. sigmodontis* female can maintain considerable immunomodulatory effects (Haben, personal communication). Thus, continued increases in *Il13* and *Arg1* gene expression and maintenance of *Retnla* and *Chil3* levels do not necessarily contradict a decreasing parasite burden. Overall, the induction of different degrees of *Il13* with alternative activation of macrophages could be confirmed on the level of gene expression for all three helminth-species tested. Although *L. sigmodontis* infection led to significantly higher degrees of *Arg1* induction than *N. brasiliensis* or *S. ratti* and persisted for a longer amount of time, no effect on susceptibility to Mtb infection was noted.

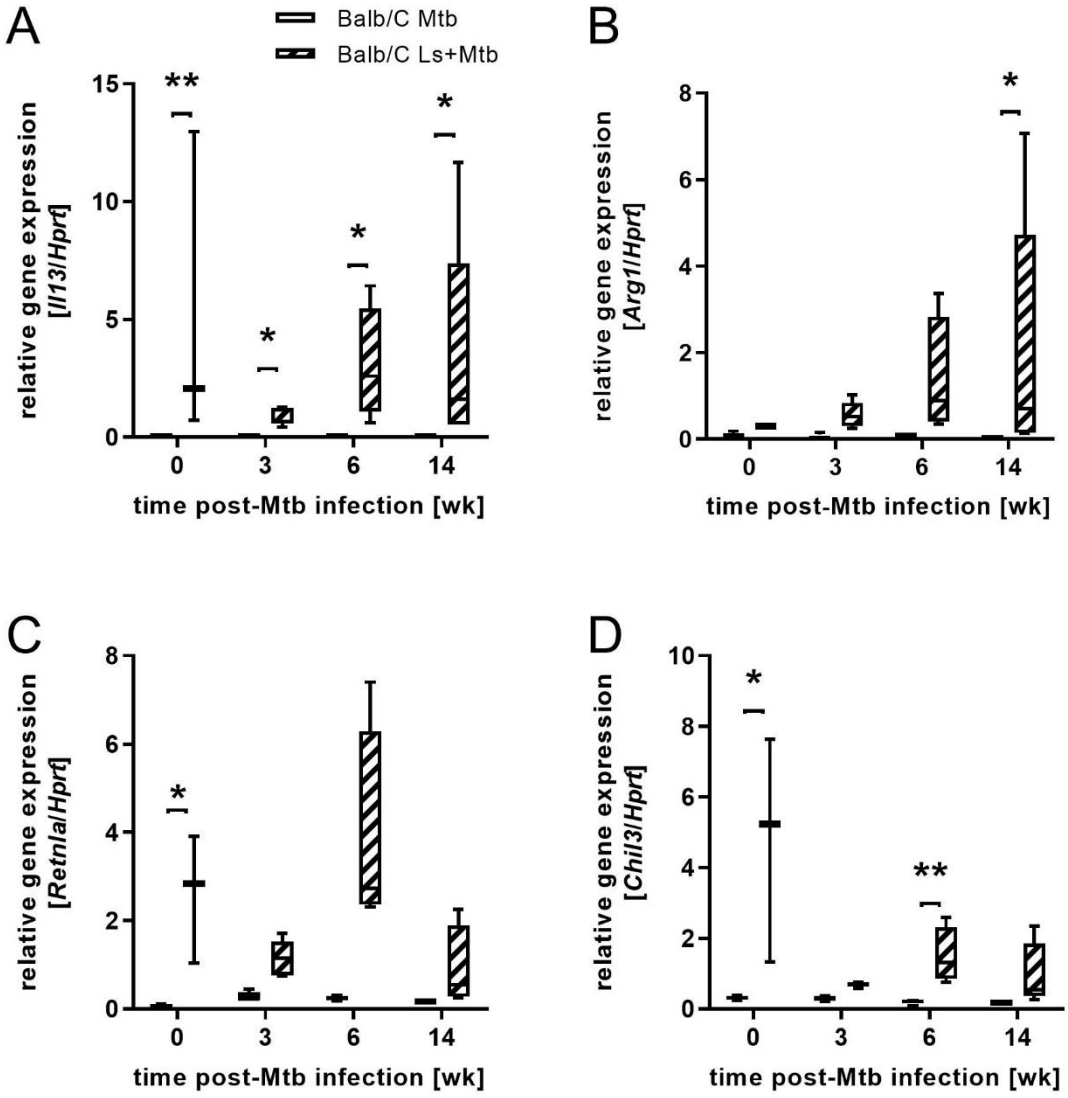

Figure 7 Relative gene expression of *Il13* and AAM-associated markers in the lungs of *L. sigmodontis*-Mtb co-infected Balb/C mice
Balb/C mice were infected with *L. sigmodontis* (Ls) via the natural route 30 days before infection with 100 CFU Mtb H37Rv via the aerosol route. Control mice were infected with Mtb alone. At the indicated time points, RNA was isolated from lung homogenates and reversely transcribed into cDNA for gene expression analysis of (A) *Il13*, (B) *Arg1*, (C) *Retnla*, and (D) *Chil3* relative to *Hprt* housekeeping gene expression by real-time quantitative PCR. Data represent the median, 25th-75th percentiles, and min. and max. values of three to five mice per group from one experiment. Statistical analysis was performed using the Kruskal-Wallis test with Dunn's post-hoc test to define differences between Mtb-infected and co-infected mice as significant (*, p≤0.05; **, p≤0.01).

3.1.4 Helminth-induced arginase activity does not affect gene expression of pro-inflammatory cytokines and CAM-associated markers during co-infection

Gene expression indicative of protective Th1- and Th17-responses and induction of CAM-associated markers was addressed as these play central roles in the control of Mtb infection. Gene expression was analyzed by real-time quantitative PCR.

3.1.4.1 Gene expression during N. brasiliensis-Mtb co-infection

In *N. brasiliensis*-Mtb co-infected Balb/C mice, gene expression of *Ifng*, *Il12b*, *Tnf*, *Il17a*, *Nos2* and *Lrg47* was similar between *N. brasiliensis*-infected mice and controls at the time of Mtb infection (week 0)

(Figure 8). Increasing gene expression levels of pro-inflammatory cytokines and CAM-associated markers were detectable at week 3 in both groups. Despite not achieving statistical significance, gene expression levels in co-infected Balb/C mice seemed to increase more slowly than those of control mice, though this tendency resolved after week 3 for all markers tested. Likewise, gene expression of pro-inflammatory cytokines and CAM-associated markers was similar between co-infected and control C57BL/6 mice at the time of aerosol infection. Gene expression levels were increased at week 3 and remained similar between both groups until the end of the experiment. Transiently higher gene expression of *Ifng* and *Il12b* was observed in co-infected C57BL/6 mice compared to co-infected Balb/C mice at week 3 ($p \leq 0.05$). In contrast to co-infected Balb/C mice, cytokine and CAM-induction appears not to be delayed in co-infected C57BL/6 mice. In light of no visible change in CFU counts between co-infected mice and control mice, this delay appears not to be biologically relevant.

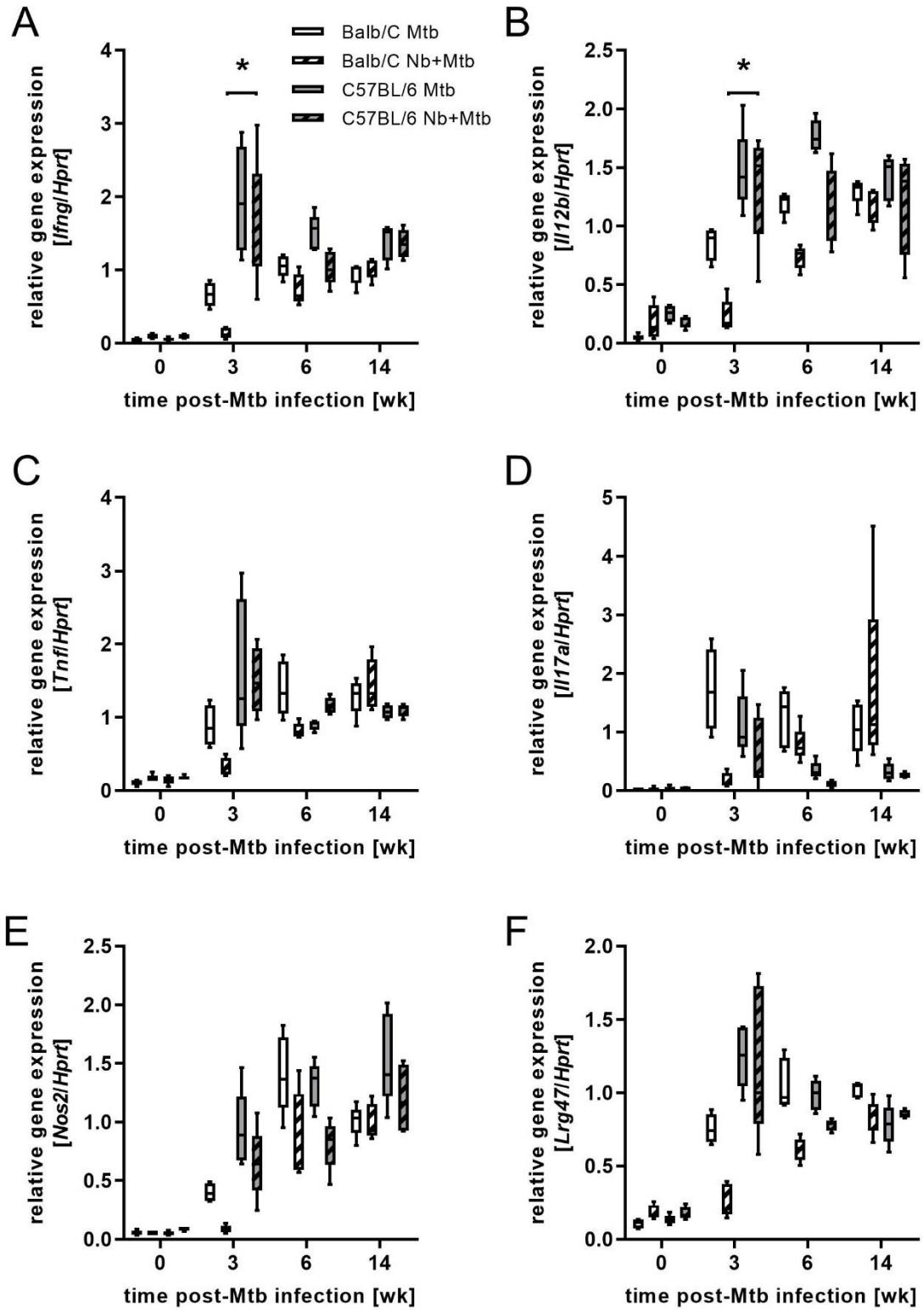

Figure 8 Gene expression of pro-inflammatory cytokines and CAM-associated markers in the lungs of *N. brasiliensis*-Mtb co-infected Balb/C and C57BL/6 mice

Balb/C and C57BL/6 mice were subcutaneously infected with 500 iL3 *N. brasiliensis* (Nb) into the scruff of the neck 5 days before infection with 100 CFU Mtb H37Rv via the aerosol route. Control mice were infected with Mtb alone. At the indicated time points, RNA was isolated from lung homogenates and reversely transcribed into cDNA for gene expression analysis of (A) *Ifng*, (B) *Il12b*, (C) *Tnf*, (D) *Il17a, (E) Nos2,* and (F) *Lrg47* relative to *Hprt* housekeeping gene expression by real-time quantitative PCR. Data represent the median, 25th-75th percentiles, and min. and max. values of five mice per group. Statistical analysis was performed using the Kruskal-Wallis test with Dunn's post-hoc test to define differences between Mtb-infected and co-infected mice, and between Balb/C and corresponding C57BL/6 mice as significant (*, p≤0.05). For C57BL/6 mice, the data shown is representative of two independent experiments; for Balb/C mice, one experiment has been performed.

3.1.4.2 Gene expression during S. ratti-Mtb co-infection

In the lungs of *S. ratti*-Mtb-infected C57BL/6 mice, gene expression of pro-inflammatory cytokines and CAM-associated markers started to increase at week 3 post-infection (Figure 9). Gene expression levels of *Ifng*, *Il12b*, *Tnf*, and *Il17a* were similar between co-infected mice and Mtb-infected control mice except for *Il17a* expression at week 14, although not statistically significant. In line with *Ifng*- and *Tnf*-levels, no differences could be observed for the down-stream induction of *Nos2* nor *Lrg47* gene expression between co-infected and Mtb-infected C57BL/6 mice.

3.1.4.3 Gene expression during L. sigmodontis-Mtb co-infection

In both Balb/C mice and C57BL/6 mice, gene expression of pro-inflammatory cytokines and CAM-associated markers (Figure 10) was similar between *L. sigmodontis*-infected mice and control mice at the time of Mtb infection. At week 3 post-infection with Mtb, gene expression of *Ifng*, *Il12b*, *Tnf*, and *Il17a* (Figure 10A-D) increased in both co-infected mice and control mice and plateaued. Following the pattern of gene expression levels of *Ifng* and *Tnf*, differences could not be observed for inducible CAM-associated markers *Nos2* or *Lrg47* either (Figure 10E-F). Overall, no significant differences could be observed between co-infected Balb/C mice and Mtb-infected controls.

Overall, gene expression of pro-inflammatory cytokines and CAM-associated markers was detectable in co-infected mice and Mtb-infected controls. Though *N. brasiliensis* infection appeared to slow this induction down initially in Balb/C mice, but not C57BL/6 mice, gene expression levels reached and maintained similar levels during the chronic phase of Mtb infection in mice co-infected with *N. brasiliensis* compared to control mice. Similarly, co-infection with *S. ratti* or *L. sigmodontis* did not seem to affect gene expression of pro-inflammatory cytokines and CAM-associated markers compared to infection with Mtb alone either. This was observed independently of the genetic background of experimental mice. These findings may explain the lack of influence of helminth infection on mycobacterial growth. Helminth-induced arginase activity appeared not to affect gene expression of markers of the protective anti-Mtb immune response or classical activation of macrophages in the lung of Balb/C and C57BL/6 mice to an extent that would thwart control of mycobacterial growth in the lung significantly.

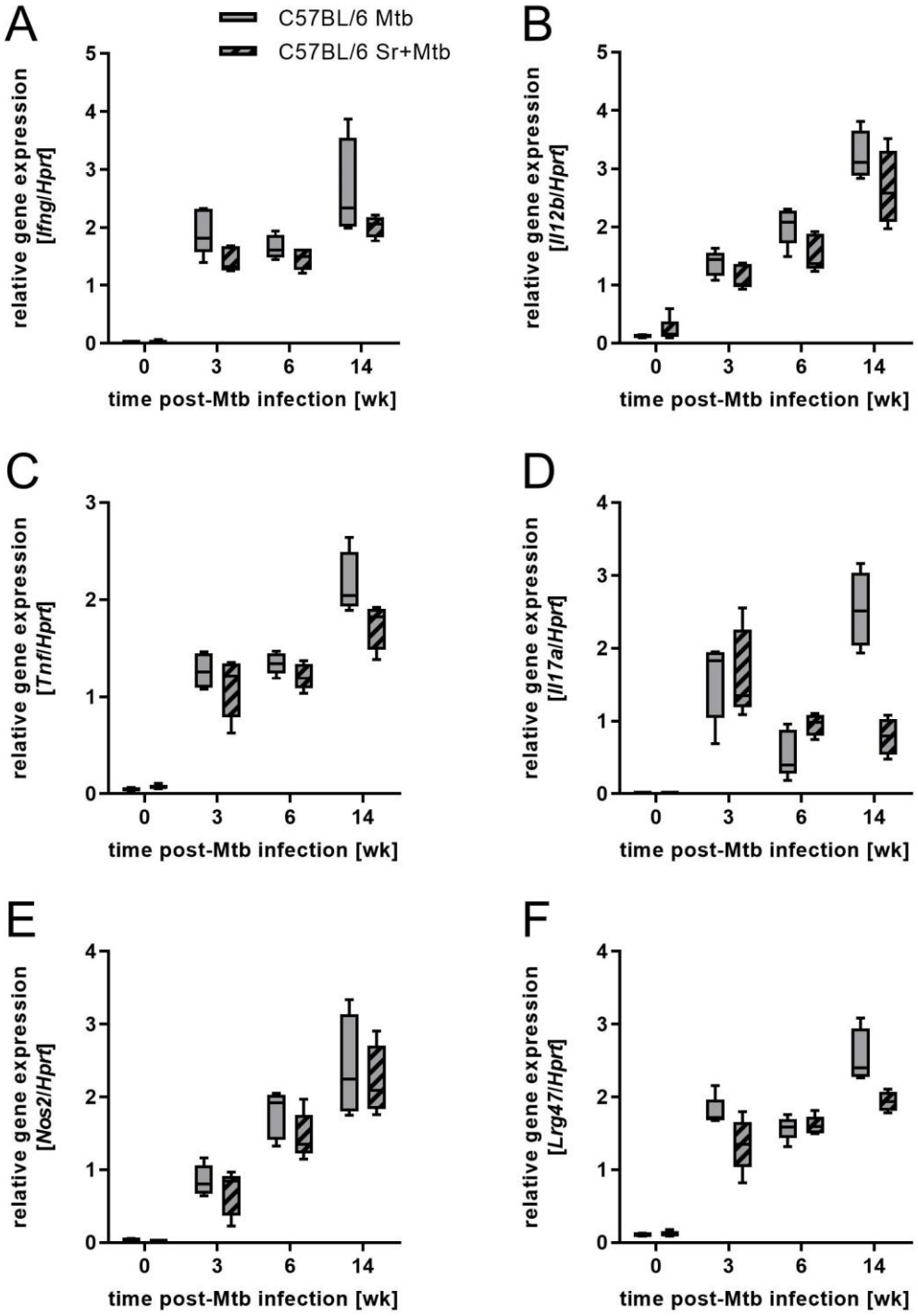

Figure 9 Gene expression of pro-inflammatory cytokines and CAM-associated markers in the lungs of *S. ratti*-Mtb co-infected C57BL/6 mice

C57BL/6 mice were subcutaneously infected with 2000 iL3 *S. ratti* (Sr) into the scruff of the neck 3 days before infection with 100 CFU Mtb H37Rv via the aerosol route. Control mice were infected with Mtb alone. At the indicated time points, RNA was isolated from lung homogenates and reversely transcribed into cDNA for gene expression analysis of (A) *Ifng*, (B) *Il12b*, (C) *Tnf*, (D) *Il17a*, (E) *Nos2*, and (F) *Lrg47* relative to *Hprt* housekeeping gene expression by real-time quantitative PCR. Data represent the median, 25th-75th percentiles, and min. and max. values of five mice per group. The data shown is representative of two independent experiments.

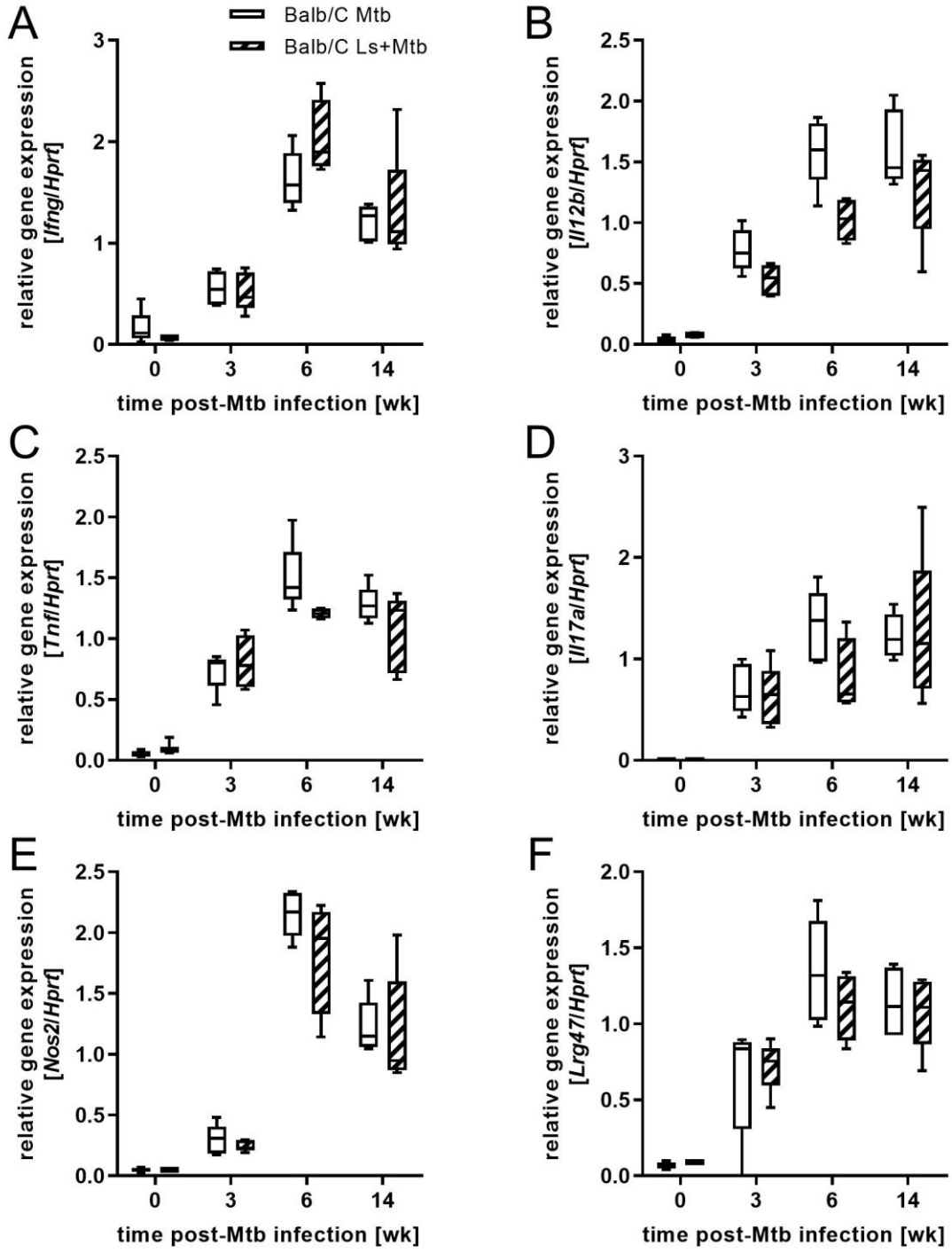

Figure 10 Gene expression of pro-inflammatory cytokines and CAMϕ-associated markers of *L. sigmodontis*-Mtb co-infected Balb/C and C57BL/6 mice

Balb/C mice were infected with *L. sigmodontis* (Ls) via the natural route 30 days before infection with 100 CFU Mtb H37Rv via the aerosol route. Control mice were infected with Mtb alone. At the indicated time points, RNA was isolated from lung homogenates and reversely transcribed into cDNA for gene expression analysis of (A) *Ifng*, (B) *Il12b*, (C) *Tnf*, (D) *Il17a*, (E) *Nos2* and (F) *Lrg47* relative to *Hprt* housekeeping gene expression by real-time quantitative PCR. Statistical analysis was performed using the Kruskal-Wallis test with Dunn's post-hoc test to define differences between Mtb-infected and co-infected mice as significant.

3.1.5 The granulomatous response in the lung appears to be unaffected by co-infection with helminths and Mtb

Helminth larvae passing through the lungs of infected animals can induce inflammation and tissue damage (116). Consequently, incoming mycobacteria encounter a different pathology in helminth-infected mice compared to the healthy lung tissue encountered in control mice. This might affect the development of pulmonary histopathology. Therefore, to investigate the granulomatous response to Mtb infection in the context of co-infection with helminths, lung histopathology was assessed by hematoxylin and eosin staining.

3.1.5.1 Lung hematoxylin and eosin staining in N. brasiliensis-Mtb co-infected Balb/C and C57BL/6 mice

At the time of Mtb infection (week 0), *N. brasiliensis*-infected Balb/C and C57BL/6 mice showed inflammation and destruction of alveolar structure in the lung caused by larval migration through the tissue. In contrast, control mice showed intact lung architecture without pathological findings (Figure 11A-D). In both Balb/C and C57BL/6 mice, early granulomatous lesions were visible at week 3 in co-infected mice and Mtb-infected mice (Figure 11E-H). At week 6 (Figure 11I-L) and week 14 (Figure 11M-P), these lesions seemed to gradually increase in size in a similar fashion in both co-infected mice and Mtb-infected mice. No major differences were visible between co-infected mice and Mtb-infected controls.

3.1.5.2 Lung hematoxylin and eosin staining in L. sigmodontis-Mtb co-infected Balb/C mice

At the day of Mtb infection (week 0), *L. sigmodontis*-infected Balb/C mice showed a normal lung architecture, which was comparable to that of control mice (Figure 12A-B). Predominantly cellular granulomatous lesions developed at week 3 (Figure 12E-F) post-infection with Mtb regardless of ongoing *L. sigmodontis* infection. Inflammation and cellular infiltration led to gradually increased lesion size at week 6 (Figure 12I-J) and week 14 (Figure 12M-N) post-infection with Mtb. Co-infected C57BL/6 mice showed a similar lung histopathology as control mice (Figure 12C-D). Granulomatous lesions could be observed at week 3 (Figure 12G-H) and were characterized by gradually increasing cellular infiltration and inflammation at week 6 (Figure 12K-L) and week 14 (Figure 12O-P). Differences in lesion structure or progression could not be observed between co-infected mice and mice infected with Mtb alone.

3.1.5.3 Lung hematoxylin and eosin staining in S. ratti-Mtb co-infected C57BL/6 mice

S. ratti-infected C57BL/6 mice showed inflammation and cellular infiltration at the time of aerosol infection (week 0) (Figure 12C-D), the characteristic response in order to contain migrating *S. ratti* larvae. In contrast, control mice showed intact lung tissue without pathological findings at the time of Mtb infection. Granulomatous lesions can be found by week 3 in co-infected mice and control mice infected with Mtb alone (Figure 12G-H). Over time, gradually increasing inflammation and extending cellular infiltration were observed which is overall similar to *N. brasiliensis* co-infection.

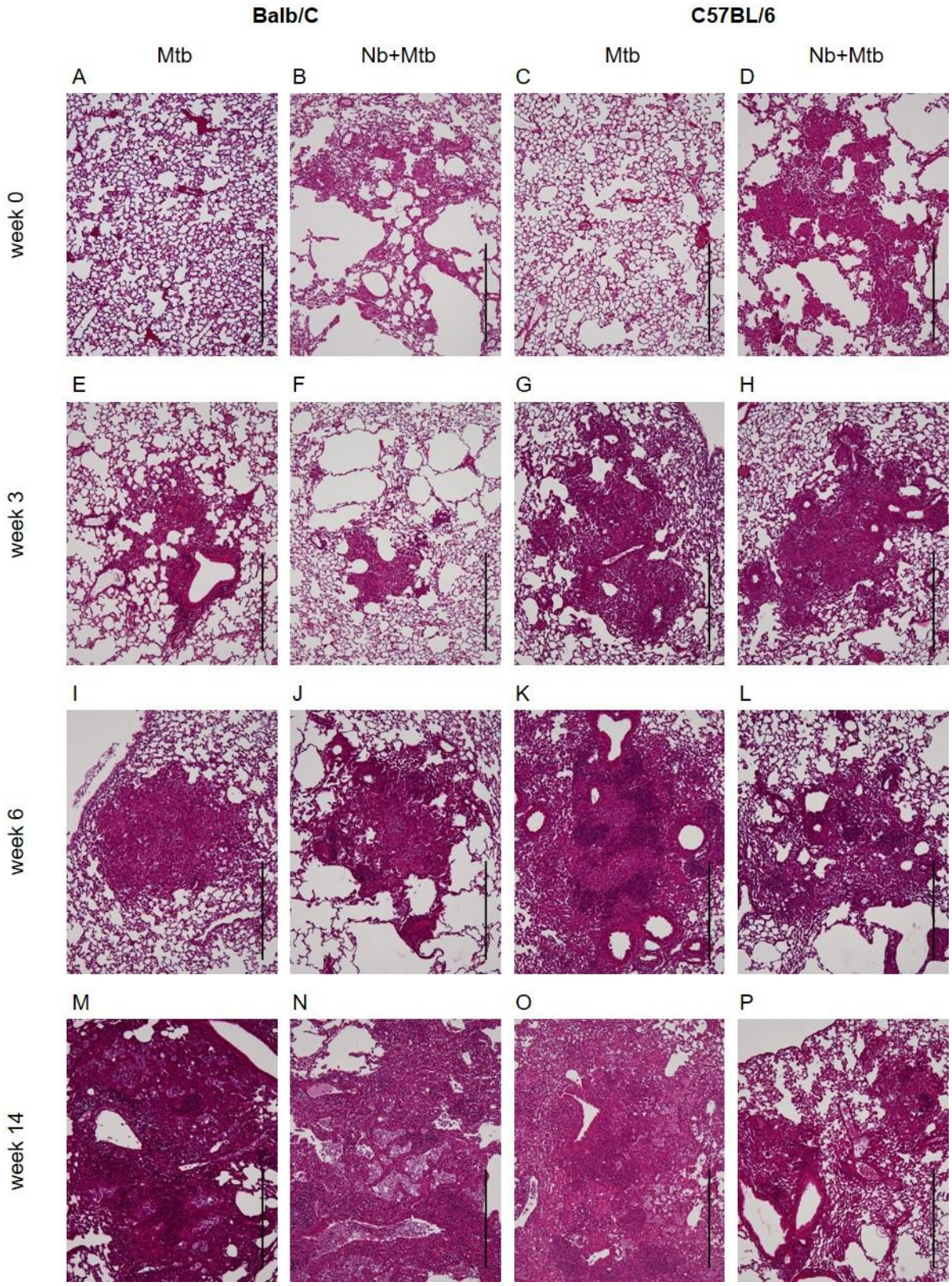

Figure 11 Lung tissue hematoxylin and eosin staining of *N. brasiliensis*-Mtb co-infected Balb/C and C57BL/6 mice
Balb/C and C57BL/6 mice were subcutaneously infected with 500 iL3 *N. brasiliensis* (Nb) into the scruff of the neck 5 days before infection with 100 CFU Mtb H37Rv via the aerosol route. Control mice were infected with Mtb alone. Sections from formalin-fixed paraffin-embedded lungs taken at (A-D) week 0, (E-H) week 3, (I-L) week 6, and (M-P) week 14 post-infection with Mtb were stained with hematoxylin and eosin staining, followed by microscopic analysis. Representative microphotograph of one out of five mice per group; scale bars: 500 µm. For C57BL/6 mice, the data shown is representative of two independent experiments; for Balb/C mice one experiment has been performed.

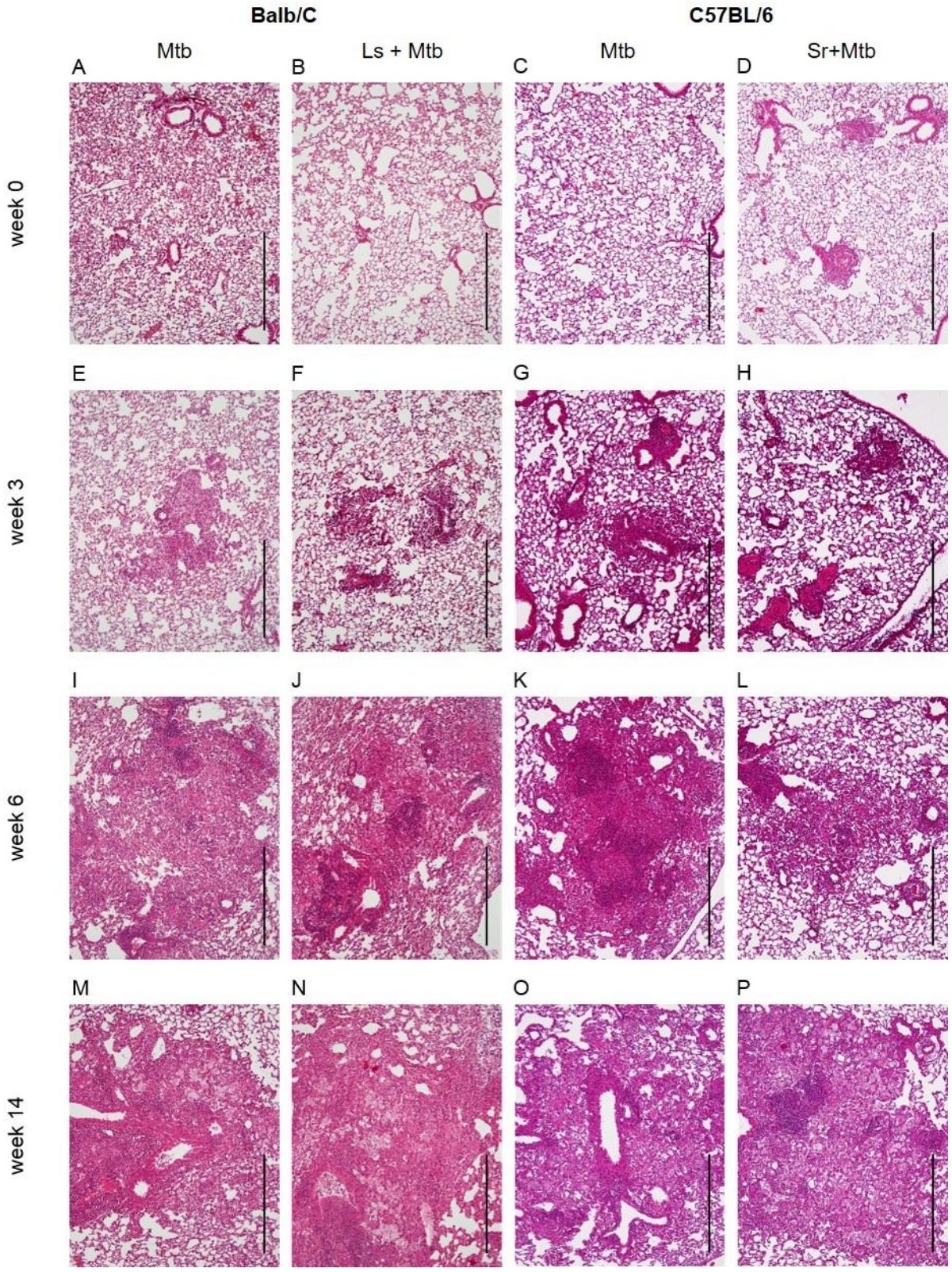

Figure 12 Lung tissue hematoxylin and eosin staining of *L. sigmodontis*- or *S. ratti*-Mtb co-infected Balb/C or C57BL/6 mice

(A-B, E-F, I-J, M-N) Balb/C mice were infected with *L. sigmodontis* (Ls) via the natural route 30 days before infection with 100 CFU Mtb H37Rv via the aerosol route and control mice were infected with Mtb alone. (C-D, G-H, K-L, O-P) C57BL/6 mice were subcutaneously infected with 2000 iL3 *S. ratti* (Sr) into the scruff of the neck 3 days before infection with 100 CFU Mtb H37Rv via the aerosol route. Control mice were infected with Mtb alone. Sections from formalin-fixed paraffin-embedded lungs were taken at (A-D) week 0, (E-H) week 3, (I-L) week 6, and (M-P) week 14 post-infection with Mtb followed by hematoxylin and eosin staining and microscopic analysis. Representative microphotograph of one out of three to five mice per group; scale bars: 500 µm. For *L. sigmodontis* co-infection, one experiment was performed; for *S. ratti* co-infection, the data shown is representative of two independent experiments.

Overall, helminth co-infection caused alveolar lung damage and inflammation in the lung at the time of Mtb infection. Predominantly cellular granulomatous lesions develop over time that were characterized by amorphous masses of infiltrating immune cells and gradually increasing size over time. Lesion development appeared to progress similarly in co-infected mice regardless of helminth species involved or mouse genetic background under the experimental circumstances tested. While there seems to be no obvious difference in histopathology based on lung hematoxylin and eosin staining, single frames do stand out (Figure 11K+P or Figure 12L). However, this needs to be interpreted with caution, as the data have not yet been substantiated by histological quantification of serial sections and it may not be excluded that sections were obtained from different planar levels of granulomatous lesions. Regardless, an absence of histopathological differences would be in line with the similarities in bacterial burden and gene expression data observed between co-infected mice and control mice and appears plausible overall. Across Mtb co-infection experiments with *N. brasiliensis*, *S. ratti*, and *L. sigmodontis*, the evidence suggests that co-infection with helminths and the concomitantly induced AAM induction and associated arginase activity did not affect susceptibility to Mtb infection of Balb/C and C57BL/6 mice in terms of bacterial growth, gene expression of Th1-, Th17- and CAM-associated markers or histopathology.

3.2 Mtb-induced Arg-1 during low- and high-dose infection of Tie2cre^{pos} Arg1$^{f/f}$ and Tie2cre^{neg} Arg1$^{f/f}$ mice

Some *in vitro* evidence suggests the existence of a Th2-independent pathway to induce Arg-1 in mycobacteria-infected macrophages independently of type 2 cytokine signaling via the Il-4Rα chain as a means to thwart intracellular control of Mtb (109). In contrast, hardly any Arg-1 induction in response to low-dose Mtb H37Rv infection could be observed for WT Balb/C and C57BL/6 mice infected with Mtb alone in the present thesis. In addition to these discrepancies between *in vitro* and *in vivo* observations, *in vitro* evidence from our lab suggests that the degree of Arg-1 induction in response to Mtb may be a function of the infectious dose of Mtb (Hölscher, unpublished). Also, it cannot be excluded that effects of Arg-1 were masked by other immunomodulatory effects of helminth-infection. In order to shed further light on the role of macrophage Arg-1 as a susceptibility factor in experimental tuberculosis, a set of experiments was designed employing low-dose and high-dose infection in the Tie2cre^{pos} Arg1$^{f/f}$ mouse model, which lacks Arg-1 specifically in macrophages. Low-dose infection was defined as aerosol infection with 100 CFU Mtb H37Rv. High-dose infection was defined as an infectious dose of 2200 CFU Mtb H37Rv. The impact of macrophage-specific Arg-1 deficiency on the susceptibility to Mtb infection was evaluated based on the analysis of mycobacterial growth, arginase activity, gene expression analysis of cytokine profiles, and lung histopathology.

3.2.1 Tie2cre^{pos} Arg1$^{f/f}$ mice and Tie2cre^{neg} Arg1$^{f/f}$ mice show similar bacterial loads in the lung during low-dose Mtb infection

Tie2cre^{neg} Arg1$^{f/f}$ and Tie2cre^{pos} Arg1$^{f/f}$ mice were infected with 100 CFU Mtb via the aerosol route, a dose that is considered to be “natural”. Tie2cre^{pos} Arg1$^{f/f}$ and competent littermates did not show

significantly induced *Arg1* gene expression, although competent mice showed wider spread of data overall (Figure 13A). Two and 4 weeks post-infection, enzyme activity in lung homogenates of Tie2cre^{pos} Arg1$^{f/f}$ mice remained at baseline levels, whereas some induction of arginase activity could be observed in Arg-1-competent littermates ($p \leq 0.05$) (Figure 13B). The magnitude of this induction was considerably lower than seen in helminth-induced arginase activity (section 3.1.1 and 3.1.2) and was transient. The absence of *Arg1* gene expression and arginase activity in Tie2cre^{pos} Arg1$^{f/f}$ mice was confirmed.

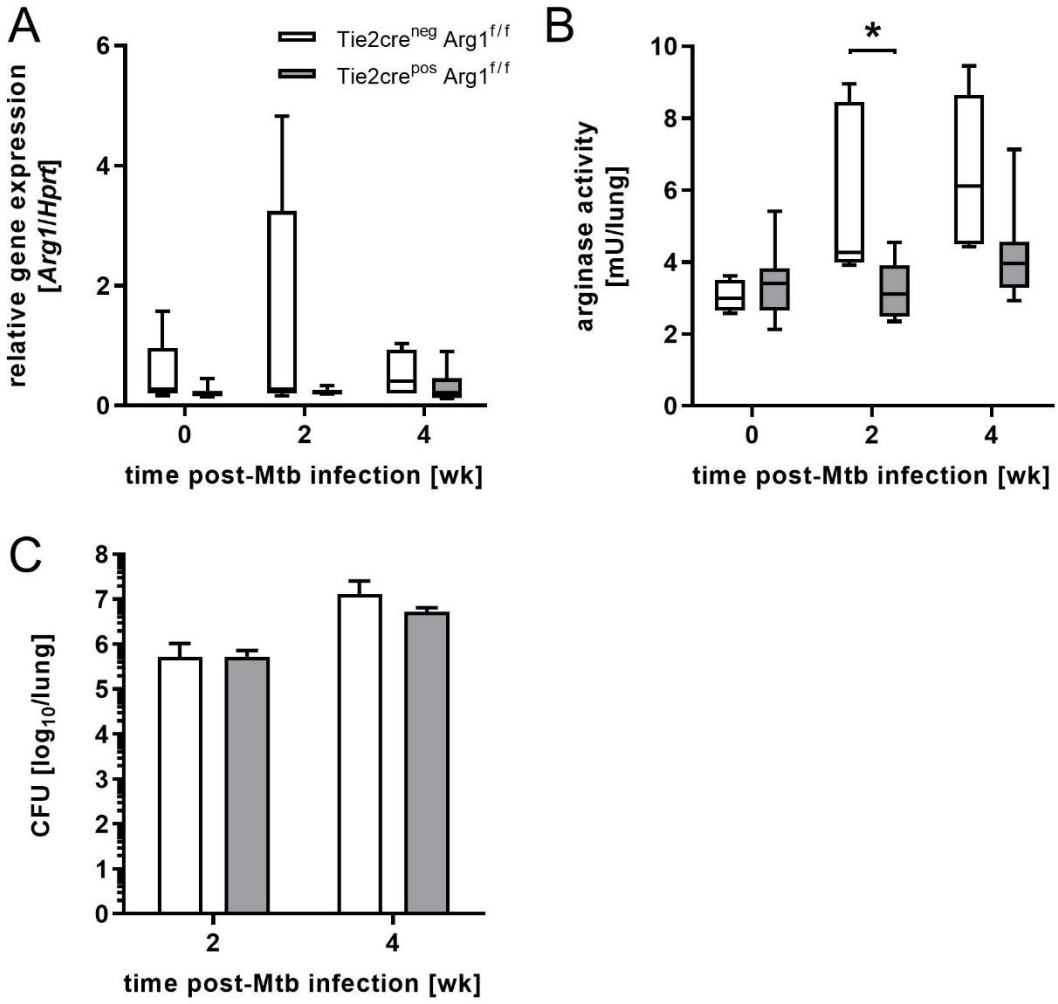

Figure 13 *Arg1* gene expression, arginase activity, and CFU counts in the lungs of low-dose Mtb-infected Tie2cre^{neg} Arg1$^{f/f}$ and Tie2cre^{pos} Arg1$^{f/f}$ mice
Tie2cre^{neg} Arg1$^{f/f}$ and Tie2cre^{pos} Arg1$^{f/f}$ mice were infected with 100 CFU Mtb H37Rv via the aerosol route. At the indicated time points, (A) RNA was isolated from lung homogenates and reversely transcribed into cDNA for gene expression analysis of *Arg1* relative to *Hprt* housekeeping gene expression by real-time quantitative PCR. (B) Arginase activity in lung homogenates was measured by L-arg conversion into urea and quantified by spectrophotometric determination of the absorbance at 540 nm. Data represent the median, 25th-75th percentiles, and min. and max. values of four to seven mice per group. Statistical analysis was performed using the Kruskal-Wallis test with Dunn's post-hoc test to define differences between Tie2cre^{neg} Arg1$^{f/f}$ and Tie2cre^{pos} Arg1$^{f/f}$ mice as significant (*, $p \leq 0.05$). (C) Bacterial loads in lung homogenates were assessed by determination of CFU counts via colony enumeration methods. Data represent the mean+SD of five to seven mice per group.

Low dose infection led to similar bacterial growth in the lungs of Tie2cre^{pos} Arg1$^{f/f}$ mice and competent littermates (Figure 13C). Bacterial loads in the lung reached approximately 10^6 CFU/lung by week 2 post-infection. At week 4 post-infection, lung bacterial loads of both groups increased to approximately 10^7 CFU/lung. Despite Arg-1 deficiency in macrophages, no significant effect on CFU could be detected after low-dose infection with Mtb H37Rv. The transient induction of Arg-1 in lung homogenates of

Tie2cre^{neg} Arg1$^{f/f}$ mice did not appear to be of biological relevance to mycobacterial growth. Hence, macrophage Arg-1 appeared not to influence the susceptibility to tuberculosis in terms of mycobacterial growth after a low dose of infection that is considered to be “natural”.

3.2.2 Tie2cre^{pos} Arg1$^{f/f}$ mice show lower bacterial loads in the lung than Tie2cre^{neg} Arg1$^{f/f}$ mice during high-dose Mtb infection

Tie2cre^{pos} Arg1$^{f/f}$ mice lacking Arg-1 in macrophages and Arg-1-competent Tie2cre^{neg} Arg1$^{f/f}$ littermates were infected with a dose of 2200 CFU Mtb H37Rv via the aerosol route. In order to confirm the absence of Arg-1 in Tie2cre^{pos} Arg1$^{f/f}$ mice compared to littermates during high-dose Mtb infection, *Arg1* gene expression in lung homogenates was determined by real-time quantitative PCR. Arginase activity in lung homogenates was measured by L-Arginine (L-Arg) conversion into urea with subsequent determination of absorbance. During high-dose infection with Mtb, *Arg1* gene expression (Figure 14A) remained at baseline levels in both Tie2cre^{pos} Arg1$^{f/f}$ mice and Arg-1-competent littermates until week 3 post-infection. At week 4, *Arg1* gene expression was significantly increased in competent mice, but remained low in Tie2cre^{pos} Arg1$^{f/f}$ mice ($p \leq 0.05$). Arginase activity in competent mice and mice lacking macrophage Arg-1 remained low until week 3 post-infection (Figure 14B). At week 4, arginase activity increased in competent mice, but remained low in Tie2cre^{pos} Arg1$^{f/f}$ mice ($p \leq 0.05$). Arginase activity in response to high-dose infection was approximately ten-fold higher than the transient induction observed during low-dose infection (Figure 13B), confirming that the degree of Arg-1 induction may be a function of the infectious dose. Next, bacterial load was quantified by determination of CFU counts in the lungs of infected animals in order to assess the effect of Arg-1 deficiency in macrophages on the growth of Mtb (Figure 14C). In high-dose infected Tie2cre^{pos} Arg1$^{f/f}$ mice and competent littermates, mycobacterial loads in the lung reached a mean CFU of approximately 10^8 CFU/lung at week 3 post-infection. At week 4, bacterial loads in the lungs of Tie2cre^{pos} Arg1$^{f/f}$ mice remained constant, whereas CFU counts in Tie2cre^{neg} Arg1$^{f/f}$ mice increased by approximately 1 log unit ($p \leq 0.01$). Arg-1 deficiency in macrophages corresponded to lower bacterial loads in the lungs of Tie2cre^{pos} Arg1$^{f/f}$ mice compared to Arg-1-competent littermates during high-dose infection. Therefore, a lack of Arg-1 in macrophages seems to be protective during high-dose infection with Mtb H37Rv.

Overall, while macrophage-specific Arg-1 deficiency appeared irrelevant to mycobacterial growth during low-dose infection with Mtb, a protective effect in terms of lower CFU counts in the lung was conferred to Tie2cre^{pos} Arg-1$^{f/f}$ mice during high-dose infection. Also, the degree of Arg-1 induction appeared to depend on the infectious dose of Mtb.

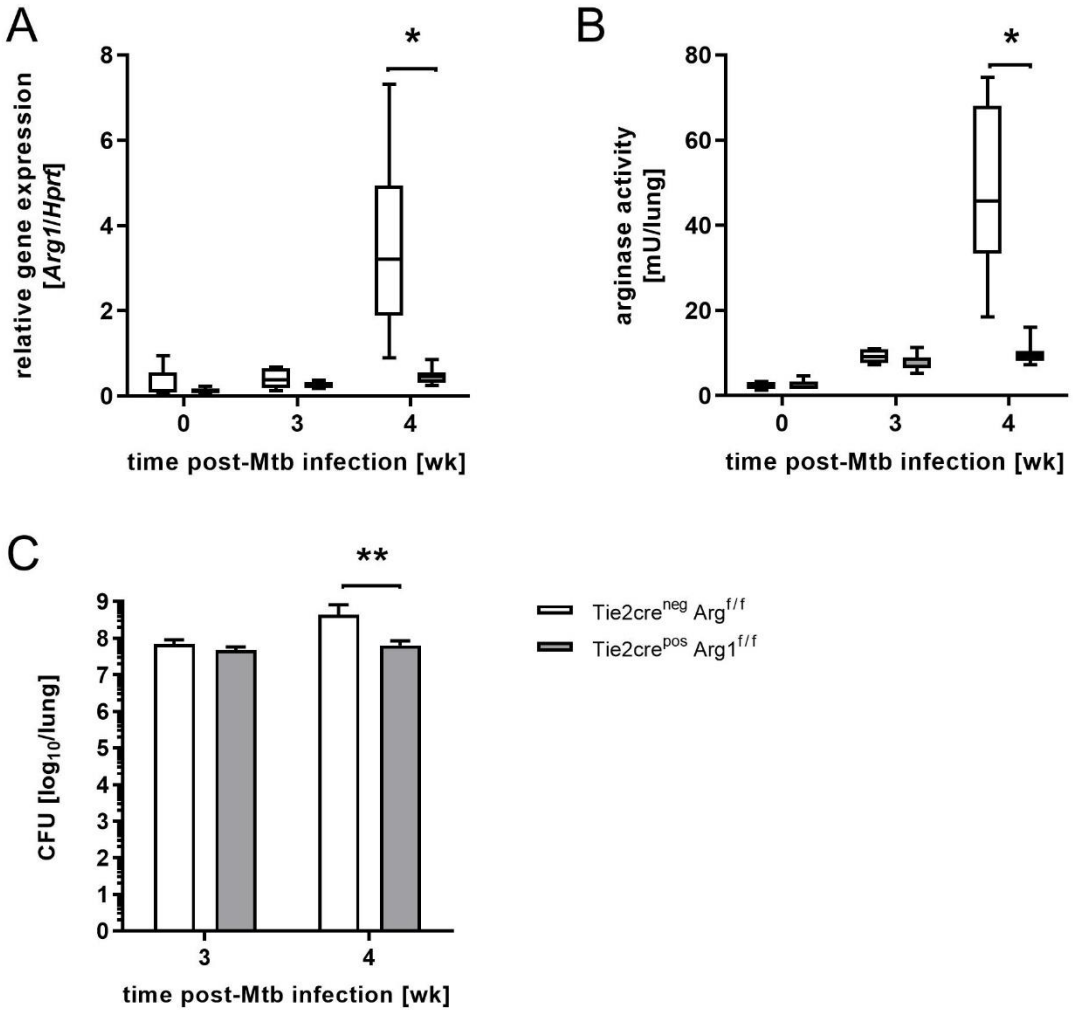

Figure 14 *Arg1* gene expression, arginase activity, and mycobacterial load in the lungs of high-dose Mtb-infected Tie2cre^{neg} Arg1$^{f/f}$ and Tie2cre^{pos} Arg1$^{f/f}$ mice
Tie2cre^{neg} Arg1$^{f/f}$ and Tie2cre^{pos} Arg1$^{f/f}$ mice were infected with 2200 CFU Mtb H37Rv via the aerosol route. At the indicated time points, (A) RNA was isolated from lung homogenates and reversely transcribed into cDNA for gene expression analysis of *Arg1* relative to *Hprt* housekeeping gene expression by real-time quantitative PCR. (B) Arginase activity in lung homogenates was measured by L-Arg conversion into urea and quantified by spectrophotometric determination of the absorbance at 540 nm. Data represent the median, 25th-75th percentiles, and min. and max. values of five to fourteen mice per group. Statistical analysis was performed using the Kruskal-Wallis test with Dunn's post-hoc test to define differences between Tie2cre^{neg} Arg1$^{f/f}$ and Tie2cre^{pos} Arg1$^{f/f}$ mice as significant (*, p≤0.05). The data shown is representative of two independent experiments. (C) At the indicated time points, bacterial loads in lung homogenates were assessed by determination of CFU. Data represent the mean+SD of four to fourteen mice per group. Statistical analysis was performed by two-way ANOVA with Bonferroni's post-hoc test to define differences between Tie2cre^{neg} Arg1$^{f/f}$ and Tie2cre^{pos} Arg1$^{f/f}$ mice as significant (**, p≤0.01). The data shown is representative of two independent experiments.

3.2.3 Macrophage-specific Arg-1 deficiency protects body weight and ameliorates disease severity during high-dose Mtb infection

Development of disease signs following infection with 2200 CFU Mtb was monitored by measuring body weight change and quantification of disease severity by assignment of disease scores (Figure 15). Body weight and disease severity started to change after week 3 post-infection. Tie2cre^{pos} Arg1$^{f/f}$ mice showed improved body weight conservation in contrast to Arg-1-competent littermates at week 4 after high-dose infection with Mtb H37Rv (p≤0.01) (Figure 15A). In line with body weight preservation, Tie2cre^{pos} Arg1$^{f/f}$

mice developed generally lower disease scores than Tie2cre^{neg} Arg1$^{f/f}$ mice (p≤0.01) (Figure 15B). Ultimately, increased disease severity in Tie2cre^{neg} Arg1$^{f/f}$ mice dictated termination of the experiment according to humane endpoint criteria at the end of week 4 post-infection. Overall, Arg-1 appeared to contribute to the development of pathology after infection with high-dose Mtb H37Rv. Consistent with the lower bacterial loads observed in Tie2cre^{pos} Arg1$^{f/f}$ animals (Figure 14), Arg-1 deficiency in macrophages seemed to ameliorate disease severity in line with improved preservation of body weight.

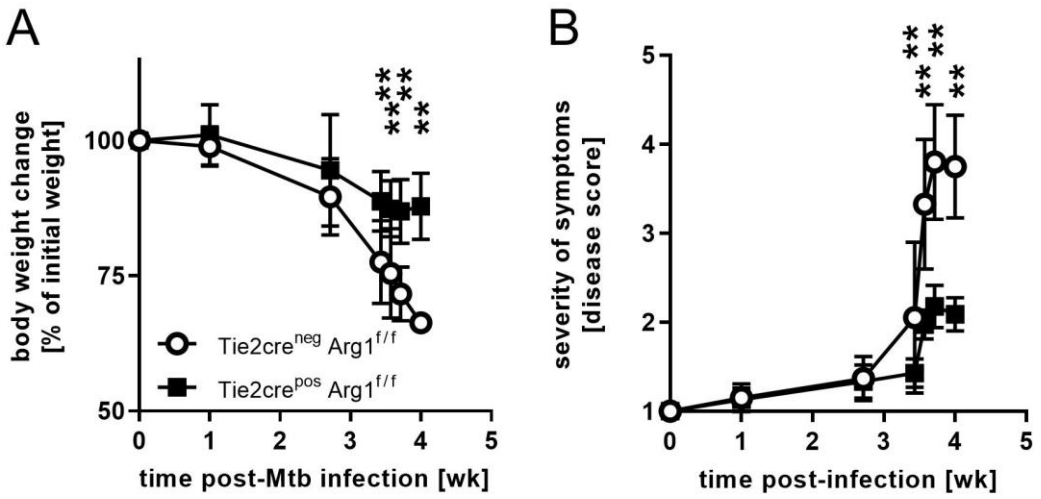

Figure 15 Body weight change and severity of symptoms of high-dose Mtb-infected Tie2cre^{neg} Arg1$^{f/f}$ and Tie2cre^{pos} Arg1$^{f/f}$ mice
Tie2cre^{neg} Arg1$^{f/f}$ and Tie2cre^{pos} Arg1$^{f/f}$ mice were infected with 2200 CFU Mtb *via* the aerosol route. At the indicated time points, (A) mice were weighed to monitor body weight change and (B) development of disease symptoms was scored according to severity. Data represent the mean±SD of four to fifteen mice per group. Statistical analysis was performed by two-way ANOVA with Bonferroni's post-hoc test to define differences between Tie2cre^{neg} Arg1$^{f/f}$ and Tie2cre^{pos} Arg1$^{f/f}$ mice as significant (**, p≤0.01). The data shown is representative of two independent experiments.

3.2.4 Gene expression of *Il6* and *Il12b* are affected by Arg-1 deficiency during high-dose Mtb infection

To assess whether Arg-1 deficiency influenced gene expression of pro-inflammatory cytokines and CAM-associated markers that characterize the anti-Mtb immune response, gene expression analysis in lung homogenates was performed by real-time quantitative PCR for high-dose infected Tie2cre^{neg} Arg1$^{f/f}$ and Tie2cre^{pos} Arg1$^{f/f}$ mice (Figure 16). IL-6 appears to be able to induce Arg-1 in macrophages independently of the IL-4Rα-chain *in vitro* (109). Therefore, *Il6* gene expression analysis was conducted. Initially, *Il6* gene expression was comparable between Tie2cre^{pos} Arg1$^{f/f}$ mice and Arg-1-competent littermates at week 0 and remained similar until week 3 post-infection (Figure 16A). At week 4, *Il6* gene expression was still at baseline level in Tie2cre^{pos} Arg1$^{f/f}$ mice whereas Arg-1-competent littermates developed significantly higher *Il6* gene expression levels (p≤0.05). *Ifng* gene expression levels were induced at week 3 post-infection and remained constant until week 4. No differences could be observed between Tie2cre^{pos} Arg1$^{f/f}$ mice and Arg-1-competent littermates (Figure 16B). Gene expression of *Il12b* was elevated at week 3 and comparable between Tie2cre^{pos} Arg1$^{f/f}$ mice and Arg-1-competent littermates. However, while *Il12b* gene expression levels decreased again in lung homogenates of

Tie2cre^{neg} Arg1$^{f/f}$ mice, they remained elevated in Tie2cre^{pos} Arg1$^{f/f}$ mice at week 4 ($p \leq 0.05$) (Figure 16C). At the same time, gene expression of *Tnf*, *Il17a*, and *Nos2* (Figure 16D-F) was elevated at week 3 and maintained until week 4 without observable differences between Tie2cre^{pos} Arg1$^{f/f}$ mice and competent littermates during the entire experiment and in line with *Ifng* gene expression.

Overall, no differences in gene expression of pro-inflammatory cytokines and *Nos2* could be observed during high-dose infection with Mtb H37Rv. In contrast, gene expression of *Il6* and *Il12b* seemed affected by macrophage Arg-1 deficiency during high-dose Mtb infection of Tie2cre^{neg} Arg1$^{f/f}$ and Tie2cre^{pos} Arg1$^{f/f}$ mice. *Il6* gene expression might be responsible for the elevated *Arg1* gene expression observed in Tie2cre^{neg} Arg1$^{f/f}$ mice. Decreased *Il12b* gene expression levels in Tie2cre^{pos} Arg1$^{f/f}$ mice may affect the recruitment of immune cells, thereby contributing to differential control of mycobacterial growth.

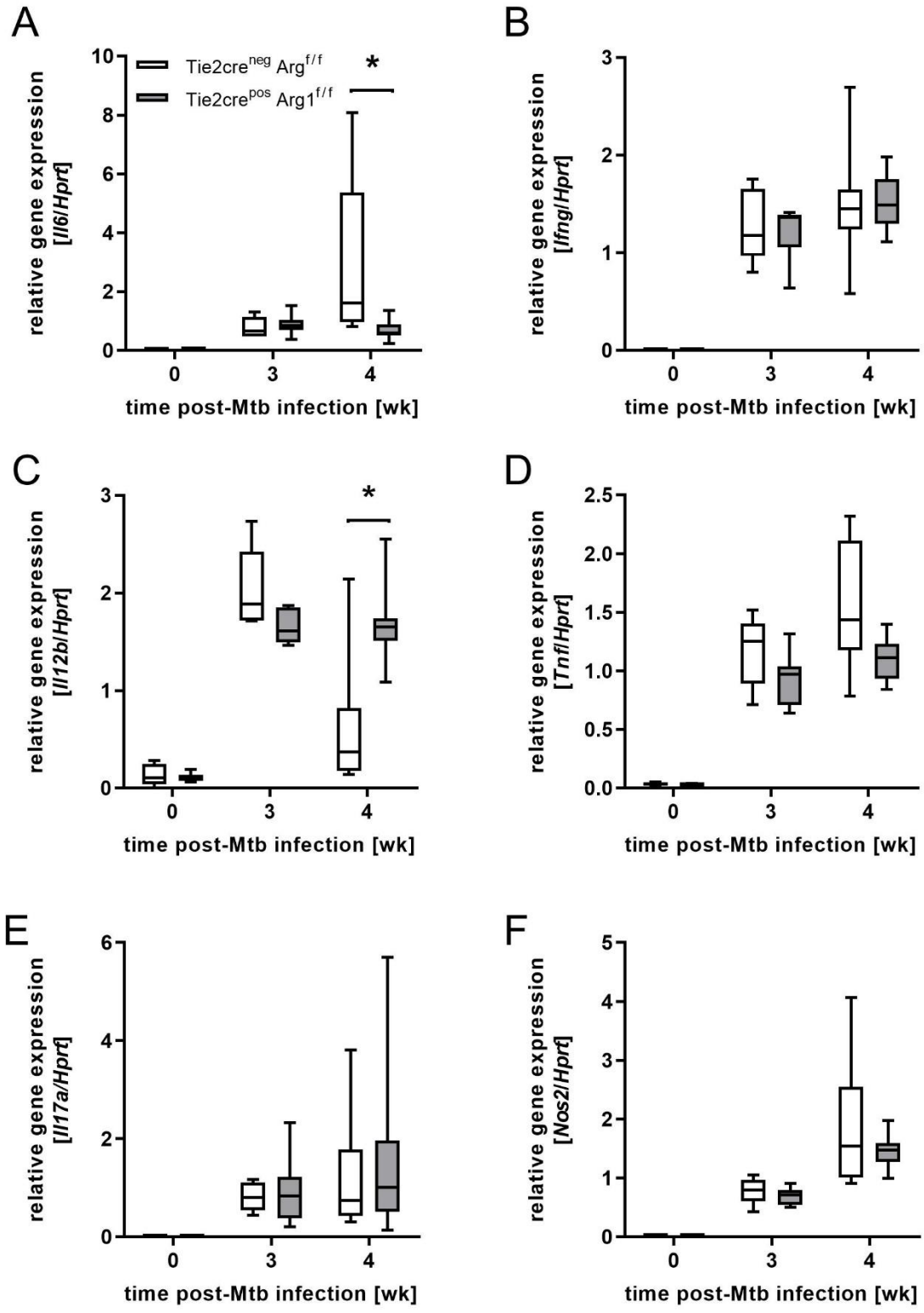

Figure 16 Gene expression of pro-inflammatory cytokines and CAM-associated markers in the lungs of high-dose Mtb-infected Tie2cre^{neg} Arg1$^{f/f}$ and Tie2cre^{pos} Arg1$^{f/f}$ mice

Tie2cre^{neg} Arg1$^{f/}$ and Tie2cre^{pos} Arg1$^{f/f}$ mice were infected with 2200 CFU Mtb H37Rv via the aerosol route. At the indicated time points, RNA was isolated from lung homogenates and reversely transcribed into cDNA for gene expression analysis of (A) *Il6*, (B) *Ifng*, (C) *Il12b*, (D) *Tnf*, (E) *Il17a*, and (G) *Nos2* relative to *Hprt* housekeeping gene expression by real-time quantitative PCR. Data represent the median, 25th-75th percentiles, and min. and max. values of five to fourteen mice per group. Statistical analysis was performed using the Kruskal-Wallis test with Dunn's post-hoc test to define differences between Tie2cre^{neg} Arg1$^{f/f}$ and Tie2cre^{pos} Arg1$^{f/f}$ mice as significant (*, p≤0.05). The data shown is representative of two independent experiments.

3.2.5 Tie2cre^{neg} and Tie2cre^{pos} Arg1$^{f/f}$ mice develop differential histopathology during high-dose infection with Mtb, while Arg-1 and NOS2 distribution within granulomatous lesions remain unchanged

Lung tissue was stained with hematoxylin and eosin staining (Figure 17) for examination by microscopy to address histopathology during high-dose infection of Tie2cre^{pos} Arg1$^{f/f}$ mice and competent littermates. Intact lung architecture without pathological findings could be observed in both Tie2cre^{pos} Arg1$^{f/f}$ mice and competent littermates at the time of Mtb infection (Figure 17A+D). Granulomatous lesions with cellular infiltrates became visible at week 3 post-infection and appeared to be similar in terms of structure in Tie2cre^{pos} Arg1$^{f/f}$ mice and competent littermates (Figure 17B+E). Within one more week however, Tie2cre^{neg} Arg1$^{f/f}$ mice appeared to develop more extensive cellular infiltrates and differentially structured lesions, whereas lesion size and structure in Tie2cre^{pos} Arg1$^{f/f}$ mice resembled week 2 morphology more closely (Figure 17C+F). In total, Tie2cre^{pos} Arg1$^{f/f}$ mice seemed to develop a less extensive, inflammatory histopathology than competent littermates.

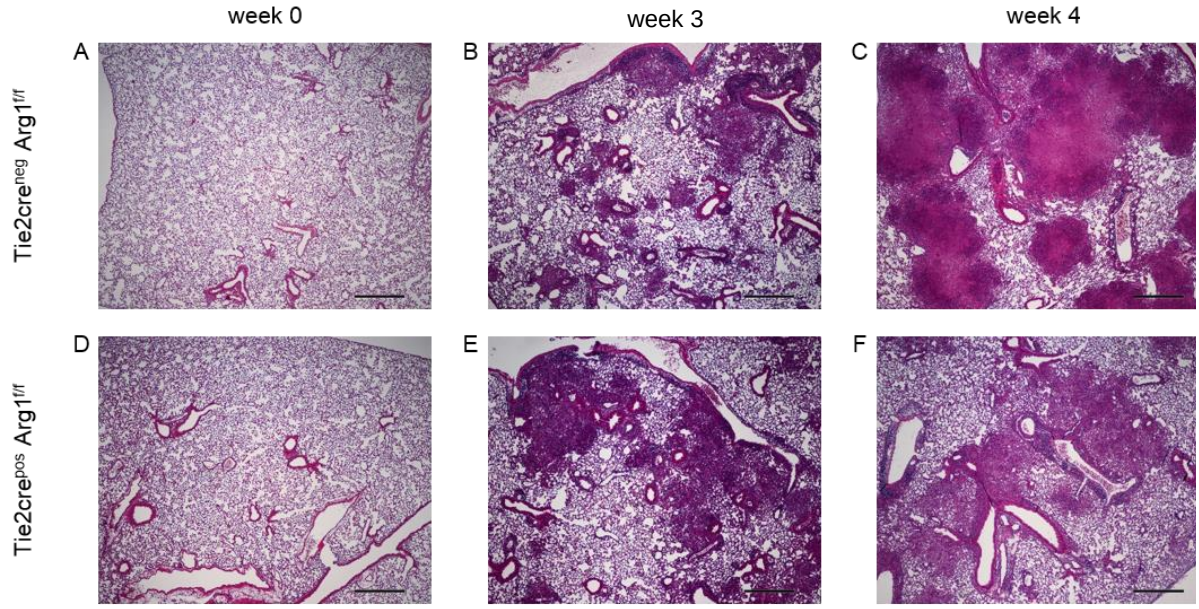

Figure 17 Lung tissue hematoxylin and eosin staining of high-dose Mtb-infected Tie2cre^{neg} Arg1$^{f/f}$ and Tie2cre^{pos} Arg1$^{f/f}$ mice
Tie2cre^{neg} Arg1$^{f/f}$ and Tie2cre^{pos} Arg1$^{f/f}$ mice were infected with 2200 CFU Mtb H37Rv via the aerosol route. Sections from formalin-fixed paraffin-embedded lungs taken at (A+D) week 0, (B+E) week 2, (C+F) week 4 post-infection were stained with hematoxylin and eosin staining followed by microscopic analysis. Representative microphotograph of one out of four to seven mice per group; scale bars: 500 µm. The data shown is representative of two independent experiments.

In order to assess whether distribution of Arg-1 and NOS2 were affected in light of the differential pathology in Tie2cre^{pos} Arg1$^{f/f}$ mice compared to competent littermates, tissue sections were immunohistochemically stained for Arg-1 (Figure 18A-F) and NOS2 (Figure 18G-L). Azan-trichrome staining was performed for visualization of collagen deposition (Figure 18M-R). Tie2cre^{neg} Arg1$^{f/f}$ mice showed scattered Arg-1 staining within granulomatous lesions and around lymphocytic aggregates, whereas Arg-1 staining was not detectable in Tie2cre^{pos} Arg1$^{f/f}$ mice (Figure 18A-F). In contrast, NOS2 distribution was detectable in both Tie2cre^{pos} Arg1$^{f/f}$ mice and competent littermates scattered through granulomatous lesions (Figure 18G-L). Arg-1 and NOS2 distribution appear similar in Tie2cre^{pos} Arg1$^{f/f}$

mice and competent littermates up to and including week 3 post-infection. Within one more week, high-dose infected Tie2cre^{neg} Arg1$^{f/f}$ mice seemed to develop a more diffuse Arg-1 distribution compared to week 3. Similarly, Tie2cre^{neg} Arg1$^{f/f}$ mice seemed to develop a more diffuse NOS2 staining than Tie2cre^{pos} Arg1$^{f/f}$ mice at week 4. Also, the localization of the Azan-trichrome staining (Figure 18M-R) in Tie2cre^{neg} Arg1$^{f/f}$ mice indicates a distinct tendency towards interstitial fibrosis, that appears dissimilar to the collagen distribution observed in the lungs of Tie2cre^{pos} Arg1$^{f/f}$ mice.

High-dose infected Tie2cre^{pos} Arg1$^{f/f}$ mice showed milder tissue pathology in terms of inflammation and fibrosis (Figure 17 and Figure 18), corresponding to lower bacterial loads in the lung (Figure 14C). Arg-1 staining was largely undetectable in Tie2cre^{pos} Arg1$^{f/f}$ mice as to be expected for Arg-1 deficient animals and in line with *Arg1* gene expression and arginase activity (Figure 14A-B). NOS2 distribution, given the difference in lesion morphology, is difficult to interpret yet appears less diffuse in Tie2cre^{pos} Arg1$^{f/f}$ mice than in Tie2cre^{neg} Arg1$^{f/f}$ littermates. Although the histological examination of Tie2cre^{neg} Arg1$^{f/f}$ mice showed increased signs of inflammation in the lung which corresponds to higher Arg-1 induction (Figure 14A-B), higher bacterial loads (Figure 14C), and more pronounced signs of disease (Figure 15), gene expression of *Ifng*, *Tnf*, *Il17* and *Nos2* appeared to be unchanged (Figure 16). The elevated levels of *Il12b* in Tie2cre^{pos} Arg1$^{f/f}$ mice might have affected cellular migration, thereby translating into this observed difference in inflammation. Interestingly, the data from high-dose infection experiments further support the speculation that the role of Arg-1 as a susceptibility factor in tuberculosis may be a function of the infectious dose.

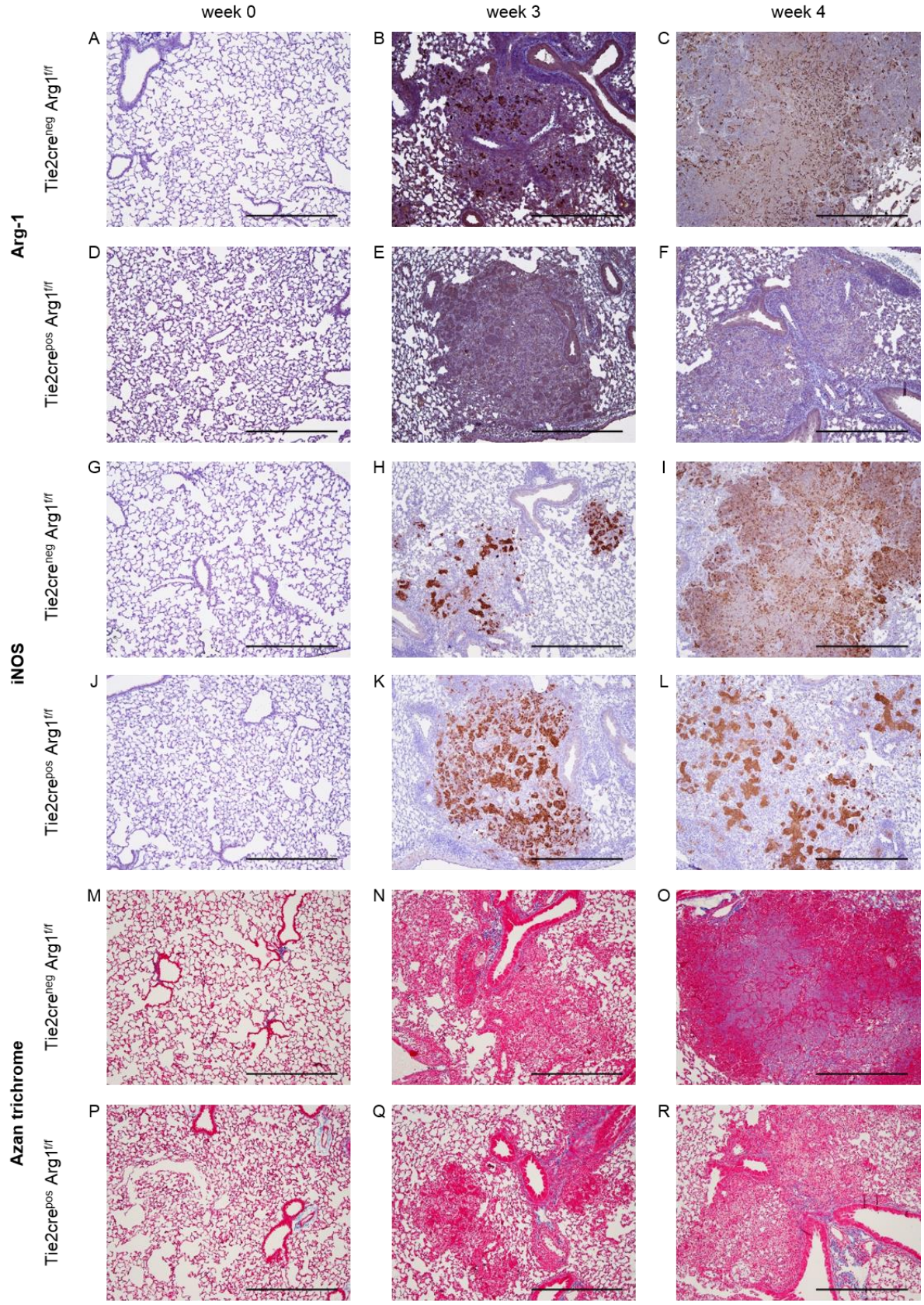

Figure 18 Distribution of Arg-1, NOS2, and collagen in granulomatous lesions of high-dose Mtb-infected Tie2cre^{neg} Arg1$^{f/f}$ and Tie2cre^{pos} Arg1$^{f/f}$ mice

Tie2cre^{neg} Arg1$^{f/f}$ and Tie2cre^{pos} Arg1$^{f/f}$ mice were infected with 2200 CFU Mtb H37Rv via the aerosol route. At the indicated time points, sections from formalin-fixed paraffin-embedded lungs were stained immunohistochemically stained for (A-F) Arg-1 or (G-L) NOS2, or stained with azan-trichrome for collagen (M-R) followed by microscopic analysis. Representative microphotograph of one out of four to seven mice per group; scale bars: 500 µm. The data shown is representative of two independent experiments

3.3 Arg-1 and Mtb HN878 infection in Tie2cre^{pos} Arg1$^{f/f}$ and Tie2cre^{neg} Arg1$^{f/f}$ mice

High-dose infection can be used to model aspects of infection with virulent Mtb strains. Virulent Mtb strains are frequent in high-endemic countries where disease is also more prevalent and often associated with higher bacterial burden. A higher bacterial burden in subjects with active disease may result in higher exposure of contact persons in an endemic setting. *In vitro* gene expression data illustrate an increased degree of *Arg1* gene expression with virulent Mtb HN878 and CDC1551 strains ((109); Hölscher, personal communication). This leads to the question whether virulent Mtb infection could be associated with higher Arg-1 induction which may then promote a higher degree of disease severity, pathology and susceptibility *in vivo*.

Tie2cre^{neg} Arg1$^{f/f}$ mice and Tie2cre^{pos} Arg1$^{f/f}$ mice, which lack Arg-1 in macrophages, were infected with 100 CFU Mtb HN878 via the aerosol route. Pulmonary bacterial loads and arginase activity in lung homogenates were determined at weeks 3, 6, and 11 post-infection (Figure 19). Bacterial loads reach and maintain a plateau at week 3 post infection and subsequent time points until the end of the experiment. No significant difference between CFU counts per lung could be detected between Tie2cre^{neg} and Tie2cre^{pos} Arg1$^{f/f}$ mice infected with Mtb HN878. In line with this, no significant arginase activity appears to be induced above background levels following HN878 infection in Tie2cre^{pos} Arg1$^{f/f}$ mice. Overall, no differences in terms of susceptibility to Mtb HN878 infection were observed in mice lacking Arg-1 expression in macrophages compared to Arg-1-competent littermates. The data presented here do not exclude a role of Arg-1 in virulent Mtb infection, but other strains such as CDC1551 would need to be investigated to form a more comprehensive picture.

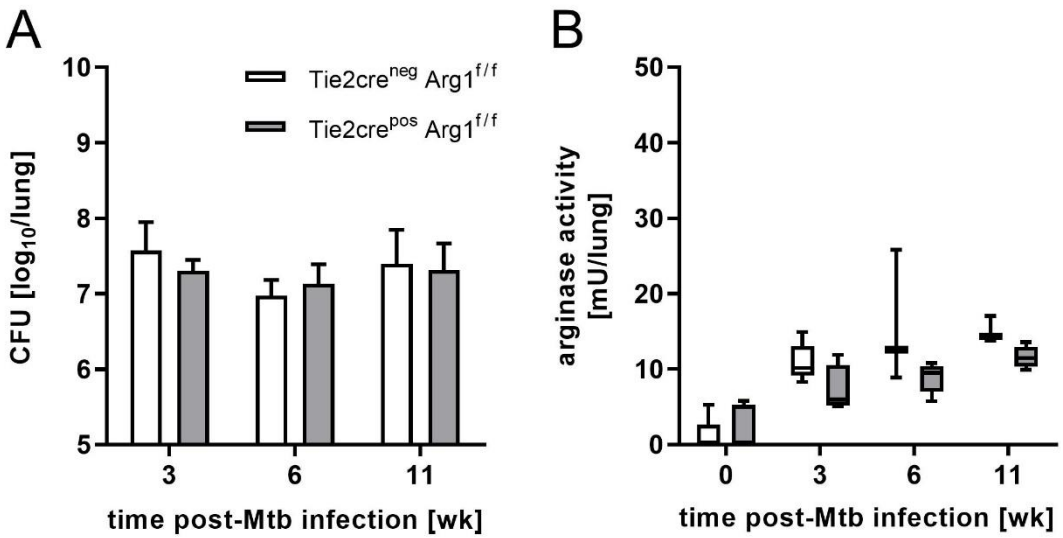

Figure 19 Lung bacterial loads and arginase activity of Mtb HN878-infected Tie2cre^{neg} Arg1$^{f/f}$ and Tie2cre^{pos} Arg1$^{f/f}$ mice
Tie2cre^{neg} Arg1$^{f/f}$ and Tie2cre^{pos} Arg1$^{f/f}$ mice were infected with 100 CFU Mtb HN878 via the aerosol route. At the indicated time points, (A) bacterial loads in lung homogenates were assessed by determination of CFU counts. Data represent the mean+SD of three to seven mice per group. (B) Arginase activity in lung homogenates was measured by L-Arg conversion into urea and quantified by spectrophotometric determination of the absorbance at 540 nm. Data represent the median, 25th-75th percentiles, and min. and max. values of three to seven mice per group. The data shown is representative of two independent experiments.

3.4 L-NIL-mediated inhibition of NOS2 in Tie2cre^{neg} Arg1$^{f/f}$ and Tie2cre^{pos} Arg1$^{f/f}$ mice during low-dose Mtb infection

Inhibition of NOS2 activity in WT mice is associated with elevated arginase activity, increased bacterial loads, and necrotizing granulomatous lesions (97). High-dose infection experiments described in the present thesis imply a possible association between the infectious dose and the degree of Arg-1 resulting in a degree of disease susceptibility and pathology. In order to investigate the importance of macrophage Arg-1 indicated by Schreiber *et al.* (96) and Heitmann *et al.* (97) while avoiding the early mortality seen in high-dose infection experiments, Tie2cre^{pos} Arg1$^{f/f}$ mice and Tie2cre^{neg} Arg1$^{f/f}$ mice were infected with a low dose of 50 CFU Mtb H37Rv. Mice then received L-NIL in drinking water to stimulate arginase activity. Control mice received plain drinking water. L-NIL stimulates arginase activity through inhibition of NOS2 activity resulting in a blockade of the endogenous Arg-1 inhibitor NOHA (Figure 2). When stimulated with L-NIL during the plateau-phase of mycobacterial growth, WT mice showed increased arginase activity accompanied by increased collagen deposition, mycobacterial growth, and development of centrally necrotizing granulomatous lesions surrounded by a rim of Arg-1 positive cells (97). Here, L-NIL administration to Tie2cre^{neg} Arg1$^{f/f}$ mice and Tie2cre^{pos} Arg1$^{f/f}$ mice was started 8 weeks post infection with Mtb H37Rv. This experimental setup shares a common factor with the high-dose infection experiments conducted earlier in terms of a relatively high bacterial load being present in the lungs of infected animals at the time of arginase induction.

3.4.1 Stimulation of arginase activity promotes Mtb growth *in vivo*

Tie2cre^{neg} Arg1$^{f/f}$ mice and Tie2cre^{pos} Arg1$^{f/f}$ mice were infected with 50 CFU Mtb H37Rv via the aerosol route. Mice received either water or a 0.01M L-NIL solution in drinking water *ad libitum* starting at week 8 post-infection and lasting until the end of the experiment. At the indicated time points, mycobacterial growth was quantified by determination of CFU counts in the lungs of infected animals (Figure 20). At week 11, Tie2cre^{neg} Arg1$^{f/f}$ mice developed significantly higher bacterial loads in the lung with L-NIL than Tie2cre^{neg} Arg1$^{f/f}$ mice receiving water ($p \leq 0.01$). Tie2cre^{pos} Arg1$^{f/f}$ mice receiving water reached similar bacterial loads as Tie2cre^{neg} Arg1$^{f/f}$ mice that received water. In Tie2cre^{pos} Arg1$^{f/f}$ mice that received L-NIL, no increase in bacterial load could be observed and CFU reached a similar level as mice that received water. Tie2cre^{neg} Arg1$^{f/f}$ mice treated with L-NIL showed significantly higher bacterial loads in the lung than Tie2cre^{pos} Arg1$^{f/f}$ mice treated with L-NIL ($p \leq 0.05$). Thus, at week 11 post-infection, administration of L-NIL led to increased bacterial loads in Arg-1-competent mice, whereas this effect was absent in mice lacking macrophage Arg-1 (Figure 20). Hence, Arg-1 appeared to mediate increased bacterial growth in Tie2cre^{neg} Arg1$^{f/f}$ mice in response to L-NIL treatment.

At week 15 post-infection, Tie2cre^{neg} Arg1$^{f/f}$ mice that received water had maintained constant lung bacterial loads, whereas Tie2cre^{neg} Arg1$^{f/f}$ mice that received L-NIL showed further increased bacterial loads ($p \leq 0.01$). Tie2cre^{pos} Arg1$^{f/f}$ mice treated with water maintained a constant CFU similar to Tie2cre^{neg} Arg1$^{f/f}$ mice treated with water. Tie2cre^{pos} Arg1$^{f/f}$ mice receiving L-NIL still showed significantly lower bacterial loads in the lung than Tie2cre^{neg} Arg1$^{f/f}$ mice receiving L-NIL ($p \leq 0.01$). However, while CFU counts were still significantly lower than those of competent littermates in response to L-NIL administration, bacterial loads in the lungs of Tie2cre^{pos} Arg1$^{f/f}$ mice that received L-NIL were also

significantly higher than the CFU counts of Tie2cre^{pos} Arg1$^{f/f}$ mice that received water (p≤0.01), thereby presenting with an intermediate phenotype. Therefore, L-NIL administration led to increased bacterial loads in the lungs of Tie2cre^{neg} Arg1$^{f/f}$ mice. However, this effect was partly abolished in Tie2cre^{pos} Arg1$^{f/f}$ mice at week 15. Thus, deficiency of Arg-1 in macrophages appeared to delay bacterial growth in response to L-NIL stimulation. This suggests that the observed increase in CFU counts was at least partially mediated by Arg-1.

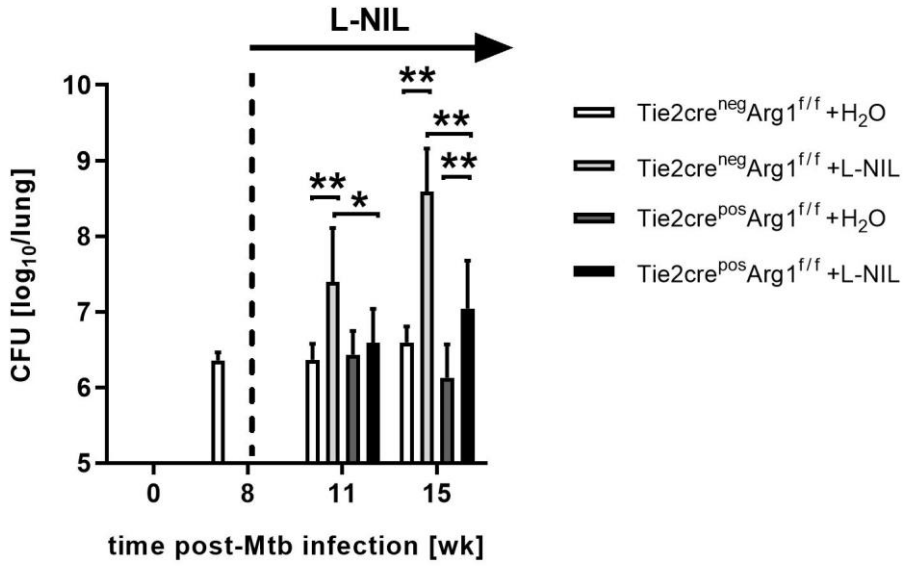

Figure 20 Effect of L-NIL treatment on lung bacterial loads of low-dose Mtb-infected Tie2cre^{neg} Arg1$^{f/f}$ and Tie2cre^{pos} Arg1$^{f/f}$ mice
Tie2cre^{neg} Arg1$^{f/f}$ and Tie2cre^{pos} Arg1$^{f/f}$ mice were infected with 50 CFU Mtb H37Rv via the aerosol route. Starting at week 8 post-infection, Tie2cre^{neg} Arg1$^{f/f}$ and Tie2cre^{pos} Arg1$^{f/f}$ mice received either water or a 0.01M L-NIL solution in drinking water *ad libitum* until the end of the experiment. At the indicated time points, bacterial loads in lung homogenates were assessed by determination of CFU. Data represent the mean+SD of five to seven mice per group. Statistical analysis was performed by 2-way ANOVA with Bonferroni's post-hoc test to define differences between Tie2cre^{neg} Arg1$^{f/f}$ and Tie2cre^{pos} Arg1$^{f/f}$ mice, and water- compared to L-NIL treated mice as significant (*, p≤0.05; **, p≤0.01).

3.4.2 Arg-1 contributes to necrosis development in response to L-NIL stimulation *in vivo*

Lung tissue sections of Mtb-infected Tie2cre^{neg} Arg1$^{f/f}$ and Tie2cre^{pos} Arg1$^{f/f}$ mice were immunohistochemically stained for Arg-1 to evaluate Arg-1 distribution in relation to histopathology (Figure 21). At week 11 and week 15 post-infection with 50 CFU Mtb H37Rv, Tie2cre^{neg} Arg1$^{f/f}$ mice that received L-NIL showed necrotizing granulomatous lesions surrounded by a rim of Arg-1-positive cells. In contrast, Tie2cre^{neg} Arg1$^{f/f}$ mice that were treated with water did not show cell death or rims of Arg-1 staining. Tie2cre^{pos} Arg1$^{f/f}$ mice that received water showed similar granulomatous lesions as competent Tie2cre^{neg} Arg1$^{f/f}$ that received water. Likewise, Tie2cre^{pos} Arg1$^{f/f}$ mice that received L-NIL showed lesions that were comparable to those of mice that received water as they lacked indicators of necrosis or stratification of Arg-1 staining. Taken together, L-NIL-treatment led to granulomatous lesions in Arg-1-competent mice, possibly with necrosis, but not in mice lacking Arg-1 specifically in macrophages. This data suggests, that Arg-1 in macrophages contributes to central granuloma necrosis in response to L-NIL stimulation. Overall, macrophage Arg-1 appeared to partially mediate effects on mycobacterial

growth in the lung and contributed to development of necrotic lesions in response to L-NIL inhibition of NOS2 in in mice infected with a low-dose of Mtb H37Rv.

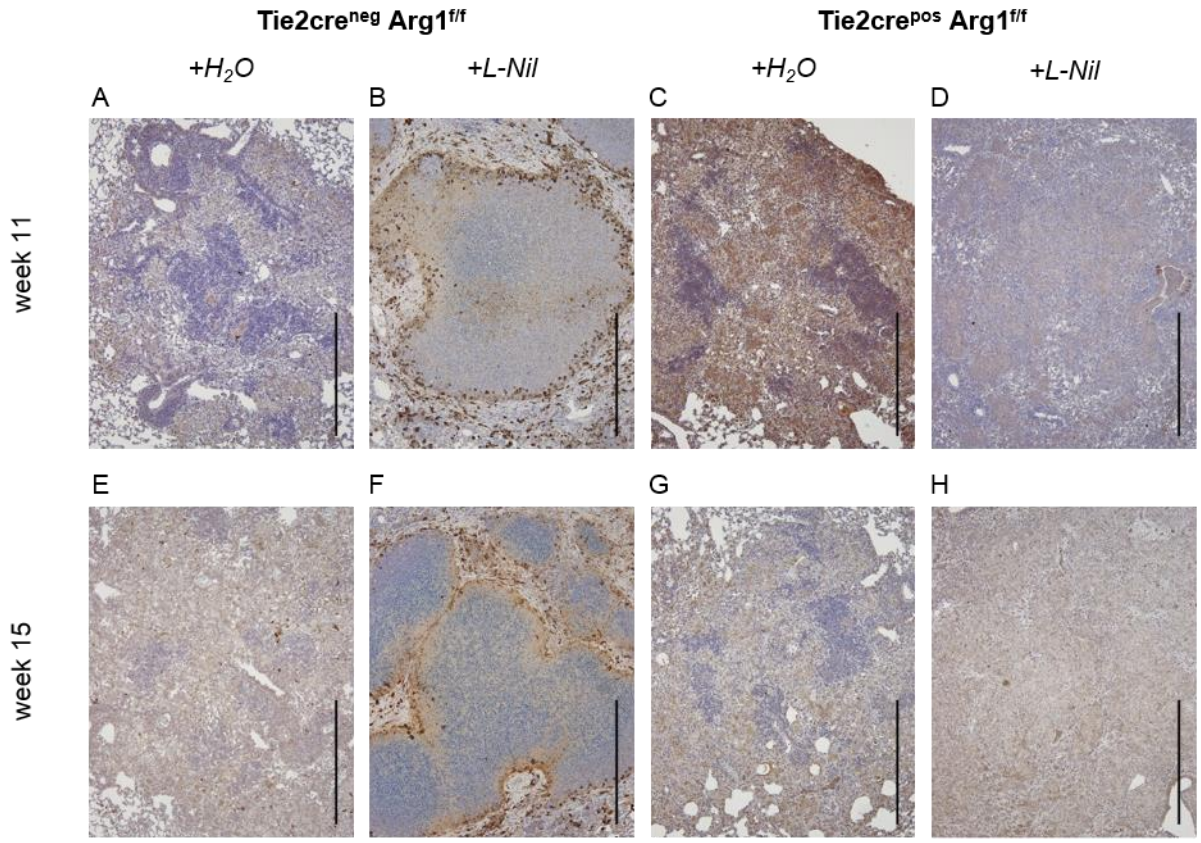

Figure 21 Distribution of Arg-1 in granulomatous lung lesions of high-dose Mtb-infected Tie2cre^{neg} Arg1$^{f/f}$ and Tie2cre^{pos} Arg1$^{f/f}$ mice
Tie2cre^{neg} Arg1$^{f/f}$ and Tie2cre^{pos} Arg1$^{f/f}$ mice were infected with 50 CFU Mtb H37Rv via the aerosol route. Starting at week 8 post-infection, Tie2cre^{neg} Arg1$^{f/f}$ and Tie2cre^{pos} Arg1$^{f/f}$ mice received either water or a 0.01M L-NIL solution in drinking water *ad libitum* until the end of the experiment. Sections from formalin-fixed paraffin-embedded lungs taken at (A-D) week 11, and (E-H) week 15 post-infection were immunohistochemically stained for Arg-1 followed by microscopic analysis. Representative microphotograph of one out of four to seven mice per group; scale bars: 500 µm.

4 Discussion

The mechanisms leading to mycobacterial reactivation and post-primary TB are incompletely understood. Experimental evidence suggests that Arg-1 in macrophages may contribute to acquisition of TB susceptibility and reactivation (97). AAMs were shown to modulate T cell responses and tissue repair. Arg-1 may promote TB pathogenesis by negative cross-regulation of NOS2, by promoting downstream collagen and polyamine synthesis, and by restricting T cell proliferation (100,103–107). Arg-1 can be induced in macrophages via Th2-dependent signaling via IL-10 and the IL-13/IL-4Rα-axis (96,97). Alternatively, it has been shown for mycobacterial infections that Th2-independent signaling via IL-6 and TLR/MyD88 may also induce Arg-1 in macrophages (108,109).

In human TB, Th2 responses have been described in patients in high-burden countries in which TB may be associated with higher exposure and infection with highly virulent strains (83). Thus, Th2 responses could drive detrimental outcomes in human TB by induction of Arg-1. Moreover, Arg-1 activity due to Th2 responses has been described in helminth-infections that are co-endemic with TB and that may pose a risk factor for post-primary TB (123). This makes it tempting to speculate that helminth-induced Arg-1 may undermine protective immune responses to Mtb. Independently of Th2 responses, Mtb has been described to induce Arg-1 in macrophages during intracellular infection (108). Experimentally, L-NIL-mediated inhibition of NOS2 has been shown to stimulate Arg-1 in macrophages during Mtb infection leading to reactivation and granuloma necrosis (97). However, most of these insights derive from *in vitro* experiments or indirect observations in transgenic animal models. *In vivo* evidence indicating a direct role for macrophage Arg-1 as a susceptibility factor in helminth-Mtb co-infection or Mtb infection alone is scarce (108,115).

The data shown in the present thesis demonstrate that helminth-Mtb co-infection does not affect the outcome of Mtb infection in WT mice despite significant Arg-1 induction in the lung. Previous authors have published co-infection data with different helminth species and mycobacteria resulting in various outcomes even for the same pathogenic nematodes (113,116). The present thesis shows for the first time a systematic approach using different helminth species within one aerosol Mtb infection model consistent in experimental setup and analytical methods and also identical in factors such as housing, animal feed, handling and scoring. Therefore, undetectable bias was minimized to a considerable extent.

In the present thesis, Mtb infection of mice with a macrophage-specific deletion of Arg-1 revealed for the first time an association between the infectious dose of Mtb and the degree of Arg-1 induction *in vivo*. While there was no association between Mtb strain virulence and macrophage Arg-1 induction, significant Arg-1 induction was observed after high-dose infection with Mtb H37Rv. High-dose Mtb infection was associated with impaired Mtb control as well as increased disease severity and pathology, all of which were reversible in mice lacking Arg-1 expression specifically in macrophages. Additionally, stimulation of arginase activity by L-NIL treatment led to development of necrotic granulomatous lesions and reactivation in mice infected with a low dose of Mtb. Mice that lacked macrophage-specific Arg-1 expression were protected against these effects. Hence, the present thesis provides direct evidence for the first time, that susceptibility and pathology in experimental TB depend on Arg-1, the level of which is induced depending on the infectious dose. Further, the data demonstrate

directly that reactivation and granuloma necrosis during pulmonary Mtb infection of mice are mediated by Arg-1 in macrophages.

4.1 Helminth-induced Arginase-1 during co-infection with Mtb

4.1.1 Helminth-induced Arg-1 and growth control of Mtb

In the present thesis, mycobacterial proliferation in the lung was unaffected by pre-existing transient or chronic helminth infections in three co-infection models with *N. brasiliensis*, *S. ratti* or *L. sigmodontis*. This demonstrates that growth control of Mtb is not compromised regardless of helminth-dependent Arg-1 induction in the lung – either transiently or over long periods of time and to a considerable degree.

The different extent and duration to which helminths induced Arg-1 appeared not to influence the growth of Mtb. While *S. ratti* was the weakest inducer of Arg-1 and *N. brasiliensis* showed a stronger but still short-lived capacity to induce Arg-1, *L. sigmodontis* established a chronic infection with ongoing Arg-1 induction in the lung which was considerably higher and of longer duration than for *N. brasiliensis* and *S. ratti*. Notably, Arg-1 induction in response to *S. ratti* infection was not detectable at the time of Mtb infection despite the fact that pre-experiments established AAM induction after *S. ratti* infection. The time window of Arg-1 induction may have escaped detection given that the day of Mtb infection was set on day 3 post-*S. ratti* infection at which time Arg-1 levels are beginning to increase. In light of the short duration of AAM induction by *S. ratti*, Arg-1 induction possibly escaped detection by being over before the first experimental endpoint at week 3 post-infection with Mtb.

The outcome of helminth-Mtb co-infection that mycobacterial growth was not affected in the present thesis conflicts with previously published results. Potian *et al.* reported a role for a helminth-induced IL-4Rα-mediated mechanism in undermining macrophage effector functions in Mtb infection, potentially due to induction of Arg-1 in the lung (116). In their model, *N. brasiliensis* induced a Th2 response in the lung with accumulation of AAMs. Subsequently, pulmonary bacterial loads in co-infected WT mice were increased significantly, because Mtb exploited AAMs as a niche for growth (116). Interestingly, the duration of *N. brasiliensis*-mediated Arg-1 induction described in this publication outlasts the duration of Arg-1 induction described in the present thesis by several weeks despite consistent approaches in dosing and timing of *N. brasiliensis* and Mtb infections. The prolonged duration of Arg-1 induction and AAM accumulation in response to *N. brasiliensis* infection that was observed by Potian *et al.* compared to the data described in the present thesis may account for the difference in disease susceptibility observed. The prolonged duration of Arg-1 induction and AAM accumulation observed by Potian *et al.* might be explained by a difference in parasite burden and/or later elimination of *N. brasiliensis* infection. Unfortunately, worm counts were not reported by the authors (116). In addition, in the *N. brasiliensis*-Mtb co-infection model by Potian *et al.*, the expression of CAM-associated markers (*Nos2*, *Lrg47*) was unaffected and CAMs were present in granulomatous lesions of co-infected mice which is at least partly consistent with gene expression of *Nos2* and *Lrg47* levels in lung homogenates of co-infected WT mice in the present thesis. Taken together, the observation that a shorter period of Arg-1 induction was not associated with increased susceptibility to Mtb infection, while a longer, potentially more pronounced Arg-1 led to increased susceptibility, supports the hypothesis,

that susceptibility to Mtb infection may depend on the degree and/or duration of Arg-1 induction. Noteworthy, Potian *et al.* report that AAMs were able to acquire features of classical activation in response to IFN-γ stimulation *in vitro* (116). It is unclear whether this also occurs *in vivo*. Thus, it is tempting to speculate that if AAMs are able to respond to IFN-γ activation, the time-to-switching could depend on the time-to-*N. brasiliensis* elimination and/or the duration over which the Th2-milieu in the lungs is maintained. In light of the shorter period of *N. brasiliensis*-induced Arg-1 described in the present thesis, AAMs may have switched to CAM effector type faster compared to the data published by Potian *et al.* (116) which may have accounted for the differences in mycobacterial growth observed.

Not only this plasticity between AAMs and CAMs is interesting to note, but also that *N. brasiliensis* has been shown to induce alveolar macrophage populations with both alternatively and classically activated characteristics in another mycobacterial co-infection model (113). *N. brasiliensis*-*M. bovis* BCG co-infection was associated with enhanced mycobacterial control after pre-existing *N. brasiliensis* infection in Balb/C mice (113). It is acknowledged that the authors used the less virulent *M. bovis* BCG strain, which is usually cleared more efficiently from the host (124), limiting the comparability of these two models regarding the general impact on TB. Nevertheless, it is interesting to observe the induction of a mixed AAM/CAM population in response to *N. brasiliensis* infection. The induction of CAM-associated markers was attributed to an early, non-specific IFN-γ release in response to *N. brasiliensis* infection (113). While some early unspecific *Ifng* gene expression was observed during pre-experiments in the present thesis, this was not sufficient to induce classical activation of macrophages after *N. brasiliensis* infection (data not shown). DuPlessis *et al.* showed that intranasal transfer of alveolar macrophages from *N. brasiliensis*-infected donor mice into *M. bovis* BCG-infected mice enhanced growth control of mycobacteria, although the authors amend that this was not mediated through direct killing of mycobacteria by donor macrophages (113). Therefore, the biological relevance of the observed *N. brasiliensis*-induced mixed AAM/CAM population reported by DuPlessis *et al.* cannot be determined for certain.

Infections with pathogenic nematodes such as *N. brasiliensis* and *S. ratti* are usually transient even though immunologic changes may persist for longer than the infection itself (116). In contrast to *N. brasiliensis* and *S. ratti*, *L. sigmodontis* infection provided a model of chronic helminth infection with high levels of arginase activity over a prolonged period of time. Given that *L. sigmodontis* adults reside in the thoracic cavity adjacent to the lung, it was tempting to speculate that the *L. sigmodontis*-induced AAMs in the thoracic cavity might influence the course of Mtb infection. Nevertheless, compartmentalization of AAMs in the thoracic cavity might have reduced Mtb interaction with AAMs, while still leaving potential for indirect effects of L-Arg depletion. The result that *L. sigmodontis* infection did not affect mycobacterial growth despite considerable arginase activity measured in lung homogenates was in line with one previous report from Hübner *et al.* (114). In a co-infection experiment with *L. sigmodontis* and Mtb in the cotton rat, the natural host of *L. sigmodontis*, no difference was observed between co-infected cotton rats and Mtb-infected controls (114). Compared to the mouse model, the cotton rat model has the advantage of replicating stratified granuloma formation in response to Mtb infection. However, Mtb H37Rv infection occurred via intranasal inoculation 11 weeks post-infection with *L. sigmodontis* (instead of 4 weeks used in the present thesis), and therefore well into the chronic and patent phase of helminth-infection. Cotton rats were sacrificed 2 months post-infection with

Mtb. Although different rodents were used and the routes and inoculum sizes of infection and the time points of sacrification differed, and arginase activity over the time course of both infections was not shown, the data obtained by Hübner *et al.* support the conclusion that pre-existing *L. sigmodontis* infection does not affect susceptibility to Mtb infection. Of note, Hübner *et al.* included *L. sigmodontis*-only infected controls. Although not reproducible across two experiments, they observed reduced adult worm counts in co-infected animals compared to *L. sigmodontis*-infected controls (114). No *L. sigmodontis*-only group has been included in the present thesis, but it was noted that adult worm counts following natural infection appeared below average. In light of these overlapping observations, Mtb infection may have negatively affected *L. sigmodontis* infection. Nevertheless, a high degree of arginase activity was still induced, regardless of relatively low parasite numbers. Overall, the data presented in the present thesis is in line with literature and supports the conclusion that helminth-induced Arg-1 does not impact susceptibility to Mtb infection in mice. Additional evidence supporting the notion that helminth-induced AAMs in the lung do not affect growth control of Mtb derives from animal experiments with *S. mansoni*. Monin *et al.* (115) generated bone marrow chimeric (BMC) mice that were reconstituted with either Arg-1-competent or Arg-1-deficient myeloid cells. These mice were co-infected with *S. mansoni* and 100 CFU Mtb H37Rv and compared to Arg-1-competent BMC mice infected with Mtb alone. Co-infection led to higher bacterial loads compared to Mtb infection alone in BMC mice with Arg-1-competent macrophages. However, this appeared unaffected by Arg-1 because co-infected mice lacking Arg-1 in macrophages displayed the same bacterial loads as Arg-1-competent BMC mice. Despite unchanged bacterial loads, AAMs in the lung drove inflammation and disease severity, suggesting that the aggravated inflammation and disease susceptibility were due to effects other than impaired growth control and high antigenic loads of Mtb. Inflammation was reversible with anthelmintic treatment (115). Arg-1-deficient mice have previously been shown to better control Mtb infection as illustrated by decreased CFU counts (108) but succumb to *S. mansoni* infection rapidly (125). Hence, the observation that *S. mansoni* and Mtb co-infection leads to similar CFU counts in both Arg-1-competent and -deficient BMC mice could imply that *S. mansoni* infection may have overrun the protective effect of Arg-1-deficiency in Mtb infection. It would have been interesting to see whether Monin *et al.* (115) could have reproduced the protective effect of macrophage Arg-1-deficiency in low-dose Mtb infection described by ElKasmi *et al.* (108). Unfortunately, this remains speculative, as Mtb infected control mice lacking Arg-1 in macrophages were not included (115).

Overall, current literature describes the impact of helminth-induced AAMs (across different species and infection models) on mycobacterial growth as of moderate magnitude and duration (113,116) or of no consequence at all (114,115). While some differences were apparent early after infection, differences in growth curves were moderate and resolved at later time points (113,116). This is consistent with the data described in the present thesis that occasionally show minor and transient differences in CFU counts (<0.5 log units) and gene expression levels of markers of protective Th1 responses and CAMs. However, these were not statistically significant. Considering the duration and extent of these changes, the impact of helminth-infection on growth control of Mtb infection in the lung appears negligible in terms of biological relevance despite the sometimes considerable Arg-1 induction.

4.1.2 Cytokine responses during co-infection

In the present thesis, gene expression analysis of markers for protective Th1 and Th17 responses and IFN-γ inducible classical activation of macrophages revealed that helminth-Mtb co-infection did not affect the expression of pro-inflammatory cytokines and CAM-associated markers in co-infected mice regardless of the helminth species used. Thus, helminth co-infection appeared not to affect the key mediators of mycobacterial growth control. Hence, it is not surprising, that no differences between pulmonary bacterial loads were observed between co-infected mice and Mtb-infected controls.

The outcome, that protective cytokine responses were unaffected by pre-existing helminth infection in the present thesis, is consistent with studies describing no or only moderate effects on T cell responses during helminth-Mtb co-infection that appeared inconsequential for control of Mtb growth (116). Although impaired T cell responses following co-infection with helminths and mycobacteria have been described in some cases (112,126,127), again other co-infection studies observed no such helminth-induced effect on Mtb-specific T cell responses (116,128). Similar observations were published on co-infection models with *M. bovis* BCG and helminths. Enhanced *M. bovis* BCG clearance in co-infected mice was associated with earlier Th1 and Th2 responses in the lungs of mice with pre-existing *N. brasiliensis* infection (113). The authors speculate that *N. brasiliensis* infection expedited macrophage and neutrophil recruitment, T cell activation, and T cell polarization. As such, an "alarmed" immune system – although not specific to *M. bovis* BCG – might have improved immune responsiveness to a subsequent infection (113). In contrast, others report that when C57BL/6 mice were infected with *N. brasiliensis* and *M. bovis* BCG, IFN-γ release from T cells in response to purified protein derivative (PPD) from Mtb was significantly decreased in the lymph node. Although this implies an inhibitory effect of helminth-infection on specific Th1 responses, mycobacterial burden was not affected (129). In a co-infection model with Mtb and filarial nematodes, no differences in spleen cell responses to PPD and IFN-γ production were observed in co-infected cotton rats compared to controls (114). Additionally, mycobacterial loads were similar between co-infected and Mtb-infected cotton rats (114). Interestingly, Balb/C mice that were injected with *Brugia malayi* microfilariae or immunized with *B. malayi* antigens to induce a Th2 response in the host. This was followed by stimulation with PPD. The data showed that the PPD-specfic immune response was biased towards a Th2 profile. However, when mice received PPD and living microfilariae at the same time, PPD-specific Th1 responses were not altered (130). Yet others have shown reduced Th1 responses and accumulation of Arg-1 expressing macrophages in the lung during *S. mansoni*-Mtb co-infection (115). Interestingly, lung bacterial burden was unaffected in co-infected BMC mice lacking Arg-1 in macrophages whereas inflammation was ameliorated, suggesting that 1) Arg-1 did not affect macrophage control of mycobacterial growth, and 2) the observed inflammatory effects were likely not mediated by high mycobacterial antigenic loads because inflammation was ameliorated whereas bacterial growth was not different (115). Both the reports by Pearlman *et al.* (130) and Monin *et al.* (115) underscore the role of timing of co-infections in experimental set-ups again, and may in part explain the variability in co-infection outcomes described in literature.

Overall, even where changes to the T cell response were described in literature, these did not consistently translate into better (or worse) protection against mycobacterial infection. Other authors report no impact on the T cell response by helminth co-infection at all. This is in line with the data reported in the present thesis, which describes no meaningful changes in markers of protective Th1/17

responses during helminth-Mtb co-infection. This is in line with the unaffected pulmonary bacterial burden in co-infected and Mtb-infected mice. In light of the important role of T cell immunity to control Mtb infection (9), the question is raised what amplitude of change would be required to impact the control of Mtb infection to a biologically relevant degree. Taken together, the present thesis and the published literature indicate that pre-existing helminth infections do not translate into a biologically relevant T cell-mediated effect on control of Mtb infection.

4.1.3 Tissue pathology

In the present thesis, the granulomatous response to Mtb infection in the lung appears to be unaffected by pre-existing *N. brasiliensis*-, *L. sigmodontis*- or *S. ratti* infections. Although the lung passage of *N. brasiliensis* larvae induces tissue damage and architectural changes which are clearly visible in co-infected mice at the time of co-infection with Mtb, Mtb granulomas develop in the common form of amorphous masses of cellular infiltration without stratification, which is to be expected in WT mice. Similarly, *S. ratti*-induced cell infiltration around larvae trapped in the lung was visible at the time of co-infection although lung tissue damage was less pronounced than for *N. brasiliensis*. Granuloma formation continues in a similar fashion in mice with pre-existing *S. ratti* infection and control mice infected with Mtb alone, without discernible differences in tissue pathology. Similarly, granuloma formation in *L. sigmodontis*-Mtb co-infected mice appeared similar to that in Mtb-infected control mice as well. Based on Heitmann *et al.*, high induction of Arg-1 alters granuloma structure to resemble a more human-like, stratified morphology with central necrosis (97). In the present thesis, this effect was clearly absent in helminth-Mtb co-infected mice. This may be due to the different sources and timing of Th2-cytokine induction between the present thesis and the publication by Heitmann *et al.* (97), which showed considerable IL-13 production under control of a T cell promoter when Th cells were activated in the course of the adaptive immune response to Mtb infection. IL-13 production was associated with considerable Arg-1 induction (97). In contrast, pre-existing helminth infection induced Arg-1 before Mtb infection in the present thesis. Therefore, it cannot be excluded that the timing of Arg-1 induction together with a different level of arginase activity may have led to this difference in granuloma morphology.

Overall, the here presented histological data are in line with the unaffected pulmonary bacterial burden and gene expression levels of markers indicative of protective immunity and macrophage activation in co-infected and Mtb-infected mice across all three helminth species tested in the present thesis.

4.1.3.1 Mechanical tissue damage due to larval migration

In the present thesis, the observation that pre-existing *N. brasiliensis* infection did not affect granuloma formation in response to a subsequent Mtb infection was a surprising result given the extent of *N. brasiliensis*-induced lung damage. Tissue damage may lead to innate IL-4 release and induction of Arg-1 which has been shown to increase susceptibility to Mtb in a filarial co-infection model (131). However, another more recent *N. brasiliensis*-Mtb co-infection model that employed IL-4Rα$^{-/-}$ mice indicates that lung tissue damage and possibly impaired lung function due to larval migration was a minor or possibly unimportant factor in development of pathology. However, the authors did not report

whether initial *N. brasiliensis*-caused lung damage was comparable between WT and IL-4Rα$^{-/-}$mice (116). Further support for the conclusion that mechanical tissue damage due to larval passage is possibly less important in driving lung pathology during Mtb infection derives also from a co-infection model with *S. mansoni* and Mtb which concluded that architectural changes and tissue damage by larvae did not seem to be an underlying factor. This was demonstrated when the authors used SEA stimulation instead of *S. mansoni* infection and obtained the same effect on granuloma formation with absent mechanical tissue damage, thus attributing pathological effects to parasite antigens rather than mechanical damage (115).

No impact on tissue pathology is seen in helminth-infected mice despite considerable damage from larval migration through the lung in the present thesis. This is overall consistent with literature and supports the conclusion that larvae-induced mechanical lung damage is less important in the development of tissue pathology associated with a concomitant Mtb infection.

4.1.3.2 AAMs and lung pathology

Granuloma integrity or lack thereof is central to the development of active disease and spread of bacilli. Unfortunately, not many publications regarding helminth-Mtb co-infection focus on the histopathological changes. This may be owed to the popularity of the mouse model in biomedical research although the mouse model is known to be largely divergent from the human host response in terms of organ pathology of TB despite its usefulness in studying aspects of the immune response (27).

Analysis of histopathology based on hematoxylin and eosin staining staining as illustrated in the present thesis showed that the granulomatous response to Mtb was unaffected in helminth-Mtb co-infected mice compared to Mtb-infected control mice. Similar to WT mice, granulomatous lesions in the lung were characterized by amorphous aggregates of immune cells.

These data are consistent with the report from Potian *et al.* that shows the same picture in *N. brasiliensis*-Mtb co-infected and Mtb infected Balb/C WT mice. Unfortunately, the authors did not further report on changes in organ pathology in co-infected and Mtb infected Balb/C WT and IL-4Rα$^{-/-}$ mice other than showing an absence of Arg-1 staining in the granulomatous lesions of co-infected IL-4Rα$^{-/-}$ mice and presence of NOS2 staining regardless of genetic background or pre-existing helminth infection (116). Along similar lines, Hübner *et al*. carried out relative quantification of granuloma size (% of total lung tissue) in *L. sigmodontis*-Mtb co-infected cotton rats and showed comparable lung lesion size between co-infected and Mtb infected cotton rats (114).

In contrast, Monin *et al*. used a *S. mansoni*-Mtb co-infection model and generated BMC mice lacking Arg-1 specifically in macrophages. In this model, co-infected BMC WT mice showed aggravated inflammation. This was characterized by larger lesion size (% area affected of total lung) with impaired B cell follicle development in granulomatous lung lesions. *S. mansoni* infection led to increased numbers of AAMs in the lung driving inflammation and disease severity. Interestingly though, AAMs in co-infected mice were found mainly in type 2 granulomatous lesions which were distinct from type 1 granulomas (containing no Arg-1 but NOS2 expressing macrophages) within the same lung. Notably, absence of Arg-1 in macrophages in co-infected mice reversed these effects (115). This would be in line with results showing that different granulomatous lesions within the same lung can have different metabolic states and immunologic statuses (99). The observation by Monin *et al.* that Arg-1 deficiency protects against

inflammation and organ pathology (115) is a striking result given that a lack of Arg-1 was shown to be detrimental in *S. mansoni* infection alone. When Tie2cre^{pos} Arg1$^{f/f}$ mice were infected with *S. mansoni* alone, mice failed to downregulate CD4 T cell responses resulting in exacerbated inflammation and fibrosis in liver and intestine during chronic *S. mansoni* infection consistent with the known role of Arg-1 in inhibition of T cell responses (115).

Since a Th1 response is induced in the first 6 weeks of *S. mansoni* infection before the release of eggs triggers the onset of a Th2 response (132), the Mtb-induced Th1 response might aid in control of the unrelated *S. mansoni* infection. This supports the hypothesis that Mtb infection may influence immune responses to other unrelated antigens. It is unfortunate though, that Monin *et al*. did not include Arg-1 deficient controls infected with Mtb only or a *S. mansoni*-only infected control group in their experimental design (115), making it difficult to discern effects of macrophage Arg-1 on Mtb infection or on *S. mansoni* infection. Nevertheless, Monin *et al.* confirmed their findings from the Tie2cre Arg1$^{f/f}$ strain with similar results observed in the LysMcre Arg-1$^{f/f}$ deleter strain which lacks Arg-1 in monocyte/macrophages and neutrophils (115). Given the limited expression of Arg-1 in neutrophils in Mtb co-infection, this too is essentially a macrophage specific Arg-1 knock-out model. Overall, they are mostly consistent with data from Potian *et al.* (116) that showed that AAMs accumulated in the lung leading to detrimental effects on development of TB, despite describing opposing effects on development of Th responses and pulmonary bacterial burden in *N. brasiliensis* and *S. mansoni* infection (115,116). Both reports concur that changes to the immune response induced by pre-existing helminth-infection (whether acute or chronic) were reversible, either in terms of AAM responsiveness to IFN-γ stimulation (116) or with anthelminthic treatment and removal of helminth antigens (115).

Overall, the histological analysis presented in the present thesis is consistent with previous literature that showed no effect of helminth-Mtb co-infection on development of pulmonary tissue pathology. This is to be expected in light of the similar bacterial load and similar gene expression levels observed for co-infected and Mtb-infected mice in the present thesis.

4.1.4 Differences in experimental models

4.1.4.1 Route of Mtb infection

In terms of technical aspects, not only analytical methods vary widely between published reports but also experimental design aspects. Even within one reasonably similar model and using the same pathogen, technical aspects may lead to differences in outcome. This is exemplified by the use of different routes of infection for Mtb. When using the natural mode of transmission, i.e. aerosol infection, Mtb appears to be more virulent than when using the intravenous route of infection (133). Moreover, meaningful comparisons between Mtb and *M. bovis* BCG are somewhat limited due to their underlying differences (124). This may account for the diversity of outcomes described in literature.

4.1.4.2 Different helminths and life cycle maintenance effects

It seems obvious that different helminth species may vary considerably in their life cycles, elicited immune response, and pathology. It could have been reasonably expected that concomitant Mtb infection may be affected differently by different helminths, accounting for the diversity in outcomes seen in literature. Immunomodulatory mechanisms other than the induction of AAM/Arg-1 may impact the

manifestation of co-infection-associated co-morbidities and thus mask effects of AAM induction on the whole-animal level. Controversy is also added by different approaches in experimental designs even when using the same species, exemplified by different immune responses induced by *N. brasiliensis* in two different laboratories (113,116).

Even when using the same helminth species in co-infection experiments including the same infectious dose and route of infection, the resulting effect may not necessarily be consistent between laboratories. It has been shown for *N. brasiliensis* that larvae from strain maintenance in rats are adapted to infect the rat but to lesser extent the mouse. When using rat-adapted larvae, the same dose of iL3 may lead to less productive infection in mice (134). To add insult to injury, the infectivity of iL3 decreases over time of storage in fecal cultures, potentially affecting subsequent infection take. Moreover, the intestinal microbiota may affect infection take of adult *N. brasiliensis* worms but is difficult to control between animal facilities (Voehringer, personal communication). It has been described, that in studies employing *N. brasiliensis* as a potent Th2 inducer, experimental mice were treated with antibiotics prior to *N. brasiliensis* infection to induce more robust responses (Voehringer, personal communication), again potentially adding to the diversity of results described in literature.

4.1.4.3 Accessibility of helminth-infected AAM to inhaled Mtb

In the present thesis, AAMs expressing Arg-1 in the lung were interspersed in granulomatous lesions induced by *N. brasiliensis* and *S. ratti* larvae in the lung. AAMs were not visible in the lung parenchyme. Whether Mtb upon entering the lung is able to infect any other AAMs except those on the border of inflammatory aggregates cannot be ascertained. Thus, the potentially higher expression of mannose receptor on AAMs (135) that could theoretically facilitate higher uptake of Mtb into AAMs might be irrelevant to invading Mtb bacilli. Although mobility of Mtb-infected macrophages and entry and efflux of infected monocytes from the granuloma has been shown, Cosma *et al*. elegantly demonstrate that homing into granulomas is pathogen specific and migrating cells may be kept out actively from entering into the “wrong” granuloma (136). Further along this notion, others have shown that macrophages inside granulomatous lesions are exposed to other cytokines than alveolar macrophages outside of granulomas (137). Aside from this, depletion of L-Arg and the resulting inhibitory effect on T cells (100,103) may hypothetically contribute to pathology in different degrees if gradients of L-Arg deficiency were ranging widely enough to affect T cells outside the larvae-induced granulomatous lesion. It is worth questioning if increased susceptibility of AAM to Mtb infection matters in practice, when AAMs are spatially distributed in larvae-induced granulomatous lesions where invading Mtb may not reach them. Hypothetically, Mtb could preferentially infect alveolar macrophages in the surrounding lung tissue and/or infiltrating monocytes/macrophages from the circulation which may be more readily accessible.

4.1.4.4 Timing of infections

Differences in timing of infections may also account for the different outcomes reported in literature. The duration of the time window in which AAMs are present expressing Arg-1 may have affected the outcome of helminth-Mtb co-infection. Considering this, also the timing of Mtb infection following helminth infection may be crucial. With transient and relatively short-lived helminth-infections such as *N. brasiliensis* and *S. ratti,* the timing in relation to Mtb infection may be critical. To complicate matters

further, different life cycle stages may elicit different immune responses and depending on the timing of infections, different immune responses and immunomodulatory mechanisms may interact. For example, a report by Elias *et al.* states that early *S. mansoni* infection enhanced resistance against Mtb while chronic *S. mansoni* infection impaired responses to Mtb challenge, likely due to different immune responses elicited by *S. mansoni* early after infection compared to later stages (127). Along the same lines, inflammation and responses to unrelated antigens may be affected by the extent and duration of infection (138).

4.1.4.5 Infection sequence

Depending on the experimental endpoint of interest (innate or adaptive immunity, acute or chronic phases of Mtb infection) different scenarios for the order of infection could be important. For example, would helminth infection just before onset of adaptive immunity of an already ongoing Mtb infection compromise adaptive responses and lead to differential control of Mtb infection? Most co-infection models have addressed the impact of a pre-existing helminth infection on a following Mtb infection. But how would a pre-existing, established Mtb infection be affected by helminth infection? Chronic Mtb infection in the murine model does not equate with latency, although WT Balb/C and C57BL/6 mice can control Mtb infection over extended periods of time without onset of weight loss and disease onset. A recent report describes the Cornell model of drug-induced latent Mtb infection in the context of *S. mansoni* and Mtb co-infection (115). When mice were infected with *S. mansoni* during drug-induced latency, co-infected mice reactivated but so did Mtb-infected controls. Co-infected mice did show a higher bacterial burden than controls, suggesting that while not necessarily causing reactivation, helminth infection may still aggravate susceptibility to disease (115).

An often neglected question is whether helminth infection might progress differently when entering a host with a pre-existing Mtb infection. Also, it cannot be determined for certain what would be the most likely sequence of infection encountered in a co-endemic setting. Is a human host more likely to be infected with Mtb first than to contract a helminth-infection? In case of high-burden, developing countries, neonates and infants are carried by parents for the majority of their early life. Thus, an early Mtb infection from a parent or close household contact may be more likely than a soil-transmitted helminthiasis at that age. The probability of infection with either pathogen may be different at later stages in life and depend e.g. on an individual's living conditions.

Infection with mycobacteria has previously led to increased *S. venezuelensis* burden (139) or delayed *Trichuris muris* elimination (140). In the present thesis, *L. sigmodontis* worm counts in co-infected mice were relatively low compared to parasite numbers usually achieved. Given that a *L. sigmodontis*-only infected control group was not included here, it is not possible to estimate whether the low parasite numbers are simply due to chance or whether the fitness of mites was reduced (which may occur in case of excessive microfilarial burden). Thus, it remains unknown whether susceptibility to *L. sigmodontis* was decreased by concomitant Mtb infection and the associated pro-inflammatory Th1 environment. A similar effect was suggested by Hübner *et al.* who described below-average parasite numbers in Mtb-*L.sigmodontis* co-infected cotton rats (114). A recent report by Wulandari *et al.* showed that macrophages were classically or alternatively activated depending on the order of co-infection with *H. polygyrus* and Mtb infection. Notably, the second infection seemed to be decisive for macrophage

polarisation (141). Together with data that showed reversal from an AAM to a CAM effector type *in vitro* (116), this provides further support for macrophage plasticity in face of a subsequent infection. Moreover, susceptibility to Mtb infection was not affected, despite different macrophage polarisation dependent on the order of Mtb and nematode infection (141). This is in line with the data shown in the present thesis and lends further support to the hypothesis that helminth co-infection does not affect immunity to Mtb infection.

Another factor scarcely investigated in co-infection models of Mtb is metabolic substrate limitation even though it can have various implications on the host metabolism and immune response but also on pathogen metabolism (142). An early publication by Kahnert *et al.* described that induction of AAMs resulted in decreased production of NO while at the same time enhancing access to iron (143). On the host side, the stress induced by malnutrition can be sufficient to override a beneficial effect of helminth infection on a concomitant infection with environmental mycobacteria (144).

Overall, the results of previously published animal studies on helminth-Mtb co-infection are contradictory and are characterized by a wide diversity in mice, helminth species, experimental designs, laboratory and analytical methodology. Their comparability may be further compromised by undetectable bias resulting from factors such as animal housing, handling, animal feed, and microbiota. Not all models, especially those employing different helminth species, may have the same role for Arg-1, the expression of which may also differ in spatial and temporal importance. As an example, Arg-1-mediated T cell inhibition may prove detrimental when T cell immunity is required for controlling an infection, but may also be beneficial to prevent excessive inflammation by timely down-modulation of the immune response once it is no longer required.

In the present thesis, for the first time, three different helminth species have been assessed in their capacity to induce AAMs and modulate susceptibility to a subsequent Mtb infection within one consistent Mtb model. While different helminth species have resulted in different outcomes of co-infection in published studies, the strength of the totality of data lies in the systematic approach comparing multiple helminth species in a Mtb co-infection model and in the control of environmental factors such as housing and handling which supports the robustness of the data shown in the present thesis.

4.1.5 Arg-1 in human helminth-Mtb co-infection studies

In the present thesis, helminth-induced Arg-1 was not associated with an impaired immune response to Mtb, resulting in a similarly sufficient control of Mtb infection and histopathology. The highly systematic approach in using three different helminth species substantiates that the impact of helminth-infection estimated by literature may have been artificially exaggerated. Similar to experimental outcomes in animals, literature suggests a diversity of outcomes is observed in human co-infection data (112,128,145–148). In light of the data presented in the present thesis, their relevance may have been overestimated due to high variability in the model parameters employed.

The current state of scientific knowledge on the role of Arg-1 in human helminth-Mtb co-infection is limited and a comparison of bacterial burden between individuals is not feasible usually. Arg-1-positive lesions in TB patients were shown by Pessanha *et al.* and indicate that the concept of Arg-1-mediated mechanisms in immunomodulation by Mtb is applicable to TB in human subjects (98). However, this

was observed in Mtb infection alone and not in helminth co-infection. One publication exists, that investigated whether Arg-1 may serve as a marker for lung inflammation in patients with active TB and concomitant helminth infection. Patients with acute TB and *S. mansoni* infection showed elevated arginase activity in serum compared to TB patients without *S. mansoni* infection (115). However, it remains unclear whether Arg-1 levels correlated with the extent of pulmonary pathology. In addition, the source of Arg-1 in these patients is not clear. Nevertheless, these data indicate a role for helminth-induced Arg-1 in the human co-infection situation. Along this line, the authors suggest a potential use of Arg-1 as a marker for lung inflammation in TB if plasma Arg-1 levels could be linked to disease severity. Hypothetically, helminth-induced, circulating regulatory monocytes or MDSCs expressing Arg-1 might inhibit inflammatory responses with the aim to sustain helminth survival (115).

4.1.5.1 Cytokines in co-infected individuals

Several authors report compromised Th1 and Th17 responses and increased Th2 responses that may imply consequences for control of Mtb infection (111,112,146,147,149). Resende *et al.* observed that patients co-infected with ≥1 intestinal helminth (mostly *S. stercoralis*) and Mtb had marked differences in their T cell compartments which were associated with decreased IFN-γ and increased IL-10 levels compared to TB patients or healthy PPD-positive control subjects. Interestingly, co-infected patients appeared to also have wider lung tissue involvement than TB patients without helminth infection, although this was not statistically significant. The authors suggest that a Th2 response may facilitate persistent TB and disease severity (111). Another clinical trial report on subjects with latent TB infection (LTBI) who were co-infected with intestinal hookworms showed depressed Th1 and Th17 responses and increased Th2 responses (149). In another study in *S. stercoralis*-Mtb co-infected patients, helminth-infected individuals appeared protected during active disease in terms of lower plasma concentrations of acute phase proteins, matrix-metallo-proteinases, and other systemic immune activation markers (146). This seems to contrast the author's previous suggestion of aggravated disease susceptibility during Strongyloides infection (149). Nevertheless, it appears plausible that hookworm co-infection during LTBI may result in different effects than during active TB. Another published report on *S. stercoralis*-Mtb co-infection showed data on T cell cytokine responses in patients with active and latent disease. Co-infected subjects had elevated type 2 cytokine levels (IL-4, IL-5 and IL-13) compared to individuals without helminth infection. In addition, LTBI subjects showed reduced type-I interferons, IL-6, IL-12, and granulocyte-macrophage colony-stimulating factor (GM-CSF) compared to co-infected patients with active TB (147). These data point to immunomodulation during LTBI and active disease and might again support the notion that latency and active disease may be affected differently. Along similar lines, another report shows that filaria-Mtb co-infection led to reduced Th1 and Th17 responses in patients with LTBI. The data suggest that filarial co-infection inhibits the production of IL-12, IFN-γ, IL-23, and IL-17 via cytotoxic T lymphocyte antigen (CTLA)– and programmed death (PD)–1–mediated mechanisms (112). Yet other data showed concurrent development of Th2 and Th1 responses in LTBI individuals co-infected with filaria (150). Antigen-specific immune responses to filarial antigens or Mtb-specific antigens in LTBI individuals were similar between subjects with or without filarial co-infection. However, memory T cell compartments for Mtb and filarial nematodes seem to be distinct. Moreover, IL-4 responses to filarial antigens seem to be attenuated in individuals with Mtb DTH responses (150).

The latter is particularly interesting in light of the observation that animal data in the present thesis as well was from literature (114) may hint at a negative impact of Mtb infection on concomitant *L. sigmodontis* infection in mice. Some evidence suggests that patients with active TB are more often co-infected with helminths and often multiple helminth species at the same time compared to Mtb-negative household contacts (151). In the context of the relatively low *L. sigmodontis* worm counts in the present thesis, this could imply that Mtb infection may affect the susceptibility to helminth infections. Hence, it cannot be excluded that Mtb infection affects the control of helminth infection, thereby limiting or enhancing helminth-induced immunomodulatory effects and their complex integration into the immune response against Mtb.

In the present thesis, cytokines characteristic for protective Th1- and Th17 responses as well as CAM induction were not compromised by co-infection with helminths. In contrast, several publications from clinical studies observed changes in the cytokine compartments important for control of Mtb infection (111,112,146,147,149). Yet the clinical relevance of these effects on the immune response to Mtb remains uncertain given that their impact on development of active TB remains unclear in absence of data on disease severity and/or rates of reactivation in co-infected individuals. Data on reactivation from latent to active disease in a human co-infection setting is scarce. Some reports describe T cell responses and cytokine levels, yet often without follow up of patients' disease progression. Data from one human study showed a (sometimes weak) association between *S. mansoni* infection and progression to TB. The study cohort consisted of 2,300 individuals infected with HIV who were enrolled between 1995 and 2003 in Uganda, mostly before wider availability of antiretroviral therapy (152). As such, conclusions from this are limited to an immunocompromised population that is not reflective of the current HIV-positive population anymore due improved standards of care in antiretroviral therapy. Moreover, HIV-helminth-Mtb co-infection may have increased the complexity of immunomodulatory interactions significantly. The only other published prospective cohort study enrolled 5096 individuals and investigated progression rates to active TB in subjects with and without helminth infection at baseline. Individuals were followed for 10 years with three follow-up visits every 2.5 years. The results demonstrate that development of active TB was not associated with any helminth infection, although the analysis is limited by the fact that patients could not be assessed for acquisition of helminth infections after baseline status determination (145). Despite this limitation, the outcome suggests a negligible impact of helminth-infection on TB in humans which is consistent with the animal data reported in the present thesis.

4.1.5.2 Human lung pathology

Data on human tissue pathology in co-infected individuals are scarce. Monin *et al.* reported a potential role for serum arginase activity in individuals with active TB as this was correlated with a higher degree of tissue damage (based on chest radiography) (115). However, this may imply a potential usefulness of serum Arg-1 as a marker, while not necessarily reflecting a causal relationship. Others have also reported aggravated lung damage in co-infected individuals as assessed based on inflammatory area involved in co-infected patients which was associated with impaired immune responses to Mtb (111). Aggravated lung tissue pathology in co-infected patients may suggest higher rates of disease transmission. Alternatively, more severe TB may compromise the host's resistance to helminth infection

which may in turn explain the sometimes higher frequencies of helminth infections observed in TB patients with active disease (151).

Overall, the data presented in the present thesis demonstrate that co-infection with helminths does not negatively affect Mtb infection in mice. It is difficult to compare murine pulmonary bacterial loads to Mtb proliferation in co-infected humans due to feasibility issues in obtaining bacterial count estimates from the human lung. However, when looking at the data on TB progression and/or reactivation, the limited information suggests a non-significant impact of co-infection with helminths. This is counterintuitive given the multitude of publications that showed an impact on the immune response to Mtb in both murine co-infection models and clinical studies. In the present thesis, no changes in protective cytokines responses and markers of classical macrophage activation or pulmonary CFU counts were observed despite significant Arg-1 induction. In the context of other mouse model data and the human co-infection setting, this leads to the questions which changes in the immune response – or what degree of change – would be required to translate into a clinically relevant effect on the course of TB disease and the development of pathology. Taken together, the expectations that were raised by several publications revealing changes to the immune response without follow-up of disease progression in co-infected individuals may have been inflated to some extent. From the totality of data, a helminth-induced modulatory effect on the immune response against Mtb cannot be denied, although it may not necessarily have translated into a biologically relevant effect. Consequently, its clinical relevance appears negligible.

4.2 Mtb-induced Arginase-1

4.2.1 A question of virulence?

In the present thesis, Tie2cre^{pos} Arg1$^{f/f}$ mice were infected for the first time with a hyper-virulent Mtb HN878 strain. The hypothesis of increased virulence being associated with the degree of Arg-1 induction and the degree of disease susceptibility was supported by *in vitro* data (108,109,153). Infection with two CDC1551 and HN878 Mtb clinical isolates led to increased gene expression of *Arg1* in macrophages *in vitro,* with HN878 leading to stronger induction of *Arg1* gene expression compared to CDC1551 (109). Along similar lines, Andrade *et al.* showed that virulence in terms of proliferation capacity of different *M. bovis* strains was associated with the capacity to induce Arg-1 to undermine protective NO production *in vitro* (153). This *in vitro* data raised the question whether an Arg-1 induction – and possibly a higher degree of arginase activity – could be associated with Mtb strains that are more virulent than the common lab strain Mtb H37Rv. Based on this published *in vitro* data, the observation that no discernable phenotype of Mtb HN878 infection could be observed in mice lacking Arg-1 in macrophages in the present thesis, was unexpected. Others have shown that when experimental mice were infected with a virulent clinical CDC1551 isolate, *Nos2* gene expression increased as expected around day 21, while a moderate *Arg1* increase could be observed at the same time. However, standard deviations were rather wide and no statistical significance was reported. Unfortunately, the methodology of this experiment including the infectious dose and the mouse strain were not disclosed by the authors (108). Thus, no meaningful comparison is possible. Few other data is available from *in vivo* infection experiments

investigating Arg-1 in the context of hyper-virulent Mtb infection. In this regard, Guler *et al.* published data from a LysMcre IL-4Rα$^{-/lox}$ mouse model in which macrophages and neutrophils lack IL-4Rα expression. Consequently, AAM induction via the IL-4/IL-13 axis was absent. When infected with Mtb HN878 or the common reference strain Mtb H37Rv, Balb/C WT and LysMcre IL-4Rα$^{-/lox}$ mice showed no major differences in terms of survival, bacterial growth, pulmonary pathology, and T cell responses. Immunohistochemical staining of NOS2 and Arg-1 did not differ between WT and LysMcre IL-4Rα$^{-/lox}$ mice (122). Since type 2 cytokines are not normally induced during low-dose Mtb infection to begin with, this is not surprising (97). Interestingly, Arg-1 induction was observed in both WT and LysMcre IL-4Rα$^{-/lox}$ mice but only after 18 weeks post-infection with 100 CFU Mtb H37Rv (122). Although the result that Mtb may induce Arg-1 independently of IL-4Rα signaling is in line with previous publications (108,109), the time points at which Arg-1 was detected vary vastly between 3 weeks for a clinical CDC1551 isolate (108) and 18 weeks for Mtb H37Rv (122) which is beyond the latest time point tested within the experiments described in the present thesis (11 weeks). Regardless, the Arg-1 expression observed in WT and LysMcre IL-4Rα$^{-/lox}$ mice may still be explained by IL-4Rα-independent mechanisms that were intact in both WT and LysMcre IL-4Rα$^{-/lox}$ mice, *i.e.* TLR-2/Myd88-signaling and autocrine-paracrine Arg-1 induction via secretion of IL-6, IL-10 and G-CSF (109). Regarding virulent Mtb infection, the significance of Arg-1 induction 18 weeks post-infection with Mtb HN878 remains unclear at this point given that no phenotype of LysMcre IL-4Rα$^{-/lox}$ mice was detected. Guler *et al.* support their claims further with *in vitro* data from IL-4/IL-13-stimulated BMDMs that were infected with Mtb HN878 (122). Genome set enrichment analysis (GSEA) showed enrichment in the IL-6, IL-10, G-CSF pathway but not in the IL-4Rα pathway following HN878 infection, but neither led to an alteration in *Arg1* gene expression. In the very least, the absence of an effect on the IL-4Rα pathway is puzzling given that BMDMs had been stimulated with IL-4 and IL-13 prior to infection. Evidence exists that these cytokines should have been able to elicit an effect on Arg-1 production *in vivo* (97). At the same time, enrichment of the IL-6, IL-10, G-CSF pathway was detected in BMDMs but did not seem extensive enough to alter *Arg1* expression *in vitro*. Moreover, autocrine-paracrine IL-10, IL-6, and G-CSF signaling could serve to induce increased IL-4Rα expression on the cell surface and thus enhance the responsiveness to IL-4/IL-13 signaling (109) - as such the absent effect in IL-4- and IL-13-stimulated cells seems baffling. While IL-10 alone has been shown to induce Arg-1 on its own, IL-10 levels might not have occurred at levels high enough to induce a discernible effect, given that IL-10-mediated Arg-1 induction was described in an IL-10^{tg} mouse model in which excessive IL-10 levels were produced (96). This begs the question whether the Mtb HN878 strain could have suppressed IL-4Rα signaling pathways or its downstream effects in IL-4- and IL-13 stimulated BMDMs. Regardless, in the present thesis, Mtb HN878 infection did not produce a phenotype in Tie2cre^{pos} Arg1$^{f/f}$ mice or competent littermates up to 11 weeks post-infection with the HN878 strain. Overall, the data from Guler *et al.* indicate no role for IL-4Rα-mediated Arg-1 induction in infection with Mtb HN878 *in vivo*. This is consistent with previously published data that showed no role for IL-4Rα-signaling in low-dose Mtb infection *in vivo* (93,94). The data shown in the present thesis confirm directly that Arg-1 may not play a prominent role as virulence factor in Mtb HN878 infection. This is particularly surprising as pulmonary CFU counts reached similar orders of magnitude as mice infected with high-dose Mtb H37Rv, though high-dose infection may have started the growth phase at a considerably higher level and may have shortened the time by which considerable CFU

counts were reached. Therefore, it cannot be excluded that a faster proliferation capacity may be associated with Arg-1 induction, or that the infectious dose may impact Arg-1 induction directly.

4.3 Exogenous Arg-1 induction

4.3.1 Arg-1-dependent disease susceptibility in high-dose Mtb H37Rv infection

A high proliferation rate resulting in rapidly increasing bacterial numbers is an established virulence factor of Mtb (153). High-dose infection mirrors the high exposure to Mtb that is faced in countries with a high burden of TB. In high-burden countries, TB is often severe, virulent strains are more prevalent and exposure is potentially higher due to high disease burden (3,28). In light of the variable, overall moderate and reversible impact of concomitant helminth infections, co-infection alone seems an insufficient explanation for this disease severity. Evidence suggests that the infectious dose may directly affect immune polarization. This is illustrated by data showing that low-dose *M. bovis* BCG infection led to a Th1 response while high-dose infection resulted in a mixed Th1/Th2 polarization (87). Surprisingly, virulent HN878 infection of Tie2cre^{pos} Arg1$^{f/f}$ mice and competent littermates showed no role for arginase-mediated induction of pathology or susceptibility in the present thesis. While El Kasmi *et al.* (108) showed that Mtb H37Rv induced Arg-1 in macrophages, the authors used 200 CFU to inoculate mice instead of the 100 CFU dose in the experimental set-up employed in the present thesis. This dose discrepancy led to the question whether the degree of Arg-1 induction may depend on the infectious dose and affect the degree of disease susceptibility induced by Mtb H37Rv. In order to investigate the impact of a high infectious dose on Arg-1-mediated disease susceptibility while avoiding the early terminal endpoint associated with high-doses of highly virulent Mtb infection in mice, Tie2cre^{pos} Arg1$^{f/f}$ mice and competent littermates were infected with low and high doses of Mtb H37Rv in the present thesis.

4.3.1.1 Mycobacterial growth

In the present thesis, low-dose Mtb H37Rv infection did not lead to Arg-1 induction and had no effect on disease susceptibility in Tie2cre^{pos} Arg1$^{f/f}$ mice or competent littermates. Some residual arginase activity was seen in Arg-1-competent mice, but the magnitude of this was low and transient, not affecting CFU counts and far below helminth-induced levels of *Arg1* gene expression or arginase activity. In contrast, mice lacking Arg-1 in macrophages were protected during high-dose infection with Mtb H37Rv. High-dose infection induced arginase activity at an approximately 10-fold higher level than low-dose infection. This elevated arginase activity was associated with higher mycobacterial load in the lung, more pronounced disease severity, and exacerbated inflammation in Arg-1-competent animals. Interestingly, the level of arginase activity in lung homogenates while higher than in low-dose infection was still considerably lower than during co-infection with helminths. Therefore, the mechanism of Arg-1 induction (Th2-dependent or -independent) appears to be highly relevant for susceptibility to TB. This may be due to the location of Arg-1 induction in close proximity to Mtb within the same cell and the absence of other potential helminth-mediated immunomodulatory effects.

Data from experiments by others using genetically diverse outbred (DO) mice offer some indication that high pulmonary Arg-1 activity was associated with increased inflammation. DO mice that showed enhanced control of Mtb infection showed lower levels of Arg-1 (115). This lends direct support to the data shown in the present thesis as it hints not only at a role for Arg-1 as a susceptibility factor in Mtb infection but also at relationship between Arg-1 and the degree of disease susceptibility. Since mice lacking macrophage Arg-1 were better protected against high-dose Mtb infection in the present thesis, a role of Arg-1 as a susceptibility factor in Mtb infection is directly confirmed.

Interestingly, another previous publication was able to show that high-dose Mtb H37Rv of LysMcre IL-4Rα$^{-/lox}$ mice showed no discernible phenotype compared to WT mice in response to intranasal infection with 10^4 CFU Mtb H37Rv (122). This could suggest that the IL-4Rα-Arg-1 axis is not relevant in high-dose infection with Mtb. The authors' histological analyses showed that Arg-1 was detected in lung tissue of high-dose infected WT and IL-4Rα$^{-/-}$ mice at week 18 post infection, possibly through a still functional Th2-independent IL-6/Arg-1 axis (109). However, caution should be exercised in comparing these data given the differences in the route of administration and dose which may account for the striking differences in seen in terms of survival time: in the present thesis, Arg-1-competent mice reached the terminal endpoint within 3-4 weeks post-Mtb infection, whereas Guler *et al.* report survival of WT mice for as long as 8 weeks (122). However, it has been shown that type 2 cytokines are not usually induced in murine models of experimental TB and, where examined, considerable IL-13 or IL-10 levels resulting from transgenic expression were needed in order to induce discernible effects (96,97). Further support of the hypothesis that the degree of Arg-1 induction and disease susceptibility may depend on the infectious dose derives from a recent publication that showed suppressor of cytokine signaling 3 (SOCS3)-mediated regulation of IL-6-dependent arginase activity. Schmok *et al.* showed Arg-1 induction in response to aerosol infection with 1000 CFU Mtb H37Rv. When Arg-1 was increased further in absence of SOCS3, mice developed a hyper-inflammatory phenotype probably facilitated by the early presence of AAMs that provided a proliferatory advantage to Mtb (117). The high dose of 1000 CFU Mtb H37Rv led to Arg-1 induction is in line with the data in the present thesis, and together they underscore the important role of the infectious dose in Arg-1 induction. Moreover, Schmok *et al.* showed that inflammation was aggravated in SOCS3-deficient mice which correlated with higher levels of Arg-1, implying that susceptibility to infection may increase with higher arginase activity. Together with this, the data in the present thesis directly substantiate a dose-response relationship between the infectious dose, the degree of Arg-1 induction, and disease susceptibility. Overall, the infectious doses used across literature and in comparison to the data described in the present thesis may also explain the varying impact on susceptibility to Mtb that was observed.

4.3.1.2 Cytokines in high-dose Mtb *infection*

In the present thesis, high-dose Mtb H37Rv infection (2200 CFU) led to increased levels of *Il6* gene expression and decreased levels of *Il12* in lung homogenates of Arg-1-competent mice, whereas *Ifng*, *Tnf*, and *Il17a* gene expression levels remained unchanged. In mice lacing Arg-1 in macrophages, *Il6* levels remained low and *Il12* levels remained high instead of dropping at week 4 post-infection. Qualls *et al.* have shown that IL-6 signaling may result in Arg-1 induction (109). Further, Schmok *et al.* demonstrate a role for dysregulated Arg-1 in the development of a hyper-inflammatory phenotype in

response to 1000 CFU Mtb H37Rv via the aerosol route. In this context, they observed increased IL-6 levels and decreased IL-12 levels in the lung and demonstrated that IL-6 is linked to Arg-1-mediated susceptibility and pathology in Mtb infection (117). While IL-6 may be responsible for the increased Arg-1 induction in macrophages of Arg-1-competent mice (109,117), the increased susceptibility to Mtb infection in the present thesis may – in part – have been mediated by a compromised Th1 response potentially resulting from a lack of IL-12 (117). Of note, IL-6-signaling has also been linked to decreased MHC class II cell surface expression on antigen presenting cells which may adversely affect activation of adaptive immunity (61). Based on CFU counts and gene expression data alone, an impaired T cell response cannot formally be excluded in the present thesis. Nevertheless, gene expression levels of *Ifng*, *Tnf*, *Il17a*, and *Nos2* in lung homogenates were similar between Tie2cre^{neg} Arg1$^{f/f}$ and Tie2cre^{pos} Arg1$^{f/f}$ mice supporting functional Th1/Th17 responses on the transcriptional level.

The data shown in the present thesis underscore a direct contribution of Arg-1 to mediating a hyper-inflammatory phenotype at higher infectious doses, possibly involving the IL-6/Arg-1 axis. It should be considered though, that *Il6* gene expression was relatively low in Tie2cre^{pos} Arg1$^{f/f}$ mice, the reasons for which are unclear as there is no obvious explanation why Mtb infection in Tie2cre^{pos} Arg1$^{f/f}$ mice should have led to lesser *Il6* induction. Based on these lower *Il6* levels, ameliorated inflammation may have been – in part – due to this more moderate *Il6* induction. The most significant change in body weight and disease score in high-dose infected mice was observed between 3-4 weeks post-infection, coinciding with the time at which onset of adaptive immunity is usually observed. Immune cell populations remain to be explored in order to characterize the contribution of T cell responses in Tie2cre^{neg} Arg1$^{f/f}$ and Tie2cre^{pos} Arg1$^{f/f}$ mice during high-dose Mtb infection. To this end, the 1000 CFU dose employed by Schmok *et al.* (117) may offer the advantage of avoiding the early terminal endpoint that was associated with the infectious dose of 2200 CFU while still inducing a degree of Arg-1 that mediates detectable effects on susceptibility to Mtb infection.

4.3.1.3 Pulmonary histopathology

In the present thesis, high-dose infection with Mtb H37Rv was associated with Arg-1 induction and resulted in exacerbated inflammation and impaired mycobacterial control. It appears that Arg-1-competent mice developed extensive inflammatory aggregates in the lung, reminiscent of the hyper-inflammatory phenotype described in the SOCS3-deficient mouse model, that was associated with dysregulated (elevated) arginase activity in the lung in response to aerosol infection with 1000 CFU Mtb H37Rv (117). This, together with the early mortality observed in the present thesis, lends further support to a dose-response relationship between the infectious dose of Mtb H37Rv (via aerosol) and the elicited degree of Arg-1 induction, which then appears to translate into more pronounced disease.

Other than this, few histopathological analyses exist in literature. Heitmann *et al.* described stratification of granulomatous lesions and subsequent necrosis upon Mtb infection in mice that overexpressed IL-13 under control of a T cell promoter, resulting in excessive IL-13 induction after Mtb infection. IL-13^{tg} mice developed stratified and necrotic lesions similar to those in human Mtb infection with elevated Arg-1 levels implying a role of Arg-1 in contributing to development of pathology (97). In the present thesis, Arg-1 induction was triggered by intracellular Mtb infection at a certain dose. As discussed, the mechanism of Arg-1 induction in macrophages appears to be important for susceptibility

to Mtb infection. Arg-1 induction in model from Heitmann *et al.* was mediated by excessive IL-13 levels and IL-4Rα-signaling (97), instead of a potentially Th2-independent mechanism as in the present thesis. Therefore, the differences in lesion morphology are not necessarily contradictory. Regardless, the data from Heitmann *et al.* provided indirect evidence that implied a role for increased Arg-1 expression in mediating susceptibility to Mtb infection. This is directly confirmed by the data described in the present thesis. With regards to collagen deposition, the histological analyses of the present thesis are difficult to interpret based on microscopic evaluation alone. Nevertheless, the distribution of collagen throughout the granulomatous lesions seems different in mice lacking Arg-1 in macrophages which presented with ameliorated pathology. It is tempting to speculate that less L-Arg may be metabolized through absent Arg-1 and thus is not available for downstream polyamine-, proline- and collagen-synthesis. Others have suggested, however, that in absence of macrophage Arg-1, more L-Arg may become available to other arginase isoforms and affect ornithine catabolizing enzymes, thereby increasing overall proline synthesis, which has been shown to be beneficial for growth of other intracellular pathogens (106). Alternatively, collagen production by neighboring fibroblasts may be increased due to a lack of substrate competition by macrophage Arg-1. Pesce *et al.* have shown that Arg-1 expressing AAMs inhibit fibrosis as well as T cell responses in the context of *S. mansoni*-caused Th2 inflammation. In this scenario, increased Th2 responses presented with inflammatory liver pathology including extensive fibrosis in *S. mansoni*-infected LysMcre^{pos} Arg1$^{-/lox}$ mice (which delete Arg-1 in macrophages and neutrophils), ultimately leading to early mortality (125). In contrast, the present thesis suggests a different outcome in the context of Mtb infection, possibly owing to specific induction of Arg-1 in Mtb-infected macrophages where Arg-1 may thwart CAM effector functions more directly.

4.3.2 Relieved endogenous Arg-1 inhibition by L-NIL treatment

In the present thesis, further support for the hypothesis that macrophage Arg-1 is a susceptibility factor in Mtb infection derives from *in vivo* experiments during which WT mice were administered L-NIL to disinhibit Arg-1, resulting in increased arginase activity. Heitmann *et al.* used L-NIL to stimulate arginase activity which was associated with increased bacterial growth and necrotizing granulomatous lesions (97). The present thesis shows for the first time that these effects are directly attributable to Arg-1 in macrophages. L-NIL treatment led to increased arginase activity in lung homogenates which was associated with increased pulmonary bacterial loads and granuloma necrosis. Mice lacking Arg-1 in macrophages were partly protected from this effect. It should be kept in mind that L-NIL stimulates arginase activity while inhibiting NOS2 at the same time, thereby relieving the inhibition exerted by the endogenous Arg-1 inhibitor NOHA. Based on the data presented in the present thesis, it is difficult to distinguish between how much of the exacerbated pathology and uncontrolled growth of Mtb seen in L-NIL treated Tie2cre^{neg} Arg1$^{f/f}$ mice was due to elevated arginase activity and how much was due to inhibition of NOS2 and CFU-mediated effects on inflammation.

By comparison, mice lacking the *Nos2* gene display increased PMN cell infiltrates with cellular debris rupturing into the airways (154). This may explain why the effect of L-NIL was only partly reversed in Tie2cre^{pos} Arg1$^{f/f}$ mice in the present thesis.

In absence of Arg-1, substrate competition between Arg-1 and NOS2 does not occur. Thus, in L-NIL-treated Arg-1-deficient mice, more L-Arg would be available for NOS2 and could potentially

overwhelm the L-NIL-mediated inhibition of NO synthesis (155). If NOS2 inhibition was thus less effective in Arg-1-deficient mice than in Arg-1-competent littermates, this might contribute to the improved mycobacterial control observed in Arg-1-deficient mice due to a relatively higher NO production. In contrast, L-NIL treatment of Arg-1-competent mice L-NIL-mediated inhibition of NOS2 could be more effective and result in increased arginase activity instead of being overwhelmed by an over-abundance of L-Arg. This may explain the increasing CFU counts and aggravated pathology. Increasing bacterial numbers in turn may lead to antigenic overload and increased inflammation. Depending on the amount of L-Arg that is metabolized by Arg-1 and how much of it is available to T cells, T cell inhibition via L-Arg depletion (100,103) may or may not work and contribute to decreased mycobacterial control and uncontrolled inflammation.

To complicate things further, L-Arg may also be used by Mtb itself for proline synthesis and growth (107). Arg-1 activity feeding into polyamine synthesis was shown to favor growth of *L. major in vivo* as well (106). Therefore, the aggravated pathology in L-NIL-treated mice may in part have been caused by increased substrate availability to Mtb. Moreover, the pathways of macrophage activation/polarization may affect the transport of L-Arg into the cell by influencing cellular transporters (156,157). In face of NOS2 inhibition by L-NIL in Tie2cre^{pos} Arg1$^{f/f}$ mice in the present thesis, where the activity of both enzymes is reduced or absent, it is tempting to speculate that L-Arg uptake by macrophages may be negatively affected as well. However, the observation of L-NIL stimulated pathology in association with increased arginase activity, which was partly reversible in mice lacking Arg-1 in macrophages, is consistent with data showing that WT mice infected with Mtb and treated with L-NIL developed TB pathology and necrotic lesions similar to IL-13^{tg} mice (97).

The role of macrophage Arg-1 in a model where NOS2 is incapacitated was also investigated in a model where Tie2cre^{pos} Arg1$^{f/f}$ mice were crossed onto a *Nos2*$^{-/-}$ background, resulting in a Tie2cre^{pos} Arg-1$^{f/f}$ NOS2$^{-/-}$ double-knockout (DKO) mouse, that is NOS2-deficient and lacks Arg-1 expression in macrophages (120). A lack of Arg-1 in macrophages appeared to drive inflammation in DKO mice infected with 10^4 CFU Mtb H37Rv via the dermal route. Hematogenous dissemination then resulted in development of hypoxic granulomatous lesions in the lung. In this model, the absence of Arg-1 in macrophages led to aggravated pulmonary pathology and increased mycobacterial growth. The presence of Arg-1 expression in hypoxic lesions was associated with reduced T cell proliferation. This suggests that Arg-1 prevents an exaggerated T cell response (120). Absence of this down-modulating effect on T cell proliferation when Arg-1 was lacking could plausibly have led to the aggravated pathology and increased CFU counts observed in DKO mice (120). Yet at the same time, NOS2 deficiency would mean that a key macrophage defense mechanism against Mtb is absent, just as likely contributing to increased CFU counts and aggravation of tissue damage. Although NOS2 is absent and the same Tie2cre Arg1$^{f/f}$ strain was used for generating DKO mice, the conditions employed in this model are vastly different and render it not entirely suitable for comparison to the data described in the present thesis. While L-NIL treatment does inhibit NOS2, this inhibition is never complete and some degree of NOS2 activity remains. This is not the case in *Nos2*$^{-/-}$ mice, which lack NOS2 expression completely. Moreover, L-NIL administration was only started after Mtb infection had already been established in the present thesis, but *Nos2*$^{-/-}$ deletion results in absence of NOS2 from the beginning of infection. The routes of infection differ between aerosol and dermal infection and a significantly higher infectious dose

was used in the latter (120). As such, both models cannot be directly compared. Yet their seemingly contrasting effects of Arg-1 deficiency are noteworthy. In the present thesis, L-NIL treatment of Mtb-infected Tie2cre^{pos} Arg1$^{f/f}$ mice led to amelioration of inflammation and lower CFU counts than in Arg-1-competent littermates, while Duque-Correa *et al.* (120) report the opposite effect: lack of Arg-1 in NOS2-deficient mice led to aggravated inflammation and increased bacterial proliferation. Aside from the contributions of NOS2 deficiency and/or Arg-1 mediated inhibition of NOS2 to impaired mycobacterial control, this begs the question whether the timing of Arg-1 mediated T cell suppression (100,103) may be crucial in development of pathology. If Arg-1 mediated T cell suppression occurs too early, control of Mtb infection may be insufficient, in which case a lack of Arg-1 may be beneficial. However, if T cell responses are not down-modulated at the right time, excessive inflammation and host tissue damage may occur. In this situation a lack of Arg-1 mediating T cell inhibition may appear detrimental.

4.3.3 A role for Arg-1 in human TB?

Given that the susceptibility to murine Mtb infection may be inducible by the degree of arginase activity, the question arises whether Arg-1 may be a potential susceptibility factor for TB in the human host. While evidence on the role of Arg-1 in human TB is scarce, a role of Arg-1 in human immunity has been documented: arginase is expressed by leukocytes of the mononuclear lineage in response to tissue injury, is detected in BAL samples of Asthma patients, and is found in skin lesions of psoriasis patients (158). In infectious diseases, Arg-1 appears to be expressed in immune cells, but not necessarily by macrophages. In a fungal infection model, Munder *et al.* showed constitutive Arg-1 expression by human PMNs. In addition, Munder *et al.* showed that Arg-1 exerts a role in antimicrobial defense by driving arginine depletion in the phagolysosome of PMNs (158). It has also been shown that Arg-1 is not only present in the phagolysosome but is also released by human PMNs during necrosis, driving extracellular L-Arg depletion in order to down-modulate T cell responses (103,159). Given the different cellular sources of Arg-1 between the mouse and the human host and the differences in pathogenesis following Mtb infection, a role for macrophage Arg-1 in human TB has been discussed controversially until Pessanha *et al.* demonstrated Arg-1 expression in human granulomas. Pessanha *et al.* were able to show that both macrophages and type II pneumocytes express Arg-1 in lung tissue sections of TB patients (98). Arg-1 expression in granulomas of non-human primates and humans, with similar Arg-1 expression levels in both species, further supports the notion of a conserved role of Arg-1 throughout different species. Therefore, the potentially detrimental role of Arg-1 in inducing susceptibility to Mtb infection and pathology may apply to TB pathogenesis in the human host as well. Interestingly, Mattila *et al.* showed considerable co-expression of Arg-1 and NOS2 in the same cells rather than a local segregation of Arg-1 and NOS2-expressing macrophages (99). Based on this, the concept of Arg-1 induction by Mtb in infected macrophages to undermine CAM-effector functions during intracellular Mtb infection may be more relevant to the human situation than previously anticipated. As such, the observation that Arg-1 induction by Mtb in macrophages depends on the infectious dose may be especially relevant in an endemic setting, where exposure to Mtb is often high due to the high burden of disease, close living quarters, and possibly suboptimal hygiene standards. Moreover, alternative activation of macrophages appears to be increased (relative to classical activation) in TB patients with

MDR-TB/XDR-TB, further supporting the association between Arg-1 and severity of TB (101) that was also shown in the murine model of TB in the present thesis.

Monin *et al.* investigated if the degree of pulmonary pathology in patients with active TB in an endemic setting was associated with Arg-1 expression to identify its potential for use as a biomarker for the extent of pulmonary pathology. In this model, a positive correlation was shown between the degree of tissue damage (determined by chest X-ray) and arginase activity measured in patient sera. Arginase activity in serum was further supported by increased *Arg1* gene expression in PBMCs isolated from TB patients (115). This suggests that the concept of TB pathology as a function of the degree of arginase induction may be applicable in the human host, although differences may exist between the cellular sources and their location. The present thesis provides evidence that the degree of Mtb-induced arginase activity is associated with disease susceptibility and pathology, providing a direct mechanistic foundation for the positive correlation in human TB patients observed by Monin *et al.* (115). In light of the relationship between the infectious dose and the degree of Arg-1 induction shown in the present thesis, it is tempting to speculate, that TB patients in an endemic setting may have been exposed to a relatively high dose compared to patients from non-endemic settings and as such may have received a dose high enough to induce a measurable degree of arginase activity (115). It remains to be seen what would be the added benefit of arginase as a biomarker when radiology is an established pillar of TB diagnosis. Even more so in light of the observation that arginase levels in serum of patients co-infected with helminths were even higher than in patients with TB alone, but no data were presented as to the extent of tissue pathology in co-infected persons with active TB. Possibly, the positive correlation between serum arginase and tissue pathology described (115) may not apply to a co-infected population. However, the principle of the extent of pathology depending on the degree of arginase induction is supported by the data described in this thesis and by the positive correlation illustrated by Monin *et al.* (115).

Beyond the experimental evidence described in the present thesis, some functional analyses shed light on the role of Arg-1 in human TB patients. Zea *et al.* observed that a decrease of CD3-ζ expression on T cells from TB patients may likely result from increased arginase activity which led to a paucity of L-Arg as a substrate in the vicinity of T cells which in turn down-regulates CD3-ζ expression on their cell surface and impairs T cell receptor function (100). Monin *et al.* suggest, that while this anti-inflammatory role of Arg-1 is relatively well studied, Arg-1 may aggravate inflammation under other conditions (115).

Overall, these studies show that Arg-1 is present in the human granuloma and in human PBMCs. Arg-1 is measurable in serum of patients, although mechanistic analyses confirming the proposed roles of Arg-1 in human patients are needed. Secondary to its meaning for virulence, the possibility exists that Arg-1 may be a used as a biomarker for the extent of lung pathology. The degree of Arg-1 induction may depend on the infectious dose and a higher degree of Arg-1 induction may be associated with a higher degree of tissue pathology, thereby translating into susceptibility to disease. The data presented in the present thesis show a potentially detrimental role of Arg-1 in TB given that a lack of Arg-1 in macrophages was protective in terms of reduced CFU counts and tissue damage. This is consistent with others who described that Mtb can induce Arg-1 in macrophages in mice and non-human primates (99,108) and supports its potentially detrimental role in enhancing disease susceptibility in human TB (115).

4.4 Targeting Arg-1 to prevent reactivation of TB?

The data shown in the present thesis high-light a potentially detrimental role for Arg-1 in inducing susceptibility to Mtb infection which may hinge on the degree of arginase activity. It has been shown that Arg-1 is a) expressed in human TB within granulomas (98), b) can be released from other human granulocytes leading to T cell suppression and impaired cytokine responses (159), and c) is present in PBMCs isolated from human TB patients (115). Thus, inhibition of Arg-1 may prevent or reduce disease susceptibility and benefit TB patients, making it a potentially interesting target for biopharmaceutical medicinal products. Small molecule arginase inhibitors have been patented (160) and the principle of Arg-1 inhibition has been picked up in other research fields years ago. In cancer research, human myeloid-derived suppressor cells (MDSCs) expressing Arg-1 have been identified as potential targets for immunotherapy (161). Studies in ovarian cancer patients have shown the potential value of arginase inhibition in promoting anti-tumor immunity by inhibition of arginase activity on systemic levels (162). In infectious diseases, Arg-1 has been suggested as a promising target in *L. major* and *T. cruzi* infections in order to interfere with polyamine biosynthesis and parasite growth (104,163–165). Although mechanistically interesting, tolerability of Arg-1 inhibition in murine models of *T. cruzi* or *L. major* infection appears variable and was in some – but not all – cases associated with an early humane endpoint in animal experiments (165). In the context of Mtb infection, myeloid-derived suppressor cells (MDSCs) have been shown to express Arg-1, are linked to immunosuppression of T cell responses, and may provide a niche for growth of Mtb (166). Additionally, numbers of MDSCs or Arg-1-expressing macrophages appear to be higher in TB patients with more severe disease, including MDR-TB/XDR-TB patients (101,167). Some evidence suggests that treatment with phosphodiesterase inhibitors, which down-regulate Arg-1 (and NOS2) expression, may relieve the immunosuppressive capacities of MDSCs and facilitate improved mycobacterial control, thereby protecting from development of pathology (168). Indirect support for a potential benefit of targeting Arg-1 in Mtb infection derives from recent data on inhibition of the IL-10/STAT-3 axis (169). The authors showed, that inhalation of peptides inhibiting IL-10 and STAT-3 signaling led to decreased arginase activity and increase NOS2 activity which was associated with improved control of Mtb proliferation in mice (169).

A second potential benefit of Arg-1 inhibition may derive from the observation that expression of heat-shock protein 16.3, which is associated with Mtb latency, may induce expression of Arg-1 and other anti-inflammatory mediators in macrophages *in vitro* (170). The role of Arg-1 in models of Mtb latency has not been investigated. However, if establishment of latency could be hindered to some extent by inhibition of Arg-1, this may be an interesting adjunctive tool for post-exposure chemoprophylaxis of contact persons of TB patients.

One complicating factor that is rarely discussed is the importance of Arg-1 in the human urea cycle. Arg-1 deficiency is a severe metabolic disorder associated with hyperammonemia and argininemia. Clinical presentations are typically observed in infancy and include growth retardation and impaired cognitive development if left untreated (171). As such, the development of arginase inhibitors would need to take into account this safety concern. Nevertheless, this may not exclude a benefit for a temporal treatment of an adult target population in which Arg-1 levels may be reduced to physiological levels at specific target sites. This begs the question whether it would be possible to realistically target Arg-1 in macrophages inside granulomas and specifically in those where Mtb is inducing Arg-1 in host

cells. The heterogeneity of human granulomas within the same lung and the heterogeneity of macrophages expressing NOS2 or Arg-1 or both within the same granulomatous lesions may provide interesting challenges to achieving target specificity. Moreover, the timing of arginase inhibition may have a crucial effect on the result, bearing in mind that while Arg-1 inhibition was associated in literature with hyper-inflammatory phenotypes (115,117), it may also inhibit immune responses in other, different infectious disease contexts (125). Thus, depending on timing, Arg-1 may suppress both excessive and helpful T cell responses. Based on these observations, arginase inhibition at the wrong time may lead to the opposite of the desired effect. The target site of specific Arg-1 inhibition as well as the right timing would complicate the identification of those TB patients who might actually benefit from a treatment with an arginase inhibitor.

In some murine models of Arg-1 inhibition, reduced Arg-1 levels were linked to increased inflammation and matrix deposition defects, therefore use of an Arg-1 inhibitor may need to take into account the possibility of impaired wound healing (172).

In the context of helminth co-infection, Arg-1 may play a limited immunomodulatory role which is illustrated by the data shown in the present thesis and the literature discussed. Therefore, targeting Arg-1 may not necessarily be desirable depending on the helminth species involved. Furthermore, the added benefit of targeting Arg-1 in co-infected individuals over de-worming and addressing food deprivation would also need to be established. Of note, studies investigating the effect of deworming on co-infected TB patients yielded some interesting observations. Immunomodulation by helminths was reversed with treatment of the helminth infection in co-infected patients (126,173,174). This implies that de-worming may achieve the same if not actually a broader effect than targeting Arg-1 specifically. Studies in TB- and helminth-endemic countries where the rate of treatment failure is high, have revealed that co-infection with helminths appeared to be an independent risk factor for therapeutic failure. Significantly more patients who failed TB therapy were co-infected with hookworms (30.9%) compared to patients with treatment success (10.4% co-infected among them) (175). However, a randomized, controlled clinical trial on the effect of de-worming (albendazole vs. placebo) in patients receiving anti-TB therapy showed no significant impact on clinical outcome of TB treatment. This was unexpected in light of measurably improved weight gain and decreased IL-10 levels (173). However, it supports the question whether any helminth-induced immunomodulation on cytokine level is clinically relevant or whether host immune control of Mtb has co-evolved to the capacity of controlling damage to the host well enough in spite of co-infecting helminths. Furthermore, the higher percentage of helminth-infected individuals among those with TB-treatment failure in combination with the non-significant effect of de-worming may further support the idea, that TB may increase the susceptibility to helminth infections.

Overall, the data shown in the present thesis suggest that Th2-dependent helminth-induced Arg-1 may not be a critical contributor to TB susceptibility in co-infected hosts for a majority of helminth species. However, based on the literature discussed, it cannot be excluded that single helminth-species, such as *S. mansoni* may affect susceptibility to Mtb infection (115). In absence of a clear characterization of a potentially limited numbers of helminth species that may involve a detrimental role for Arg-1, deworming, improved hygiene, vector control, and nutrition rather than Arg-1-inhibition may be more beneficial to the common co-infected patient, as they hey may be more accessible and target more than Arg-1-mediated immunomodulatory effects alone. Moreover, anthelminthic therapy may

overall reduce comorbidity, nutritional impairment, developmental, and cognitive defects associated with helminth infections (8) - and would not need to distinguish between helminth infections that are associated with Arg-1-mediated negative effects or not.

A potentially different means of targeting Arg-1-mediated immunosuppression could be L-Arg supplementation. The literature on the use of L-Arg supplementation is contradictory and beneficial effects seem to depend on the disease under study (176). L-Arg supplementation may also bear the risk of facilitating pathogen growth through provision of amino acids for polyamine synthesis. Interestingly, L-Arg supplementation was helpful in *T. cruzi* infection in mice as evidenced by elevated NO levels in heart and plasma as well as electrocardiogram improvements (177). Similarly, L-Arg supplementation was able to rescue macrophage killing mechanisms in *Toxoplasma gondii* infection (102). In contrast, mice that received dietary L-Arg supplementation showed no discernible effect on Mtb infection (Hölscher, unpublished). This is consistent with evidence from clinical trials with TB patients. L-Arg supplementation in human patients at a dose of 6 g per day for 8 weeks did not result in changes in sputum culture conversion rate and disease severity in a randomized, double-blind, placebo-controlled clinical trial (178). Interestingly, others had previously shown the results of a randomized, double-blind, placebo-controlled study concluding on a benefit of a much lower dose (1 g) L-Arg hydrochloride adjunctive therapy for 4 weeks when investigating sputum conversion and disease manifestation (179). Nevertheless, this improvement may have been temporary. Unfortunately, no dose finding rationale was provided in either publication. A third clinical trial investigated the effect of dietary supplementation with peanuts (corresponding to a daily dose of 1 g L-Arg) but found no clinical effect other than in a secondary subgroup analysis according to HIV-status: HIV-positive TB patients who received peanut supplementation adjunctive to therapy showed improved clinical cure compared to HIV-positive TB patients receiving placebo instead of peanuts (180). However, patient numbers were low and secondary subgroup analyses were post-hoc and not powered. Overall, the more recent trial results seem to suggest no benefit of adjunctive L-Arg supplementation in therapy of TB (178).

Yet others have investigated the role of Arg-1 in asthma pathogenesis and found no role for Arg-1 in myeloid cells suggesting that while Arg-1 is a general marker of AAMs its function in regulation of Th2 responses may be limited (181). Other asthma models suggest a benefit of Arg-1 inhibition in asthma e.g. by promoting production of NO, which has prominent vasodilatory effects (182).

While targeting Arg-1 might relieve its immunosuppressive effects, safety concerns may arise if T cell responses were affected at the wrong time. Toxicity associated with malfunctioning of the urea cycle should also be limited. Overall, there is diversity in the data reported in literature on the potential usefulness of Arg-1 inhibition depending on the disease, timing, and the anti- and pro-inflammatory roles of Arg-1 which further complicate the evaluation of Arg-1 as a useful therapeutic target. However, arginase activity has been shown in the plasma of TB patients and correlated with the extent of tissue pathology (115). In addition, MDSCs may exert their immunosuppressive function through Arg-1-mediated mechanisms (168) and Arg-1 may well be associated with more severe disease in human TB patients (101,115,167). Support for Arg-1 as a useful target derives from animal experiments showing improved control of chronic Mtb infection when up-stream signaling pathways that are known to lead to Arg-1 induction, were inhibited (169). In the context of the literature discussed, the data shown in the present thesis provide direct evidence for a detrimental role of Mtb-induced Arg-1 in induction of disease

susceptibility and development of pathology, making it a potentially interesting target for relieving immunosuppression to enhance control of Mtb infection, potential challenges notwithstanding.

5 Overall conclusions and Outlook

In the present thesis, helminth-induced alternative activation of macrophages and expression of Arg-1 in the lung did not lead to increased susceptibility to TB in terms of bacterial burden, gene expression of pro-inflammatory and CAM-associated markers or changes in the granulomatous response during acute and chronic Mtb infection.

Th2-dependent Arg-1 induction appeared to be less influential for the control of Mtb infection than Th2-independent Arg-1 induction during high-dose Mtb infection *in vivo*. Therefore, the IL-6/Arg-1 axis (109) and/or TLR2/MyD88 (108) may be more relevant mechanisms of Arg-1 induction in macrophages regarding development of TB pathology and disease severity.

While no obvious role for Arg-1 could be observed in virulent HN878 infection, the outcome of high-dose Mtb H37Rv infection still implies an involvement of Arg-1 in virulent Mtb infection considering that high-dose infection is supposed to reflect high exposure observed in endemic countries and that virulent infection is often associated with a high mycobacterial burden. Strain-specific effects may not be excluded bearing in mind the potentially higher *Arg1*-inducing potential of CDC1551 compared to HN878 reported in *in vitro* (109). The observation that the degree of Arg-1 induction may depend on the infectious dose and may translate into increased pathology and disease severity may account for the diversity in outcomes observed in literature regarding the role of Arg-1 in murine aerosol infection models using Mtb H37Rv infection specifically (108,117), not accounting for mouse backgrounds, housing effects, and other factors.

Blocking the endogenous Arg-1 inhibitor by L-NIL treatment led to increased arginase activity, elevated bacterial counts, and granulomatous lesions that were characterized by a rim of Arg-1 positive cells and necrosis, effects which were partly reversible when macrophage-Arg-1 was lacking.

Taken together, these data provide direct evidence for a role of Mtb-induced Arg-1 as a susceptibility factor in Mtb H37Rv infection *in vivo*. When looking at low-dose compared to high-dose Mtb infection, bacterial growth, tissue pathology and disease severity were inducible by a higher infectious dose, which may have implications for Mtb infection in endemic regions where virulent strains are common and exposure is high due to high prevalence of TB.

Specific parameters remain to be investigated, most importantly the roles of IL-6 and IL-12 prompt further thoughts along the role of the IL-6/Arg-1 axis and DC migration to the draining lymph nodes. It is unclear whether Arg-1-expressing macrophages may leave granulomatous lesions and migrate to the lymph nodes where they may suppress T cell activation.

In the present thesis, arginase activity (artificially induced after an already established Mtb infection) was associated with necrotizing granulomatous lesions. Based on this, a possible role of Arg-1 in reactivation TB should be considered and could be explored in murine models of latency and reactivation.

Summary

The role of macrophage Arginase-1 (Arg-1) in modulation of immunity against *Mycobacterium tuberculosis* (Mtb) was investigated in the present thesis in order to elucidate whether susceptibility to Mtb infection and pathology may be acquired through Arg-1-mediated mechanisms. Arg-1 was induced by different means and under diverse conditions, including T helper cell type (Th)2-dependent Arg-1 induction during helminth-Mtb co-infection and Th2-independent Arg-1-induction by different doses and strains of Mtb. The present thesis demonstrates that helminth-Mtb co-infection did not influence susceptibility to Mtb infection *in vivo.* No significant differences in the outcome of Mtb infection in terms of pulmonary bacterial burden, gene expression of Th1 and Th17 responses as well as classically activated macrophages, and histopathology were detected in either acute and transient co-infection with *Nippostrongylus brasiliensis* or *Strongyloides ratti,* or in chronic co-infection with *Litomosoides sigmodontis*. This was observed in spite of considerable degrees of Arg-1 induction in lungs of co-infected wild type mice. Although other authors have published co-infection data with Mtb and different helminth species and various outcomes, the present thesis shows for the first time a highly systematic approach that employed multiple helminth species within the otherwise identical *Mtb* infection model also allowing for harmonization of potential confounders, such as animal housing or scoring of animals.

The present thesis showed for the first time that the extent of Arg-1 induction is linked to the infectious Mtb dose *in vivo*. Infection with virulent Mtb HN878 appeared not to be associated with significant Arg-1 induction. However, high-dose Mtb H37rv infection led to elevated arginase activity accompanied by increased mycobacterial growth, disease severity as well as aggravated pulmonary pathology compared to low-dose infection. These effects were partly reversed in mice lacking Arg-1 specifically in macrophages, indicating Arg-1 as a susceptibility factor in TB. Along this line, stimulation of arginase activity by inhibition of nitric oxide synthase 2 (NOS2) and thus relief of endogenous Arginase-1 inhibition led to increased mycobacterial growth and pathology in Arg-1-competent mice. These effects were partially reversed in mice deficient for macrophage Arg-1.

Overall, the present thesis provides direct evidence for the hypothesis that Arg-1 induction depends on the infectious dose and translates into increased susceptibility to Mtb infection and pathology *in vivo*. Further, the here presented data demonstrate directly that reactivation and granuloma necrosis are induced by arginase activity in macrophages during pulmonary Mtb infection.

Zusammenfassung

In der vorliegenden Dissertation wurde die Bedeutung der Arginase-1 (Arg-1) in Makrophagen für die Immunmodulation durch *Mycobacterium tuberculosis* (Mtb) untersucht, um festzustellen ob die Suszeptibilität gegenüber einer Mtb-Infektion und der damit verbundenen Pathologie durch Arg-1-vermittelte Mechanismen erwerbbar ist. Arg-1 wurde mittels unterschiedlicher Bedingungen induziert. Diese beinhalteten eine Typ2-T-Helferzell (Th2)-abhängige Arg-1 Induktion durch Co-Infektion mit Helminthen und eine Th2-unabhängige Arg-1 Induktion durch Infektion mit unterschiedlichen Mtb-Stämmen und Infektionsdosen. Die vorliegende Arbeit zeigt, dass eine Co-Infektion mit Helminthen die Suszeptibilität gegenüber einer Mtb-Infektion *in vivo* nicht beeinflusst. Mit Bezug auf die pulmonale Keimlast, die Genexpression von Typ1- und Typ17-T-Helferzell-vermittelten Immunantworten, die klassische Aktivierung von Makrophagen und die Histopathologie, wurden keine signifikanten Unterschiede im Verlauf einer Mtb Infektion gesehen. Dies betraf sowohl die akute, transiente Co-Infektion mit *N. brasiliensis* oder *S. ratti*, als auch die chronische Co-Infektion mit *L. sigmodontis*, obwohl es zu einer beträchtlichen Arginase-1 Induktion in den Lungen von Wildtyp-Mäusen kam. Obwohl Co-Infektionsdaten anderer Autoren zu divergenten Ergebnissen kommen, zeigt die vorliegende Dissertation zum ersten Mal einen hochgradig systematischen Versuchsansatz, bei dem mehrere Helminthen-Spezies innerhalb desselben Mtb Infektionsmodels eingesetzt wurden. Potenzielle Störvariablen, wie z. B. Tierhaltungsbedingungen, wurden dabei harmonisiert. Neben der Co-Infektion wurden verschieden Parameter im Mtb-Aerosol-Infektionsmodel getestet, um die Bedeutung der Th2-unabhängigen Arg-1 Induktion durch Mtb selbst in Makrophagen-spezifischen Arg-1-defizienten Mäusen zu untersuchen. Mit der vorliegenden Arbeit wurde zum ersten Mal ein Zusammenhang zwischen dem Grad der Arg-1 Induktion und der Infektionsdosis gezeigt. Die Infektion mit virulentem Mtb HN878 konnte mit keiner signifikanten Arg-1 Induktion in Verbindung gebracht werden. Dahingegen führte eine Hochdosis-Infektion mit Mtb H37Rv auch im Vergleich zu einer Niedrig-Dosis Infektion zu einer erhöhten Arginase-Aktivität, die mit einer Steigerung der mykobakteriellen Proliferation, des Krankheitsschweregrads und einer Verschlechterung der pulmonalen Pathologie verbunden war. Diese Effekte waren in Mäusen mit einer Makrophagen-spezifischen Arg-1-Deletion teilweise aufgehoben. Dies deutet auf Arg-1 als einen Suszeptibilitätsfaktor in der Tuberkulose hin. Anknüpfend an diese Ergebnisse konnte mittels Stimulation der Arginase-Aktivität durch Inhibition der Stickoxid-Synthase 2 (und Aufhebung der endogenen Arg-1 Inhibition) ein gesteigertes Mykobakterienwachstum und eine Verschlechterung der Pathologie in Arg-1-kompetenten Mäusen gezeigt werden. Diese Effekte waren in Mäusen mit einer Makrophagen-spezifischen Arginase-1 Deletion ebenfalls partiell aufgehoben. Die vorliegende Dissertation bestätigt somit die Hypothese, dass die Arg-1 Induktion *in vivo* von der Infektionsdosis abhängt und eine erhöhte Suszeptibilität gegenüber einer Mtb-Infektion und der damit verbundenen Pathologie vermittelt. Darüber hinaus bestätigt die vorliegende Arbeit, dass eine Reaktivierung und Granulomnekrose während einer Mtb-Infektion *in vivo* durch Arginase-Aktivität in Makrophagen induzierbar sind.

Appendix

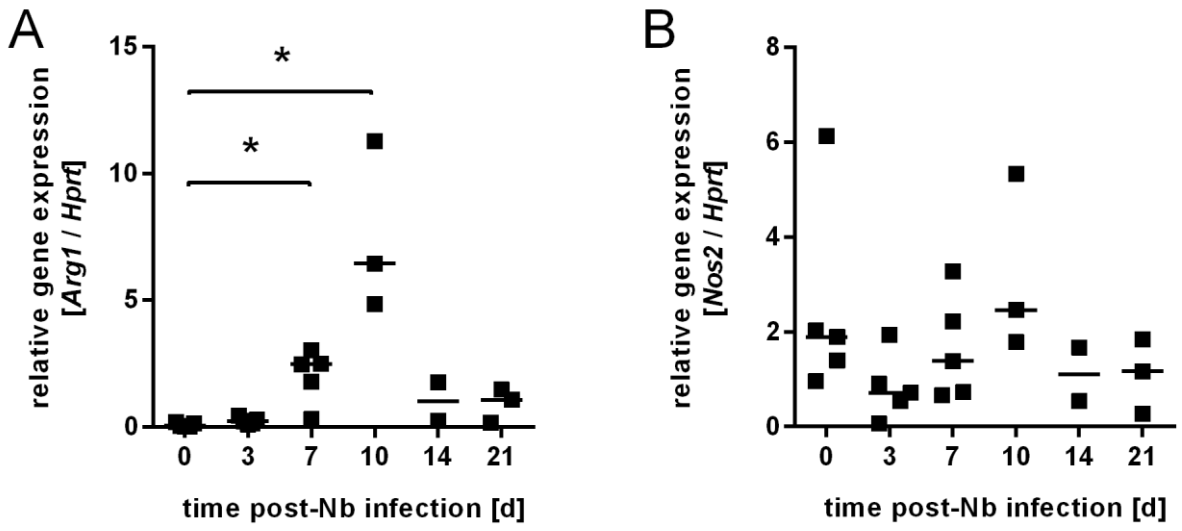

Supplementary Figure 1 Gene expression of *Arg1* and *Nos2* in the lungs of *N. brasiliensis*-infected C57BL/6 mice
C57BL/6 mice were subcutaneously infected with 500 iL3 *N. brasiliensis* into the scruff of the neck. At the indicated time points, RNA was isolated from lung homogenates and reversely transcribed into cDNA for gene expression analysis of (A) *Arg1* and (B) *Nos2* by real-time quantitative PCR. Data represent the median of two to five mice per group with each dot representing one mouse. Statistical analysis was performed using the Kruskal-Wallis test with Dunn's post-hoc test to define differences between day 0 and later time points as significant.

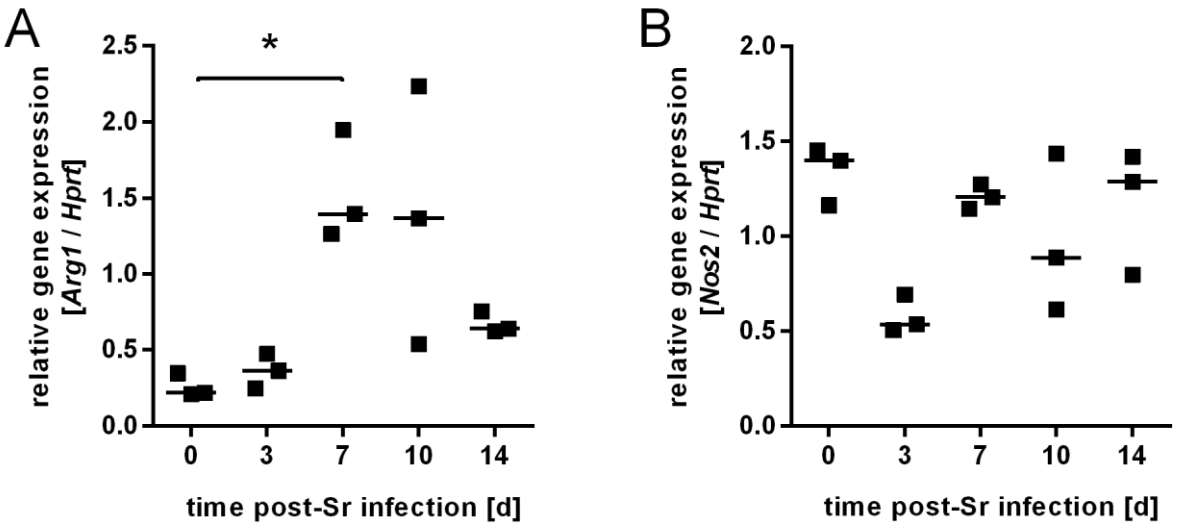

Supplementary Figure 2 Gene expression of *Arg1* and *Nos2* in the lung of *S. ratti*-infected C57BL/6 mice
C57BL/6 mice were subcutaneously infected with 2000 iL3 *S. ratti* into the scruff of the neck. At the indicated time points, RNA was isolated from lung homogenates and reversely transcribed into cDNA for gene expression analysis of (A) *Arg1* and (B) *Nos2* by real-time quantitative PCR. Data represent the median of three mice per group with each dot representing one mouse. Statistical analysis was performed using the Kruskal-Wallis test with Dunn's post-hoc test to define differences between day 0 and later time points as significant.

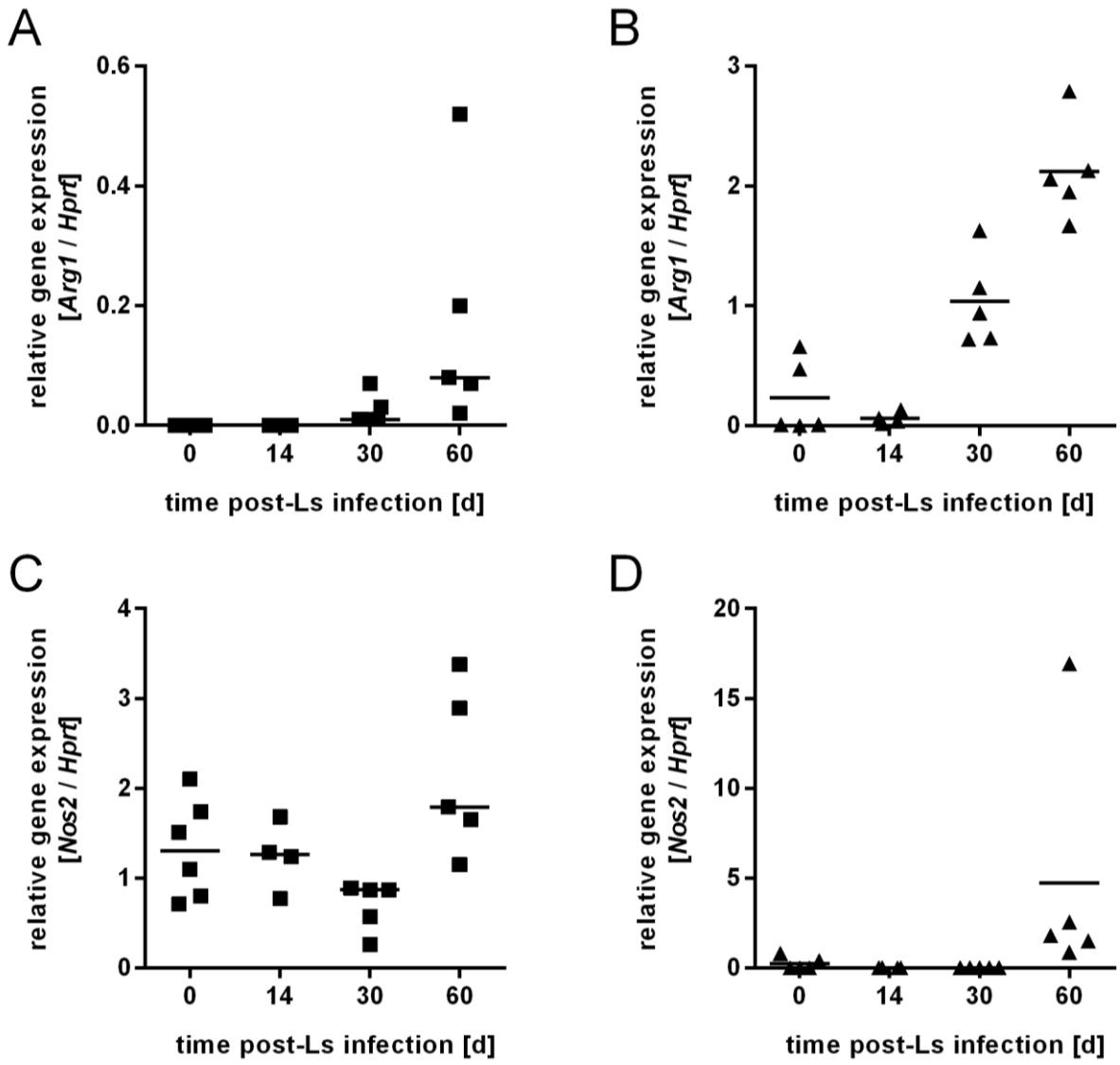

Supplementary Figure 3 Gene expression of *Arg1* and *Nos2* in the lungs and in cells from pleural wash of *L. sigmodontis*-infected Balb/C mice
Balb/C mice were infected with *L. sigmodontis* by exposure to larvae-carrying *O. bacoti* mites. At the indicated time points, RNA was isolated from lung homogenates (A+C) and cells from pleural wash (B+D), and reversely transcribed into cDNA for gene expression analysis of (A-B) *Arg1* and (C-D) *Nos2* by real-time quantitative PCR. Data represent the median of four to six mice per group, with each dot representing one mouse. Data are representative of two independent experiments.

Filarial nematodes, in contrast to hookworms like *N. brasiliensis* und *S. ratti*, establish long-lasting chronic infection. *L. sigmodontis* is known for its immunosuppressive capacities by interference with Th1- and Th2-associated IgG2- and IgG1-antibody responses to thymus-dependent antigens through interaction with follicular T-helper cells at lymph node germinal centers (183). Also, *L. sigmodontis* potently induces AAMs in the thoracic cavity over long periods of time. The complex life cycle of *L. sigmodontis* reaches patency and chronic infection in Balb/C mice, but not in C57BL/6 mice, where larval stages do not fully mature to the adult stage. Patent infection with generation of microfilariae/offspring is not reached in C57BL/6 mice. Instead, the infection is terminated after approximately 60 days. Supplementary Table 1 shows what endpoint after Mtb infection corresponds to which life stage of *L. sigmodontis* in Balb/C mice.

Supplementary Table 1 *L. sigmodontis* life stages at respective experimental endpoints of *L. sigmodontis*-Mtb co-infection experiments

Time post-Mtb infection [wk]	**Time post-*L.sigmodontis* infection [wk]**	***L. sigmodontis* life stage**
0	**4.5** (30 days)	young adult, pre-patency
3	**7.5** (51 days)	adult, patent
6	**10.5** (72 days)	adult, patent
14	**18.5** (128 days)	adult, patent

Literature

1. Koch R. The etiology of tuberculosis. Berl Klin Wochenschr. 1882 Apr 10;(15):221–30.

2. Kumar V, Robbins SL, editors. In: Robbins basic pathology. 8th ed. Philadelphia, PA: Saunders/Elsevier; 2007. p. 516–24.

3. World Health Organization. Global tuberculosis report 2021. World Health Organization; 2021. Available from: https://apps.who.int/iris/handle/10665/346387

4. Fox GJ, Barry SE, Britton WJ, Marks GB. Contact investigation for tuberculosis: a systematic review and meta-analysis. Eur Respir J. 2013 Jan 1;41(1):140–56.

5. European Concerted Action on New Generation Genetic Markers and Techniques for the Epidemiology and Control of Tuberculosis. Beijing/W genotype *Mycobacterium tuberculosis* and drug resistance. Emerg Infect Dis. 2006 May;12(5):736–43.

6. Abate E, Belayneh M, Gelaw A, Idh J, Getachew A, Alemu S, et al. The impact of asymptomatic helminth co-infection in patients with newly diagnosed tuberculosis in north-west Ethiopia. PloS One. 2012;7(8):e42901.

7. Wong W-K, Mohd-Nor N, Noordin R, Foo P-C, Mohamed Z, Haq JA, et al. Parasitic infections in Malaysian aborigines with pulmonary tuberculosis: a comparative cross-sectional study. Parasitol Res. 2019 Sep;118(9):2635–42.

8. World Health Organization, Department of Control of Neglected Tropical Diseases. Integrating neglected tropical diseases into global health and development: fourth WHO report on neglected tropical diseases. World Health Organization; 2017. Available from: https://apps.who.int/iris/handle/10665/255011.

9. O'Garra A, Redford PS, McNab FW, Bloom CI, Wilkinson RJ, Berry MPR. The Immune Response in Tuberculosis. Annu Rev Immunol. 2013 Mar 21;31(1):475–527.

10. Tadolini M, Codecasa LR, García-García J-M, Blanc F-X, Borisov S, Alffenaar J-W, et al. Active tuberculosis, sequelae and COVID-19 co-infection: first cohort of 49 cases. Eur Respir J. 2020 Jul;56(1):2001398.

11. Herchline TE, Amorosa JK. Tuberculosis (TB) Clinical Presentation [Internet]. Medscape. 2020 [cited 2022 Jan 29]. Available from: https://emedicine.medscape.com/article/230802-clinical

12. Natarajan A, Beena PM, Devnikar AV, Mali S. A systemic review on tuberculosis. Indian J Tuberc. 2020 Jul;67(3):295–311.

13. Flynn JL, Chan J, Lin PL. Macrophages and control of granulomatous inflammation in tuberculosis. Mucosal Immunol. 2011 May;4(3):271–8.

14. Lösslein AK, Lohrmann F, Scheuermann L, Gharun K, Neuber J, Kolter J, et al. Monocyte progenitors give rise to multinucleated giant cells. Nat Commun. 2021 Dec;12(1):2027.

15. Helming L, Gordon S. Macrophage fusion induced by IL-4 alternative activation is a multistage process involving multiple target molecules. Eur J Immunol. 2007 Jan;37(1):33–42.

16. Helming L, Gordon S. The molecular basis of macrophage fusion. Immunobiology. 2007;212(9–10):785–93.

17. Herrtwich L, Nanda I, Evangelou K, Nikolova T, Horn V, Sagar null, et al. DNA Damage Signaling Instructs Polyploid Macrophage Fate in Granulomas. Cell. 2016 17;167(5):1264-1280.e18.

18. Ulrichs T, Kaufmann SHE. New insights into the function of granulomas in human tuberculosis. J Pathol. 2006 Jan;208(2):261–9.

19. Russell DG. Who puts the tubercle in tuberculosis? Nat Rev Microbiol. 2007 Jan;5(1):39–47.

20. Russell DG, Cardona P-J, Kim M-J, Allain S, Altare F. Foamy macrophages and the progression of the human tuberculosis granuloma. Nat Immunol. 2009 Sep;10(9):943–8.

21. Reece ST, Kaufmann SHE. Floating between the poles of pathology and protection: can we pin down the granuloma in tuberculosis? Curr Opin Microbiol. 2012 Feb;15(1):63–70.

22. Ehlers S, Hölscher C. DTH-associated pathology. In: Microbiology and Microbial Infections, S H Kaufmann, Ed. London, UK: Arnold Publishing; 2005. p. 705–20.

23. Fortin A, Abel L, Casanova JL, Gros P. Host genetics of mycobacterial diseases in mice and men: forward genetic studies of BCG-osis and tuberculosis. Annu Rev Genomics Hum Genet. 2007;8:163–92.

24. Tsai MC, Chakravarty S, Zhu G, Xu J, Tanaka K, Koch C, et al. Characterization of the tuberculous granuloma in murine and human lungs: cellular composition and relative tissue oxygen tension. Cell Microbiol. 2006 Feb;8(2):218–32.

25. Apt A, Kramnik I. Man and mouse TB: contradictions and solutions. Tuberc Edinb Scotl. 2009 May;89(3):195–8.

26. Orme IM, Ordway DJ. Mouse and Guinea Pig Models of Tuberculosis. Microbiol Spectr. 2016;4(4).

27. Leong FJW-M, Dartois V, Dick T, editors. Immunopathology of Tuberculosis Disease across Species. In: A color atlas of comparative pathology of pulmonary tuberculosis. Boca Raton: CRC Press; 2011. p. 21–7.

28. Rook GAW, Hernández-Pando R, Zumla A. Tuberculosis Due to High-Dose Challenge in Partially Immune Individuals: A Problem for Vaccination? J Infect Dis. 2009 Mar 1;199(5):613–8.

29. Pierce CH, Dubos RJ, Schaefer WB. Multiplication and survival of tubercle bacilli in the organs of mice. J Exp Med. 1953 Feb 1;97(2):189–206.

30. Rhoades ER, Frank AA, Orme IM. Progression of chronic pulmonary tuberculosis in mice aerogenically infected with virulent *Mycobacterium tuberculosis*. Tuber Lung Dis Off J Int Union Tuberc Lung Dis. 1997;78(1):57–66.

31. North RJ, Jung Y-J. Immunity to Tuberculosis. Annu Rev Immunol. 2004 Apr;22(1):599–623.

32. Cooper AM, Magram J, Ferrante J, Orme IM. Interleukin 12 (IL-12) is crucial to the development of protective immunity in mice intravenously infected with *Mycobacterium tuberculosis*. J Exp Med. 1997 Jul 7;186(1):39–45.

33. Flynn JL, Chan J, Triebold KJ, Dalton DK, Stewart TA, Bloom BR. An essential role for interferon gamma in resistance to *Mycobacterium tuberculosis* infection. J Exp Med. 1993 Dec 1;178(6):2249–54.

34. Flynn JL, Goldstein MM, Chan J, Triebold KJ, Pfeffer K, Lowenstein CJ, et al. Tumor necrosis factor-alpha is required in the protective immune response against *Mycobacterium tuberculosis* in mice. Immunity. 1995 Jun;2(6):561–72.

35. MacMicking JD, North RJ, LaCourse R, Mudgett JS, Shah SK, Nathan CF. Identification of nitric oxide synthase as a protective locus against tuberculosis. Proc Natl Acad Sci U S A. 1997 May 13;94(10):5243–8.

36. Domingo-Gonzalez R, Prince O, Cooper A, Khader SA. Cytokines and Chemokines in *Mycobacterium tuberculosis* Infection. Microbiol Spectr. 2016 Oct;4(5).

37. Schlesinger LS. Macrophage phagocytosis of virulent but not attenuated strains of *Mycobacterium tuberculosis* is mediated by mannose receptors in addition to complement receptors. J Immunol Baltim Md 1950. 1993 Apr 1;150(7):2920–30.

38. Weikert LF, Edwards K, Chroneos ZC, Hager C, Hoffman L, Shepherd VL. SP-A enhances uptake of bacillus Calmette-Guerin by macrophages through a specific SP-A receptor. Am J Physiol-Lung Cell Mol Physiol. 1997 May 1;272(5):L989–95.

39. Kleinnijenhuis J, Oosting M, Joosten LAB, Netea MG, Van Crevel R. Innate immune recognition of *Mycobacterium tuberculosis*. Clin Dev Immunol. 2011;2011:405310.

40. Reiling N, Ehlers S, Hölscher C. MyDths and un-TOLLed truths: sensor, instructive and effector immunity to tuberculosis. Immunol Lett. 2008 Feb 15;116(1):15–23.

41. Hölscher C, Reiling N, Schaible UE, Hölscher A, Bathmann C, Korbel D, et al. Containment of aerogenic *Mycobacterium tuberculosis* infection in mice does not require MyD88 adaptor function for TLR2, -4 and -9. Eur J Immunol. 2008 Mar;38(3):680–94.

42. Bafica A, Scanga CA, Feng CG, Leifer C, Cheever A, Sher A. TLR9 regulates Th1 responses and cooperates with TLR2 in mediating optimal resistance to *Mycobacterium tuberculosis*. J Exp Med. 2005 Dec 19;202(12):1715–24.

43. Mishra A, Akhtar S, Jagannath C, Khan A. Pattern recognition receptors and coordinated cellular pathways involved in tuberculosis immunopathogenesis: Emerging concepts and perspectives. Mol Immunol. 2017 Jul;87:240–8.

44. Weiss G, Schaible UE. Macrophage defense mechanisms against intracellular bacteria. Immunol Rev. 2015 Mar;264(1):182–203.

45. Behar SM, Divangahi M, Remold HG. Evasion of innate immunity by *Mycobacterium tuberculosis*: is death an exit strategy? Nat Rev Microbiol. 2010 Sep;8(9):668–74.

46. Divangahi M, Desjardins D, Nunes-Alves C, Remold HG, Behar SM. Eicosanoid pathways regulate adaptive immunity to *Mycobacterium tuberculosis*. Nat Immunol. 2010 Aug;11(8):751–8.

47. Blomgran R, Desvignes L, Briken V, Ernst JD. *Mycobacterium tuberculosis* inhibits neutrophil apoptosis, leading to delayed activation of naive CD4 T cells. Cell Host Microbe. 2012 Jan 19;11(1):81–90.

48. Armstrong JA, Hart PD. Response of cultured macrophages to *Mycobacterium tuberculosis*, with observations on fusion of lysosomes with phagosomes. J Exp Med. 1971 Sep 1;134(3 Pt 1):713–40.

49. Cooper AM, Dalton DK, Stewart TA, Griffin JP, Russell DG, Orme IM. Disseminated tuberculosis in interferon gamma gene-disrupted mice. J Exp Med. 1993 Dec 1;178(6):2243–7.

50. Dalton DK, Pitts-Meek S, Keshav S, Figari IS, Bradley A, Stewart TA. Multiple defects of immune cell function in mice with disrupted interferon-gamma genes. Science. 1993 Mar 19;259(5102):1739–42.

51. Smith D, Hänsch H, Bancroft G, Ehlers S. T-cell-independent granuloma formation in response to *Mycobacterium avium*: role of tumour necrosis factor-alpha and interferon-gamma. Immunology. 1997 Dec;92(4):413–21.

52. Ehlers S, Schaible UE. The granuloma in tuberculosis: dynamics of a host-pathogen collusion. Front Immunol. 2012;3:411.

53. Robinson CM, Jung J-Y, Nau GJ. Interferon-γ, tumor necrosis factor, and interleukin-18 cooperate to control growth of *Mycobacterium tuberculosis* in human macrophages. Cytokine. 2012 Oct;60(1):233–41.

54. Mogues T, Goodrich ME, Ryan L, LaCourse R, North RJ. The relative importance of T cell subsets in immunity and immunopathology of airborne *Mycobacterium tuberculosis* infection in mice. J Exp Med. 2001 Feb 5;193(3):271–80.

55. Green AM, Difazio R, Flynn JL. IFN-γ from CD4 T cells is essential for host survival and enhances CD8 T cell function during *Mycobacterium tuberculosis* infection. J Immunol Baltim Md 1950. 2013 Jan 1;190(1):270–7.

56. Keller C, Hoffmann R, Lang R, Brandau S, Hermann C, Ehlers S. Genetically determined susceptibility to tuberculosis in mice causally involves accelerated and enhanced recruitment of granulocytes. Infect Immun. 2006 Jul;74(7):4295–309.

57. Fabri M, Stenger S, Shin D-M, Yuk J-M, Liu PT, Realegeno S, et al. Vitamin D is required for IFN-gamma-mediated antimicrobial activity of human macrophages. Sci Transl Med. 2011 Oct 12;3(104):104ra102.

58. Appelberg R. Protective role of interferon gamma, tumor necrosis factor alpha and interleukin-6 in *Mycobacterium tuberculosis* and *M. avium* infections. Immunobiology. 1994 Oct;191(4–5):520–5.

59. Saunders BM, Frank AA, Orme IM, Cooper AM. Interleukin-6 induces early gamma interferon production in the infected lung but is not required for generation of specific immunity to *Mycobacterium tuberculosis* infection. Infect Immun. 2000 Jun;68(6):3322–6.

60. Ladel CH, Blum C, Dreher A, Reifenberg K, Kopf M, Kaufmann SH. Lethal tuberculosis in interleukin-6-deficient mutant mice. Infect Immun. 1997 Nov;65(11):4843–9.

61. Nagabhushanam V, Solache A, Ting L-M, Escaron CJ, Zhang JY, Ernst JD. Innate inhibition of adaptive immunity: *Mycobacterium tuberculosis*-induced IL-6 inhibits macrophage responses to IFN-gamma. J Immunol Baltim Md 1950. 2003 Nov 1;171(9):4750–7.

62. VanHeyningen TK, Collins HL, Russell DG. IL-6 produced by macrophages infected with Mycobacterium species suppresses T cell responses. J Immunol Baltim Md 1950. 1997 Jan 1;158(1):330–7.

63. Hölscher C, Atkinson RA, Arendse B, Brown N, Myburgh E, Alber G, et al. A Protective and Agonistic Function of IL-12p40 in Mycobacterial Infection. J Immunol. 2001 Dec 15;167(12):6957–66.

64. Feng CG, Jankovic D, Kullberg M, Cheever A, Scanga CA, Hieny S, et al. Maintenance of Pulmonary Th1 Effector Function in Chronic Tuberculosis Requires Persistent IL-12 Production. J Immunol. 2005 Apr 1;174(7):4185–92.

65. Schreiber T, Ehlers S, Aly S, Hölscher A, Hartmann S, Lipp M, et al. Selectin Ligand-Independent Priming and Maintenance of T Cell Immunity during Airborne Tuberculosis. J Immunol. 2006 Jan 15;176(2):1131–40.

66. Torrado E, Cooper AM. IL-17 and Th17 cells in tuberculosis. Cytokine Growth Factor Rev. 2010 Dec;21(6):455–62.

67. Khader SA, Pearl JE, Sakamoto K, Gilmartin L, Bell GK, Jelley-Gibbs DM, et al. IL-23 compensates for the absence of IL-12p70 and is essential for the IL-17 response during tuberculosis but is dispensable for protection and antigen-specific IFN-gamma responses if IL-12p70 is available. J Immunol Baltim Md 1950. 2005 Jul 15;175(2):788–95.

68. Khader SA, Bell GK, Pearl JE, Fountain JJ, Rangel-Moreno J, Cilley GE, et al. IL-23 and IL-17 in the establishment of protective pulmonary CD4+ T cell responses after vaccination and during *Mycobacterium tuberculosis* challenge. Nat Immunol. 2007 Apr;8(4):369–77.

69. Hibbs JB, Taintor RR, Vavrin Z, Rachlin EM. Nitric oxide: a cytotoxic activated macrophage effector molecule. Biochem Biophys Res Commun. 1988 Nov 30;157(1):87–94.

70. Flesch IE, Kaufmann SH. Mechanisms involved in mycobacterial growth inhibition by gamma interferon-activated bone marrow macrophages: role of reactive nitrogen intermediates. Infect Immun. 1991 Sep;59(9):3213–8.

71. Ehrt S, Schnappinger D. Mycobacterial survival strategies in the phagosome: defence against host stresses. Cell Microbiol. 2009 Aug;11(8):1170–8.

72. Chan J, Tanaka K, Carroll D, Flynn J, Bloom BR. Effects of nitric oxide synthase inhibitors on murine infection with *Mycobacterium tuberculosis*. Infect Immun. 1995 Feb;63(2):736–40.

73. MacMicking JD, Taylor GA, McKinney JD. Immune control of tuberculosis by IFN-gamma-inducible LRG-47. Science. 2003 Oct 24;302(5645):654–9.

74. Singh SB, Davis AS, Taylor GA, Deretic V. Human IRGM induces autophagy to eliminate intracellular mycobacteria. Science. 2006 Sep 8;313(5792):1438–41.

75. Via LE, Lin PL, Ray SM, Carrillo J, Allen SS, Eum SY, et al. Tuberculous granulomas are hypoxic in guinea pigs, rabbits, and nonhuman primates. Infect Immun. 2008 Jun;76(6):2333–40.

76. Aly S, Wagner K, Keller C, Malm S, Malzan A, Brandau S, et al. Oxygen status of lung granulomas in *Mycobacterium tuberculosis*-infected mice. J Pathol. 2006 Nov;210(3):298–305.

77. Barnes PF, Lu S, Abrams JS, Wang E, Yamamura M, Modlin RL. Cytokine production at the site of disease in human tuberculosis. Infect Immun. 1993 Aug;61(8):3482–9.

78. Seah GT, Scott GM, Rook GA. Type 2 cytokine gene activation and its relationship to extent of disease in patients with tuberculosis. J Infect Dis. 2000 Jan;181(1):385–9.

79. Mihret A, Bekele Y, Bobosha K, Kidd M, Aseffa A, Howe R, et al. Plasma cytokines and chemokines differentiate between active disease and non-active tuberculosis infection. J Infect. 2013 Apr;66(4):357–65.

80. Surcel HM, Troye-Blomberg M, Paulie S, Andersson G, Moreno C, Pasvol G, et al. Th1/Th2 profiles in tuberculosis, based on the proliferation and cytokine response of blood lymphocytes to mycobacterial antigens. Immunology. 1994 Feb;81(2):171–6.

81. Hölscher C, Heitmann L, Owusu-Dabo E, Horstmann RD, Meyer CG, Ehlers S, et al. A Mutation in IL4RA Is Associated with the Degree of Pathology in Human TB Patients. Mediators Inflamm. 2016;2016:4245028.

82. Rook GAW, Hernandez-Pando R, Dheda K, Teng Seah G. IL-4 in tuberculosis: implications for vaccine design. Trends Immunol. 2004 Sep;25(9):483–8.

83. W. Rook G. Th2 Cytokines in Susceptibility to Tuberculosis. Curr Mol Med. 2007 May 1;7(3):327–37.

84. Schauf V, Rom WN, Smith KA, Sampaio EP, Meyn PA, Tramontana JM, et al. Cytokine gene activation and modified responsiveness to interleukin-2 in the blood of tuberculosis patients. J Infect Dis. 1993 Oct;168(4):1056–9.

85. Demissie A, Abebe M, Aseffa A, Rook G, Fletcher H, Zumla A, et al. Healthy individuals that control a latent infection with *Mycobacterium tuberculosis* express high levels of Th1 cytokines and the IL-4 antagonist IL-4delta2. J Immunol Baltim Md 1950. 2004 Jun 1;172(11):6938–43.

86. Fletcher HA, Owiafe P, Jeffries D, Hill P, Rook GAW, Zumla A, et al. Increased expression of mRNA encoding interleukin (IL)-4 and its splice variant IL-4delta2 in cells from contacts of *Mycobacterium tuberculosis*, in the absence of in vitro stimulation. Immunology. 2004 Aug;112(4):669–73.

87. Power CA, Wei G, Bretscher PA. Mycobacterial dose defines the Th1/Th2 nature of the immune response independently of whether immunization is administered by the intravenous, subcutaneous, or intradermal route. Infect Immun. 1998 Dec;66(12):5743–50.

88. Hernandez-Pando R, Aguilar D, Hernandez MLG, Orozco H, Rook G. Pulmonary tuberculosis in BALB/c mice with non-functional IL-4 genes: changes in the inflammatory effects of TNF-alpha and in the regulation of fibrosis. Eur J Immunol. 2004 Jan;34(1):174–83.

89. Roy E, Brennan J, Jolles S, Lowrie DB. Beneficial effect of anti-interleukin-4 antibody when administered in a murine model of tuberculosis infection. Tuberc Edinb Scotl. 2008 May;88(3):197–202.

90. Buccheri S, Reljic R, Caccamo N, Ivanyi J, Singh M, Salerno A, et al. IL-4 depletion enhances host resistance and passive IgA protection against tuberculosis infection in BALB/c mice. Eur J Immunol. 2007 Mar;37(3):729–37.

91. Hernandez-Pando R, Pavön L, Arriaga K, Orozco H, Madrid-Marina V, Rook G. Pathogenesis of tuberculosis in mice exposed to low and high doses of an environmental mycobacterial saprophyte before infection. Infect Immun. 1997 Aug;65(8):3317–27.

92. Hernández-Pando R, Orozcoe H, Sampieri A, Pavón L, Velasquillo C, Larriva-Sahd J, et al. Correlation between the kinetics of Th1, Th2 cells and pathology in a murine model of experimental pulmonary tuberculosis. Immunology. 1996 Sep;89(1):26–33.

93. North RJ. Mice incapable of making IL-4 or IL-10 display normal resistance to infection with *Mycobacterium tuberculosis*. Clin Exp Immunol. 1998 Jul;113(1):55–8.

94. Jung Y-J, LaCourse R, Ryan L, North RJ. Evidence inconsistent with a negative influence of T helper 2 cells on protection afforded by a dominant T helper 1 response against *Mycobacterium tuberculosis* lung infection in mice. Infect Immun. 2002 Nov;70(11):6436–43.

95. Morris KR, Lutz RD, Bai X, McGibney MT, Cook D, Ordway D, et al. Suppression of IFNgamma+mycobacterial lipoarabinomannan-induced NO by IL-4 is due to decreased IRF-1 expression. Tuberc Edinb Scotl. 2009 Jul;89(4):294–303.

96. Schreiber T, Ehlers S, Heitmann L, Rausch A, Mages J, Murray PJ, et al. Autocrine IL-10 induces hallmarks of alternative activation in macrophages and suppresses antituberculosis effector mechanisms without compromising T cell immunity. J Immunol Baltim Md 1950. 2009 Jul 15;183(2):1301–12.

97. Heitmann L, Abad Dar M, Schreiber T, Erdmann H, Behrends J, Mckenzie AN, et al. The IL-13/IL-4Rα axis is involved in tuberculosis-associated pathology. J Pathol. 2014 Nov;234(3):338–50.

98. Pessanha AP, Martins RAP, Mattos-Guaraldi AL, Vianna A, Moreira LO. Arginase-1 expression in granulomas of tuberculosis patients. FEMS Immunol Med Microbiol. 2012 Nov;66(2):265–8.

99. Mattila JT, Ojo OO, Kepka-Lenhart D, Marino S, Kim JH, Eum SY, et al. Microenvironments in Tuberculous Granulomas Are Delineated by Distinct Populations of Macrophage Subsets and Expression of Nitric Oxide Synthase and Arginase Isoforms. J Immunol Baltim Md 1950. 2013 Jun 7;

100. Zea AH, Culotta KS, Ali J, Mason C, Park H-J, Zabaleta J, et al. Decreased expression of CD3zeta and nuclear transcription factor kappa B in patients with pulmonary tuberculosis: potential mechanisms and reversibility with treatment. J Infect Dis. 2006 Nov 15;194(10):1385–93.

101. Cho HJ, Lim Y-J, Kim J, Koh W-J, Song C-H, Kang M-W. Different macrophage polarization between drug-susceptible and multidrug-resistant pulmonary tuberculosis. BMC Infect Dis. 2020 Dec;20(1):81.

102. Rutschman R, Lang R, Hesse M, Ihle JN, Wynn TA, Murray PJ. Cutting edge: Stat6-dependent substrate depletion regulates nitric oxide production. J Immunol Baltim Md 1950. 2001 Feb 15;166(4):2173–7.

103. Zea AH, Rodriguez PC, Culotta KS, Hernandez CP, DeSalvo J, Ochoa JB, et al. L-Arginine modulates CD3zeta expression and T cell function in activated human T lymphocytes. Cell Immunol. 2004 Dec;232(1–2):21–31.

104. Hölscher C, Arendse B, Schwegmann A, Myburgh E, Brombacher F. Impairment of alternative macrophage activation delays cutaneous leishmaniasis in nonhealing BALB/c mice. J Immunol Baltim Md 1950. 2006 Jan 15;176(2):1115–21.

105. Rath M, Müller I, Kropf P, Closs EI, Munder M. Metabolism via Arginase or Nitric Oxide Synthase: Two Competing Arginine Pathways in Macrophages. Front Immunol. 2014;5:532.

106. Kropf P, Fuentes JM, Fähnrich E, Arpa L, Herath S, Weber V, et al. Arginase and polyamine synthesis are key factors in the regulation of experimental leishmaniasis in vivo. FASEB J Off Publ Fed Am Soc Exp Biol. 2005 Jun;19(8):1000–2.

107. Hampel A, Huber C, Geffers R, Spona-Friedl M, Eisenreich W, Bange F-C. *Mycobacterium tuberculosis* Is a Natural Ornithine Aminotransferase (rocD) Mutant and Depends on Rv2323c for Growth on Arginine. PloS One. 2015;10(9):e0136914.

108. El Kasmi KC, Qualls JE, Pesce JT, Smith AM, Thompson RW, Henao-Tamayo M, et al. Toll-like receptor-induced arginase 1 in macrophages thwarts effective immunity against intracellular pathogens. Nat Immunol. 2008 Dec;9(12):1399–406.

109. Qualls JE, Neale G, Smith AM, Koo M-S, DeFreitas AA, Zhang H, et al. Arginine usage in mycobacteria-infected macrophages depends on autocrine-paracrine cytokine signaling. Sci Signal. 2010;3(135):ra62.

110. Bowcutt R, Bell LV, Little M, Wilson J, Booth C, Murray PJ, et al. Arginase-1-expressing macrophages are dispensable for resistance to infection with the gastrointestinal helminth *Trichuris muris*. Parasite Immunol. 2011 Jul;33(7):411–20.

111. Resende Co T, Hirsch CS, Toossi Z, Dietze R, Ribeiro-Rodrigues R. Intestinal helminth co-infection has a negative impact on both anti-*Mycobacterium tuberculosis* immunity and clinical response to tuberculosis therapy. Clin Exp Immunol. 2007 Jan;147(1):45–52.

112. Babu S, Bhat SQ, Kumar NP, Jayantasri S, Rukmani S, Kumaran P, et al. Human type 1 and 17 responses in latent tuberculosis are modulated by coincident filarial infection through cytotoxic T lymphocyte antigen-4 and programmed death-1. J Infect Dis. 2009 Jul 15;200(2):288–98.

113. du Plessis N, Kleynhans L, Thiart L, van Helden PD, Brombacher F, Horsnell WGC, et al. Acute helminth infection enhances early macrophage mediated control of mycobacterial infection. Mucosal Immunol. 2012 Dec 19;

114. Hübner MP, Killoran KE, Rajnik M, Wilson S, Yim KC, Torrero MN, et al. Chronic Helminth Infection Does Not Exacerbate *Mycobacterium tuberculosis* Infection. MacDonald AS, editor. PLoS Negl Trop Dis. 2012 Dec 20;6(12):e1970.

115. Monin L, Griffiths KL, Lam WY, Gopal R, Kang DD, Ahmed M, et al. Helminth-induced arginase-1 exacerbates lung inflammation and disease severity in tuberculosis. J Clin Invest. 2015 Nov 16;

116. Potian JA, Rafi W, Bhatt K, McBride A, Gause WC, Salgame P. Preexisting helminth infection induces inhibition of innate pulmonary anti-tuberculosis defense by engaging the IL-4 receptor pathway. J Exp Med. 2011 Aug 29;208(9):1863–74.

117. Schmok E, Abad Dar M, Behrends J, Erdmann H, Rückerl D, Endermann T, et al. Suppressor of Cytokine Signaling 3 in Macrophages Prevents Exacerbated Interleukin-6-Dependent Arginase-1 Activity and Early Permissiveness to Experimental Tuberculosis. Front Immunol [Internet]. 2017

Nov 10 [cited 2018 May 9];8. Available from: http://journal.frontiersin.org/article/10.3389/fimmu.2017.01537/full

118. Stuehr DJ, Kwon NS, Nathan CF, Griffith OW, Feldman PL, Wiseman J. N omega-hydroxy-L-arginine is an intermediate in the biosynthesis of nitric oxide from L-arginine. J Biol Chem. 1991 Apr 5;266(10):6259–63.

119. Hecker M, Nematollahi H, Hey C, Busse R, Racké K. Inhibition of arginase by NG-hydroxy-L-arginine in alveolar macrophages: implications for the utilization of L-arginine for nitric oxide synthesis. FEBS Lett. 1995 Feb 13;359(2–3):251–4.

120. Duque-Correa MA, Kühl AA, Rodriguez PC, Zedler U, Schommer-Leitner S, Rao M, et al. Macrophage arginase-1 controls bacterial growth and pathology in hypoxic tuberculosis granulomas. Proc Natl Acad Sci U S A. 2014 Sep 23;111(38):E4024-4032.

121. Mylonas KJ, Hoeve MA, MacDonald AS, Allen JE. Alternative activation of macrophages by filarial nematodes is MyD88-independent. Immunobiology. 2013 Apr;218(4):570–8.

122. Guler R, Parihar SP, Savvi S, Logan E, Schwegmann A, Roy S, et al. IL-4Rα-dependent alternative activation of macrophages is not decisive for *Mycobacterium tuberculosis* pathology and bacterial burden in mice. PloS One. 2015;10(3):e0121070.

123. du Plessis N, Walzl G. Helminth-M. tb co-infection. Adv Exp Med Biol. 2014;828:49–74.

124. Fulton SA, Martin TD, Redline RW, Henry Boom W. Pulmonary immune responses during primary *Mycobacterium bovis*-Calmette-Guerin bacillus infection in C57Bl/6 mice. Am J Respir Cell Mol Biol. 2000 Mar;22(3):333–43.

125. Pesce JT, Ramalingam TR, Mentink-Kane MM, Wilson MS, El Kasmi KC, Smith AM, et al. Arginase-1-expressing macrophages suppress Th2 cytokine-driven inflammation and fibrosis. PLoS Pathog. 2009 Apr;5(4):e1000371.

126. Elias D, Wolday D, Akuffo H, Petros B, Bronner U, Britton S. Effect of deworming on human T cell responses to mycobacterial antigens in helminth-exposed individuals before and after bacille Calmette-Guérin (BCG) vaccination. Clin Exp Immunol. 2001 Feb;123(2):219–25.

127. Elias D, Akuffo H, Thors C, Pawlowski A, Britton S. Low dose chronic Schistosoma mansoni infection increases susceptibility to *Mycobacterium bovis* BCG infection in mice. Clin Exp Immunol. 2005 Mar;139(3):398–404.

128. Rafi W, Bhatt K, Gause WC, Salgame P. Neither primary nor memory immunity to *Mycobacterium tuberculosis* infection is compromised in mice with chronic enteric helminth infection. Infect Immun. 2015 Mar;83(3):1217–23.

129. Erb KJ, Trujillo C, Fugate M, Moll H. Infection with the helminth *Nippostrongylus brasiliensis* does not interfere with efficient elimination of *Mycobacterium bovis* BCG from the lungs of mice. Clin Diagn Lab Immunol. 2002 May;9(3):727–30.

130. Pearlman E, Kazura JW, Hazlett FE Jr, Boom WH. Modulation of murine cytokine responses to mycobacterial antigens by helminth-induced T helper 2 cell responses. J Immunol Baltim Md 1950. 1993 Nov 1;151(9):4857–64.

131. Loke P, Gallagher I, Nair MG, Zang X, Brombacher F, Mohrs M, et al. Alternative activation is an innate response to injury that requires CD4+ T cells to be sustained during chronic infection. J Immunol Baltim Md 1950. 2007 Sep 15;179(6):3926–36.

132. Pearce EJ, MacDonald AS. The immunobiology of schistosomiasis. Nat Rev Immunol. 2002 Jul;2(7):499–511.

133. North RJ. *Mycobacterium tuberculosis* is strikingly more virulent for mice when given via the respiratory than via the intravenous route. J Infect Dis. 1995 Dec;172(6):1550–3.

134. Camberis M, Le Gros G, Urban J Jr. Animal model of *Nippostrongylus brasiliensis* and *Heligmosomoides polygyrus*. Curr Protoc Immunol Ed John E Coligan Al. 2003 Aug;Chapter 19:Unit 19.12.

135. Gordon S, Martinez FO. Alternative activation of macrophages: mechanism and functions. Immunity. 2010 May 28;32(5):593–604.

136. Cosma CL, Humbert O, Ramakrishnan L. Superinfecting mycobacteria home to established tuberculous granulomas. Nat Immunol. 2004 Aug;5(8):828–35.

137. Redente EF, Higgins DM, Dwyer-Nield LD, Orme IM, Gonzalez-Juarrero M, Malkinson AM. Differential polarization of alveolar macrophages and bone marrow-derived monocytes following chemically and pathogen-induced chronic lung inflammation. J Leukoc Biol. 2010 Jul;88(1):159–68.

138. Smits HH, Hammad H, van Nimwegen M, Soullie T, Willart MA, Lievers E, et al. Protective effect of *Schistosoma mansoni* infection on allergic airway inflammation depends on the intensity and chronicity of infection. J Allergy Clin Immunol. 2007 Oct;120(4):932–40.

139. Carmo AM, Vicentini MA, Dias AT, Alves LL, Alves CCS, Brandi JS, et al. Increased susceptibility to *Strongyloides venezuelensis* in mice due to *Mycobacterium bovis* co-infection which modulates production of Th2 cytokines. Parasitology. 2009 Aug 7;136(11):1357.

140. Nel HJ, du Plessis N, Kleynhans L, Loxton AG, van Helden PD, Walzl G. *Mycobacterium bovis* BCG infection severely delays *Trichuris muris* expulsion and co-infection suppresses immune responsiveness to both pathogens. BMC Microbiol. 2014;14:9.

141. Wulandari L, Amin M, Soedarto null, Soegiarto G, Ishiwata K. Sequential Co-infection of *Heligmosomoides polygyrus* and *Mycobacterium tuberculosis* Determine Lung Macrophage Polarization and Histopathological Changes. Indian J Tuberc. 2021 Jul;68(3):340–9.

142. Budischak SA, Sakamoto K, Megow LC, Cummings KR, Urban JF, Ezenwa VO. Resource limitation alters the consequences of co-infection for both hosts and parasites. Int J Parasitol. 2015 Jun;45(7):455–63.

143. Kahnert A, Seiler P, Stein M, Bandermann S, Hahnke K, Mollenkopf H, et al. Alternative activation deprives macrophages of a coordinated defense program to *Mycobacterium tuberculosis*. Eur J Immunol. 2006 Mar;36(3):631–47.

144. Garrido-Amaro C, Cardona P, Gassó D, Arias L, Velarde R, Tvarijonativiciute A, et al. Protective Effect of Intestinal Helminthiasis Against Tuberculosis Progression Is Abrogated by Intermittent Food Deprivation. Front Immunol. 2021 Apr 14;12:627638.

145. Chatterjee S, Kolappan C, Subramani R, Gopi PG, Chandrasekaran V, Fay MP, et al. Incidence of active pulmonary tuberculosis in patients with coincident filarial and/or intestinal helminth infections followed longitudinally in South India. PloS One. 2014;9(4):e94603.

146. George PJ, Kumar NP, Sridhar R, Hanna LE, Nair D, Banurekha VV, et al. Coincident helminth infection modulates systemic inflammation and immune activation in active pulmonary tuberculosis. PLoS Negl Trop Dis. 2014 Nov;8(11):e3289.

147. George PJ, Pavan Kumar N, Jaganathan J, Dolla C, Kumaran P, Nair D, et al. Modulation of pro- and anti-inflammatory cytokines in active and latent tuberculosis by coexistent *Strongyloides stercoralis* infection. Tuberculosis. 2015 Dec;95(6):822–8.

148. Babu S, Nutman TB. Helminth-Tuberculosis Co-infection: An Immunologic Perspective. Trends Immunol. 2016 Aug 5;

149. George PJ, Anuradha R, Kumaran PP, Chandrasekaran V, Nutman TB, Babu S. Modulation of Mycobacterial-Specific Th1 and Th17 Cells in Latent Tuberculosis by Coincident Hookworm Infection. J Immunol Baltim Md 1950. 2013 Apr 10;

150. Chatterjee S, Clark CE, Lugli E, Roederer M, Nutman TB. Filarial infection modulates the immune response to *Mycobacterium tuberculosis* through expansion of CD4+ IL-4 memory T cells. J Immunol Baltim Md 1950. 2015 Mar 15;194(6):2706–14.

151. Elias D, Mengistu G, Akuffo H, Britton S. Are intestinal helminths risk factors for developing active tuberculosis? Trop Med Int Health TM IH. 2006 Apr;11(4):551–8.

152. Brown M, Miiro G, Nkurunziza P, Watera C, Quigley MA, Dunne DW, et al. *Schistosoma mansoni*, nematode infections, and progression to active tuberculosis among HIV-1-infected Ugandans. Am J Trop Med Hyg. 2006 May;74(5):819–25.

153. Andrade MR, Amaral EP, Ribeiro SC, Almeida FM, Peres TV, Lanes V, et al. Pathogenic *Mycobacterium bovis* strains differ in their ability to modulate the proinflammatory activation phenotype of macrophages. BMC Microbiol. 2012;12(1):166.

154. Cooper AM, Pearl JE, Brooks JV, Ehlers S, Orme IM. Expression of the nitric oxide synthase 2 gene is not essential for early control of *Mycobacterium tuberculosis* in the murine lung. Infect Immun. 2000 Dec;68(12):6879–82.

155. Denis M. Interferon-gamma-treated murine macrophages inhibit growth of tubercle bacilli via the generation of reactive nitrogen intermediates. Cell Immunol. 1991 Jan;132(1):150–7.

156. Peteroy-Kelly M, Venketaraman V, Connell ND. Effects of *Mycobacterium bovis* BCG infection on regulation of L-arginine uptake and synthesis of reactive nitrogen intermediates in J774.1 murine macrophages. Infect Immun. 2001 Sep;69(9):5823–31.

157. Talaue MT, Venketaraman V, Hazbón MH, Peteroy-Kelly M, Seth A, Colangeli R, et al. Arginine homeostasis in J774.1 macrophages in the context of *Mycobacterium bovis* BCG infection. J Bacteriol. 2006 Jul;188(13):4830–40.

158. Munder M, Mollinedo F, Calafat J, Canchado J, Gil-Lamaignere C, Fuentes JM, et al. Arginase I is constitutively expressed in human granulocytes and participates in fungicidal activity. Blood. 2005 Mar 15;105(6):2549–56.

159. Munder M, Schneider H, Luckner C, Giese T, Langhans C-D, Fuentes JM, et al. Suppression of T-cell functions by human granulocyte arginase. Blood. 2006 Sep 1;108(5):1627–34.

160. Ivanenkov YA, Chufarova NV. Small-molecule arginase inhibitors. Pharm Pat Anal. 2014 Jan;3(1):65–85.

161. Zea AH, Rodriguez PC, Atkins MB, Hernandez C, Signoretti S, Zabaleta J, et al. Arginase-producing myeloid suppressor cells in renal cell carcinoma patients: a mechanism of tumor evasion. Cancer Res. 2005 Apr 15;65(8):3044–8.

162. Czystowska-Kuzmicz M, Sosnowska A, Nowis D, Ramji K, Szajnik M, Chlebowska-Tuz J, et al. Small extracellular vesicles containing arginase-1 suppress T-cell responses and promote tumor growth in ovarian carcinoma. Nat Commun. 2019 05;10(1):3000.

163. D'Antonio EL, Ullman B, Roberts SC, Dixit UG, Wilson ME, Hai Y, et al. Crystal structure of arginase from *Leishmania mexicana* and implications for the inhibition of polyamine biosynthesis in parasitic infections. Arch Biochem Biophys. 2013 Jul 15;535(2):163–76.

164. Heby O, Persson L, Rentala M. Targeting the polyamine biosynthetic enzymes: a promising approach to therapy of African sleeping sickness, Chagas' disease, and leishmaniasis. Amino Acids. 2007 Aug;33(2):359–66.

165. Abad Dar M, Hölscher C. Arginase-1 Is Responsible for IL-13-Mediated Susceptibility to *Trypanosoma cruzi* Infection. Front Immunol. 2018;9:2790.

166. Knaul JK, Jörg S, Oberbeck-Mueller D, Heinemann E, Scheuermann L, Brinkmann V, et al. Lung-residing myeloid-derived suppressors display dual functionality in murine pulmonary tuberculosis. Am J Respir Crit Care Med. 2014 Nov 1;190(9):1053–66.

167. Jøntvedt Jørgensen M, Jenum S, Tonby K, Mortensen R, Walzl G, Du Plessis N, et al. Monocytic myeloid-derived suppressor cells reflect tuberculosis severity and are influenced by cyclooxygenase-2 inhibitors. J Leukoc Biol. 2021 Jul;110(1):177–86.

168. Leukes V, Walzl G, du Plessis N. Myeloid-Derived Suppressor Cells as Target of Phosphodiesterase-5 Inhibitors in Host-Directed Therapeutics for Tuberculosis. Front Immunol. 2020 Mar 25;11:451.

169. Upadhyay R, Sanchez-Hidalgo A, Wilusz CJ, Lenaerts AJ, Arab J, Yeh J, et al. Host Directed Therapy for Chronic Tuberculosis via Intrapulmonary Delivery of Aerosolized Peptide Inhibitors Targeting the IL-10-STAT3 Pathway. Sci Rep. 2018 Nov 9;8(1):16610.

170. Zhang Y, Li S, Liu Q, Long R, Feng J, Qin H, et al. *Mycobacterium tuberculosis* Heat-Shock Protein 16.3 Induces Macrophage M2 Polarization Through CCRL2/CX3CR1. Inflammation. 2020 Apr;43(2):487–506.

171. Morales JA, Sticco KL. Arginase Deficiency (Argininemia). In: StatPearls [Internet]. Treasure Island (FL): StatPearls Publishing; 2019 [cited 2020 Jan 7]. Available from: http://www.ncbi.nlm.nih.gov/books/NBK482365/

172. Campbell L, Saville CR, Murray PJ, Cruickshank SM, Hardman MJ. Local Arginase 1 Activity Is Required for Cutaneous Wound Healing. J Invest Dermatol. 2013 Apr 3;

173. Abate E, Elias D, Getachew A, Alemu S, Diro E, Britton S, et al. Effects of albendazole on the clinical outcome and immunological responses in helminth co-infected tuberculosis patients: a double blind randomised clinical trial. Int J Parasitol. 2015 Feb;45(2–3):133–40.

174. Anuradha R, Munisankar S, Bhootra Y, Dolla C, Kumaran P, Nutman TB, et al. Modulation of *Mycobacterium tuberculosis*-specific humoral immune responses is associated with *Strongyloides stercoralis* co-infection. PLoS Negl Trop Dis. 2017 May;11(5):e0005569.

175. Hasanain AFA, Zayed AA-AH, Mahdy RE, Nafee AMA, Attia RA-MH, Mohamed AO. Hookworm infection among patients with pulmonary tuberculosis: Impact of co-infection on the therapeutic failure of pulmonary tuberculosis. Int J Mycobacteriology. 2015 Dec;4(4):318–22.

176. Ochoa JB. Arginine deficiency caused by myeloid cells: importance, identification and treatment. Nestlé Nutr Inst Workshop Ser. 2013;77:29–45.

177. Carbajosa S, Rodríguez-Angulo HO, Gea S, Chillón-Marinas C, Poveda C, Maza MC, et al. L-arginine supplementation reduces mortality and improves disease outcome in mice infected with *Trypanosoma cruzi*. PLoS Negl Trop Dis. 2018;12(1):e0006179.

178. Ralph AP, Waramori G, Pontororing GJ, Kenangalem E, Wiguna A, Tjitra E, et al. L-arginine and vitamin D adjunctive therapies in pulmonary tuberculosis: a randomised, double-blind, placebo-controlled trial. PloS One. 2013;8(8):e70032.

179. Schön T, Elias D, Moges F, Melese E, Tessema T, Stendahl O, et al. Arginine as an adjuvant to chemotherapy improves clinical outcome in active tuberculosis. Eur Respir J. 2003 Mar;21(3):483–8.

180. Schön T, Idh J, Westman A, Elias D, Abate E, Diro E, et al. Effects of a food supplement rich in arginine in patients with smear positive pulmonary tuberculosis--a randomised trial. Tuberc Edinb Scotl. 2011 Sep;91(5):370–7.

181. Barron L, Smith AM, El Kasmi KC, Qualls JE, Huang X, Cheever A, et al. Role of arginase 1 from myeloid cells in th2-dominated lung inflammation. PloS One. 2013;8(4):e61961.

182. Maarsingh H, Pera T, Meurs H. Arginase and pulmonary diseases. Naunyn Schmiedebergs Arch Pharmacol. 2008 Aug;378(2):171–84.

183. Haben I, Hartmann W, Breloer M. Nematode-induced interference with vaccination efficacy targets follicular T helper cell induction and is preserved after termination of infection. PLoS Negl Trop Dis. 2014 Sep;8(9):e3170.

Acknowledgments

I would like to thank the Leibniz Center Infection for funding the research project “Helminth-induced interleukin-4-receptor-alpha-dependent mechanisms in alternatively activated macrophages that subvert protective immune responses against *Mycobacterium tuberculosis”* and the Research Center Borstel for the financial support of my work.

I thank Prof. Dr. Ulrich Schaible and Prof. Dr. Jürgen Westermann for taking up the positions as referees and Prof. Dr. Norbert Tautz for presiding over the oral examination.

My sincere gratitude goes to my PhD supervisor, Dr. Christoph Hölscher, for provision of this interesting topic, for many fruitful discussions and his expert scientific support, for his trust, and for supporting my participation at national and international congresses and scientific meetings. Thank you for believing in me and for your patience that allowed me to grow into my scientific career.

I would also like to thank my co-supervisor, PD Dr. Minka Breloer, for her expert supervision and scientific insight, and for many helpful discussions that sparked new ideas. In addition, I would like to thank her for making her established *S. ratti*- and *L. sigmodontis* life cycles available for my co-infection experiments and for giving me the opportunity to learn at her lab. I would also like to thank her team, Marie-Luise Brunn, Dr. Martina Reitz, Dr. Wiebke Hartmann, and Dr. Irma Haben, for their help with *S. ratti* and *L. sigmodontis* infection procedures for co-infection experiments and for sharing their laboratory skills and knowledge with me.

I want to thank Prof. Dr. David Voehringer and Dr. Adriana Turqueti-Neves for providing *N. brasiliensis* larvae and protocol assistance for establishment of the *N. brasiliensis* life cycle at the Research Center Borstel.

Many special thanks go out to the infection immunology group at the Research Center Borstel, in particular to Alexandra Hölscher, Johanna Volz, and Ann-Kathrin Lemm for their technical support and the gracious sharing of their knowledge. Their help was invaluable and their kindness always lifted me up. My heartfelt thanks go to Mahin Abad Dar, Melanie Wannick, Miriam Krusch, Kristina Ritter, Filipa Varela, Fengyuan Deng, Hanna Erdmann, Kerstin Walter, Jochen Behrends, and Katharina Bayer. Their scientific spirit and friendship made working with them a pleasure.

Furthermore, I would like to thank everyone at the Research Center Borstel who made my doctorate studies such an educational and enjoyable experience.

I would also like to thank my close friends, Anna and Martha, for their friendship and emotional support.

Finally, I would like to thank my family, in particular my parents, Yvonne and Peter, my brother, Hans, and my husband, Christoph, for having faith in me and for their love and support during this endeavor. This work is dedicated to them.